İSTANBUL TECHNICAL UNIVERSITY ★ INSTITUTE OF SCIENCE AND TECHNOLOGY

THE EFFECT OF CYLINDER BORE DISTORTION ON LUBE OIL CONSUMPTION AND BLOW-BY

M.Sc. Thesis by
Fatih KAĞNICI

Department : Mechanical Engineering

Programme : Automotive

JUNE 2010

İSTANBUL TECHNICAL UNIVERSITY ★ INSTITUTE OF SCIENCE AND TECHNOLOGY

THE EFFECT OF CYLINDER BORE DISTORTION ON LUBE OIL CONSUMPTION AND BLOW-BY

M.Sc. Thesis by
Fatih KAĞNICI
(503081732)

Date of submission : **07 May 2010**
Date of defence examination: **10 June 2010**

Supervisor (Chairman) : **Assis. Prof. Dr. Özgen AKALIN (ITU)**
Members of the Examining Committee : **Prof. Dr. Metin ERGENEMAN (ITU)**
Prof. Dr. İrfan YAVAŞLIOL (YTU)

JUNE 2010

İSTANBUL TEKNİK ÜNİVERSİTESİ ★ FEN BİLİMLERİ ENSTİTÜSÜ

SİLİNDİR İÇİ DEFORMASYONUN YAĞ TÜKETİMİ ÜZERİNE ETKİSİNİN İNCELENMESİ

YÜKSEK LİSANS TEZİ
Fatih KAĞNICI
(503081732)

Tezin Enstitüye Verildiği Tarih : 07 Mayıs 2010
Tezin Savunulduğu Tarih : 10 Haziran 2010

Tez Danışmanı : Yrd. Doç. Dr. Özgen AKALIN (İTÜ)
Diğer Jüri Üyeleri : Prof. Dr. Metin ERGENEMAN (ITU
Prof. Dr. İrfan YAVAŞLIOL (YTU)

HAZİRAN 2010

FOREWORD

I would like to express my deepest appreciation to my thesis advisor Assist. Prof. Dr. Özgen AKALIN who has inspired and guided me throughout the research.

I also would like to thank my colleagues in Ford Otomotiv Sanayi A.Ş., especially to my supervisor Alper TEKELİ, Nedim Güngör SOYDEMİR, Kayhan ÖZDEMİR and Bilal BİTİKÇİOĞLU for their kind support throughout the project.

At last but not least, I would like to thank my family for their encouragement and assistance over my life.

May 2010

Fatih KAĞNICI

Mechanical Engineer

TABLE OF CONTENTS

Page

ABBREVIATIONS

FEM	: Finite Element Method
TS	: Thrust Side
ATS	: Anti-thrust Side
CFD	: Computational Fluid Dynamics
CA	: Crank Angle
LOC	: Lube Oil Consumption

LIST OF TABLES

Page

LIST OF FIGURES

Page

LIST OF SYMBOLS

m_p : Piston mass

I_p : Piston moment of inertia around pin center

F_g : Weight of piston

F_{gas} : Force due to combustion pressure

F_r : Piston ring contact force

F_{ci} : Liner contact force at thrust and anti-thrust sides at i'th cross section

F_{pin} : Force exerted by piston pin on piston

M_{ci} : Moment due to piston-liner contact at i'th cross section

M_g : Moment due to piston weight

M_{gas} : Moment due to gas force (active when the combustion chamber is non- symmetric)

M_r : Moment due to ring axial and radial contact force

M_p : Moment due to friction at piston pin

$\ddot{\kappa}$: Angular acceleration of piston

m_r : Mass of piston ring

$F_{fric,ax}$: Friction between liner and ring surface

$F_{gas,ax}$: Gas force

$F_{hydr,ax}$: Axial damping force caused by the oil filling of the groove

F_{bend} : Bending force caused by the interaction between TS and ATS

$F_{tension}$: Force caused by the tension of the ring

$F_{gas,rad}$: Radial gas force

$F_{fric,rad}$: Friction force between ring and ring groove

$F_{hydr,rad}$: Force caused by the hydrodynamic gap between liner and ring running face

$M_{elastic}$: Elastic bending moment due to ring twisting

$M_{pre-twist}$: Elastic moment due to pre-twist angle

h_i : Moment arm for each force component

p_c : Chamber pressure

T_c : Chamber temperature

V_c : Chamber volume

p_o : Surrounding or neighboring chamber pressure

T_o : Surrounding or neighboring chamber temperature

V_o : Neighboring chamber volume

R : Gas constant of combustion gas

k : Isentropic exponent

ψ : Gas flow coefficient

A : Cross sectional area

Δt : Time step

h : Nominal film thickness

$\overline{h}_T$: The average gap

$\overline{p}$: Mean hydrodynamic pressure

σ : Composite surface roughness

Φ_x : Pressure flow factor

Φ_s : Shear flow factor

U : Sliding velocity

β : Mass transfer coefficient

c_{film} : Concentration of lube oil at film surface

c_∞ : Concentration of lube oil in combustion chamber

$\dot{m}$: Mass flow rate into boundary surface

y : Coordinate perpendicular to boundary surface

Δs : Movement of the piston during time step Δt

s_{film} : Uncovered area of the oil film

a_0 : Acceleration at the beginning of motion

h_{film} : Height of oil film between top land and liner

d_{film} : Diameter of oil film

THE EFFECT OF CYLINDER BORE DISTORTION ON LUBE OIL CONSUMPTION AND BLOW-BY

SUMMARY

It is a well-known fact that cylinder bore deformations in engine operation involves a number of problems in terms of lubrication, and the deterioration of piston ring conformability to the bore, in particular, increases the lubricating oil consumption (LOC). Therefore, identification and understanding of bore distortion influencing oil consumption has been an important subject.

The inherent complexities in power cylinder system and large amount of testing cost and time necessitates analytical tools, which enables engineers to optimize their design prior to any prototype build and testing. This requires the advancement of the understanding of the characteristics, sources, and driving mechanisms of cylinder bore distortion, consequently oil consumption. Such an analytical model does not only provide early predictions for power cylinder performance but also provides a means for the identification and prevention of failure modes.

In this study, analytical lubricating oil consumption model was established for a diesel engine. Piston stiffness was determined as an important input for the oil consumption model. So, stiffness measurement test-rig was simulated via FEM in order to calculate the stiffness matrix. In addition, finite element analysis of cylinder bore distortion was performed at engine operating conditions for identifying the distorted bore and its Fourier coefficients. Results were used for obtaining the orders of bore distortion. In addition to distorted liner shape, straight liner and from order 0 to order 4 shape liners which are thought significant for LOC were used as an input in the oil consumption model at certain steady state operating conditions. Measured pressure curves were used for the analyses. Consequently, bore distortion was found to be an effective parameter on oil consumption.

SİLİNDİR İÇİ DEFORMASYONUN YAĞ TÜKETİMİ ÜZERİNE ETKİSİNİN İNCELENMESİ

ÖZET

Silindir içi deformasyonlar, içten yanmalı motorlarda yağlama ve segmanların silindir içine oturmaması gibi problemlerden dolayı yağ tüketimini etkilediği bilinen bir gerçektir. Bu nedenle, yağ tüketimi üzerinde etkili olan silindir içi deformasyonlarının belirlenmesi ve anlaşılması oldukça önem arz etmektedir.

Güç silindir sistemlerinin kendine özgü zorluklarından ve test için gereken zamanın ve yüksek meblağlardaki masraflarından dolayı, mühendislerin kendi tasarımlarının eniyileme çalışmalarını ve bunun için gerekli olan bilgisayar ortamındaki analitik ekipmanlardan yararlanmalarını bir ihtiyaç haline getirmiştir. Bu durum, silindir içi deformasyonların ve bunun sonucunda yağ tüketiminin karakteristik özelliklerini, sebeblerini ve bunların altında yatan mekanizmayı ileri düzeyde anlamayı gerektirmektedir. Bahsi geçen bu analitik model, güç silindirlerin performanslarını önceden hesaplamanın yanında sistemin hata mekanizmalarını da önlemek için de kullanılmaya imkan sağlamalıdır

Bu çalışmada, bir dizel motor için yağ tüketim modeli oluşturulmuştur. Piston rijitliği, yağ tüketimi modeli için önemli bir parametre olduğu için, çalışma koşullarındaki değerlerini bire bir yansıtması için; test şartları bilgisayar ortamında simüle edilip yağ tüketimi modeline girdi olarak yerleştirilmiştir. Silindir içi deformasyonlar, motorun çalışma şartlarına göre bilgisayar ortamında analizi yapılarak, düz silindir, deforme olmuş silindir ve onun değişik sıklıkdaki şekilleri analiz sonucunda ayrı ayrı elde edilmiştir. Bu şekillerdeki silindirler, yağ tüketimi modeline girilerek sabit rejim çalışma noktalarında incelenmiş ve etkileri karşılaştırılmıştır. Yapılan simülasyonlarda ölçülen silindir içi basınç eğrileri kullanılmıştır. Yapılan karşılaştırmalar sonucunda deforme olmuş silindirin değişik sıklıklarda farklı olarak, yağ tüketimi üzerinde farklı etkileri gözlenmiştir.

1. INTRODUCTION

Engine oil consumption is one of the most important criteria for the modern internal combustion engine performance and, consequently, customer satisfaction. Engine oil consumption is also recognized to be a significant source of pollutant emissions in automotive engines.

The ring-pack inside a power cylinder system plays an important role in an internal combustion engine. Its main function is to provide a moving seal between the piston and cylinder liner, which prevents the gas leakage from the combustion chamber to the crankcase, and at the same time minimizes the oil transport in the opposite direction. The lubrication occurring in the interface between the ring running-face and cylinder liner surface greatly influences the ring sealing performance. Developing capabilities to understand the ring-pack lubrication has always been an active subject in engine research. Among them, the numerical simulation is one of the powerful means. (Liu and Tian, 2005)

The conformability of the ring-pack is an important issue for the engine oil consumption and blow-by. If the sealing mechanism does not work very well because of the conformability problems of the ring, then oil consumption may occur as a serious problem in an engine. When a block is subjected to operating loads, assembly loads and manufacturing problems, the piston bores of the block will deform. Any change in the block structure may cause significant ring-bore seal issues.

Any non-circular cylinder bore distortion has an important influence on the operational behavior of an engine. Because of the limited ability of the piston rings to conform to the distorted bore shape, the oil consumption increases. Mainly, several loads which cause the liner to deviate from the ideal condition in addition to manufacturing tolerances. These are;

- Assembly loads (assembly of the cylinder head and gasket)
- Gas Pressure during fired operation.

- Thermal loads (thermal expansion differences between cylinder block and head)
- Temperature gradients during fired operation.

According to Liu and Tian (2005), bore distortion is found to have an important influence on the oil transport. Due to the reduced conformability of the top ring caused by the bore distortion, a relatively large amount of oil is left on the liner by the top ring during intake stroke. Under the impact of increasing gas pressure acting on the back, the top ring can carry some oil to the upper region of liner, and even up-scraping of oil is observed. Both up and down-scraping of oil by the top ring are found to increase with the amplitude of bore distortion.

There are few studies have been done for the effect of bore distortion on lube oil consumption and blow-by. Most of them are focused on experimental studies. However, the computerized investigations barely focusing on this issue has not been found. Moreover, the inherent complexities in power cylinder system and large amount of testing cost and time necessitates analytical tools, which enables engineers to optimize their design prior to any prototype build and testing. This requires the advancement of the understanding of the characteristics, sources, and driving mechanisms of cylinder bore distortion, consequently oil consumption. Such an analytical model does not only provide early predictions for power cylinder performance, but also provides a means for the identification and prevention of failure modes.

1.1 Oil Consumption Mechanisms

Understanding the primary investigation, the oil consumption in the modern internal combustion engines describes the combustion oil consumption sources. Four potential oil consumption paths have been proposed by Froelund and Ertan (2004). These sources consist of piston-ring-liner system, crankcase ventilation system, valve stem seals and turbocharger.

Furthermore, being the major source of oil consumption, oil consumption in the power cylinder is in the scope of the text and other oil consumption due to valve stem seal and turbocharger is ignored.

Research has been made in identifying and classifying significant oil consumption sources in internal combustion engines. Mainly, four potential sources of oil consumption were determined to contributing to total oil consumption in the use

1. Oil throw-off from the top compression ring
2. Transport of oil with reverse gas flow into the combustion chamber
3. Evaporation of oil from the liner wall
4. Oil scraping by piston top land

These oil consumption mechanisms are shown in Figure 1.1

Yilmaz et al., (2004) describe the throw-off mechanism as a hypothesis supported by experimental data concerning oil consumption of the mechanical transport of liquid oil in the combustion chamber due to inertia forces caused by acceleration and deceleration of the piston assembly (see Figure 1.1a). The importance of this drive is assumed that from the information collected on the oil film on the top land and ring. Oil throw-off was visualized in research with single cylinder engine spark ignition engine at low load conditions (Inagaki et. al., 1995, Thirouard et. al., 1998) .

The direct oil transport with the reverse gas flow from the second land into the combustion chamber is also main oil consumption mechanism of piston-ring-liner system (see Figure 1.1.b). During several periods of the engine cycle, when the second land pressure becomes greater than the combustion chamber pressure, reverse gas flows back into the combustion chamber through the top ring gap and around the top ring groove if the top ring loses its stability in the groove.(Yilmaz et al., 2004)

Oil evaporation, as illustrated schematically in Figure 1.1.c, is also found to be a strong contributor to the oil consumption from the piston-ring-liner system, especially during severe operation conditions when the thermal loading of engine components is high (Yilmaz et al., 2002). They also underline that oil evaporation from the cylinder liner, the piston, and the oil sump, which are different regions of the engine, are main oil consumption contributor because of the evaporation. On the other hand, the oil presenting in these regions is exposed higher gas flow rates and temperatures dominate evaporation from the piston-ring-liner system. Wahiduzzaman et. al., (1991) presented a complete evaporation model which treats

oil vaporization as the diffusion of oil vapor through a gas boundary layer on the cylinder's surface.

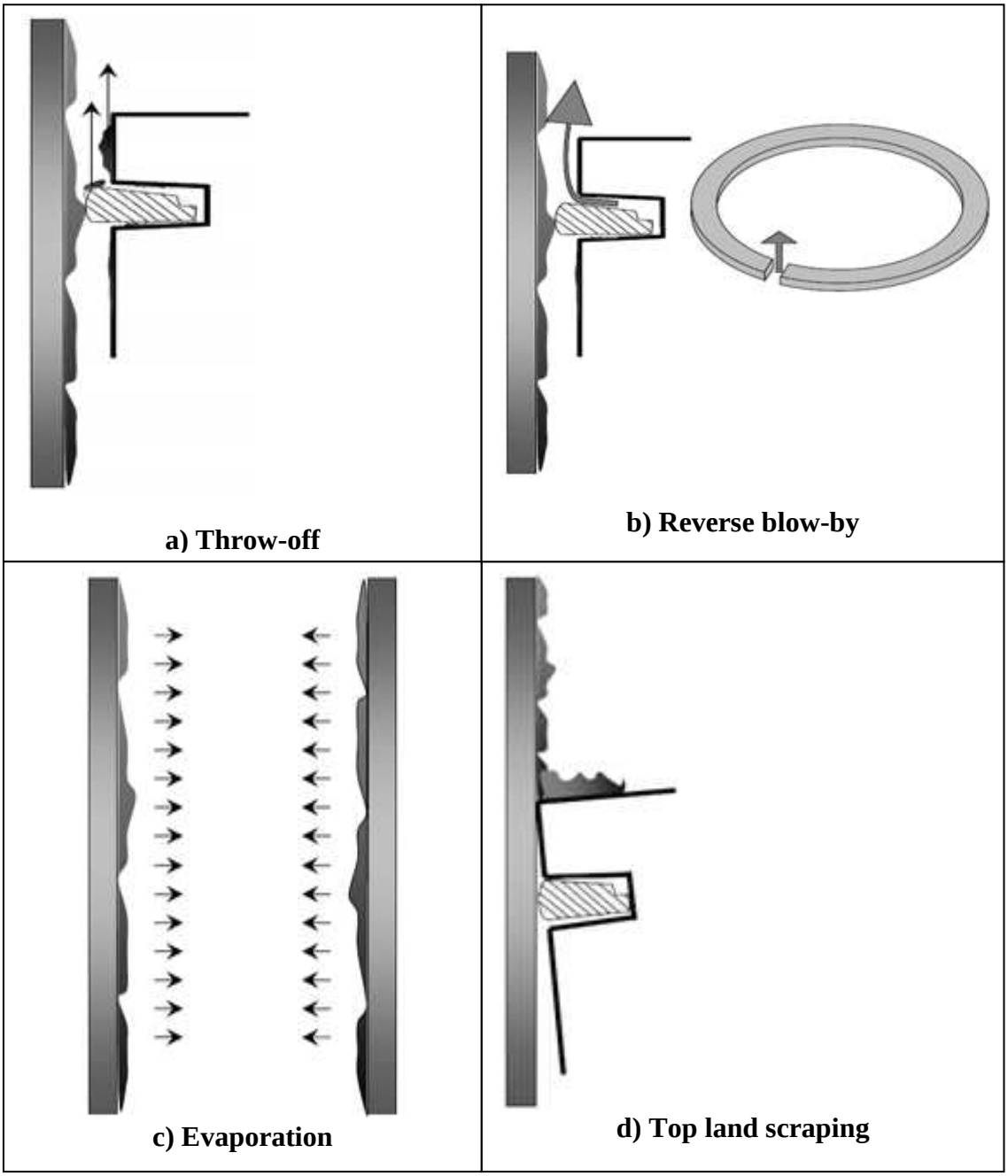

Figure 1.1 : Oil Consumption Mechanisms in Piston Ring Liner System (Scania, 2009)

Moreover, Audette and Wong (1999) have developed a similar model to Wahiduzzaman's, extending the model capability to consider variation of oil composition along the liner. Furthermore, according to Yilmaz et al. (2002), oil volatility directly governs the oil evaporation rate from surfaces during the engine cycles.

Top land scraping of oil can be described that the top land clearance of a piston is rather low under engine running conditions. Deposits on the top land and lateral motion due to piston secondary movement cause contact with the liner wall. At each upward stroke, the piston top edge scrapes along the liner wall and pushes oil into the combustion chamber

1.2 Cylinder Bore Distortion

In view of the fact that the piston and the piston rings are moving in the cylinder, the cylinder liner constitutes an important tribological element as a sliding surface against the piston and piston rings. (Andersson et. al., 2002)

In a typical power cylinder assembly, there are three rings: two compression rings and an oil control ring. The compression rings seal piston in its combustion chamber, so that pressure from exploding gasoline can be converted to mechanical energy. Also, the rings support the dissipation of heat through the cylinder wall and control oil consumption.

The radial deformation of a cylinder bore is called cylinder bore distortion. Cylinder bore distortion has taken on significance to engine designers, as well as to manufacturers of cylinder liners, pistons, cylinder head gaskets and head bolts. The interest in bore distortion is directly attributed to the trend to lighter weight castings, new materials and fuel economy. (Ford Handbook, 2001)

The cylinder may distort before and during operation because of defects in design and assembly, gas pressure and thermal variations. So, the circular piston ring must conform to a slightly imperfect cylinder bore. Since the piston ring performs like an elastic beam, we expect the ring to successfully conform to a slightly distorted bore. If the ring cannot follow these deformations, a localized lack of contact will occur. This seal violate may cause increased oil consumption and leakage, blowby, and engine wear; also fuel efficiency may decrease. (Bardizmashvilli et. al., 2004)

In order to achieve the best conditions for the function of the piston, ring and liner tribological system, the shape of the liner should be as circular as possible.

In addition to the manufacturing tolerances, which cause a deviation to the liner from the ideal condition, the liner will deviate from the ideal geometry because of the loads acting on it. (Koch et. al., 1998)

According to Leonne and Ziemba (1988) the causes of cylinder bore deformation can be categorized into the following groups:

- Distortion caused by the manufacturing process.
- Deformations caused by the assembly of the cylinder head with the cylinder head gasket and the peripheral components, called cold-static initial clamping distortion. These elastic distortions can be influenced by design changes of the installed components.
- Deformations caused by dynamic gas forces.
- Cylinder distortions through friction-related sliding movements in the sealing plane, caused by differing thermal expansion of cylinder head and block.
- In engine running conditions, there are also distortions caused by temperature differences around the cylinder bores. For example the cold-static distortion of the 2nd order in lateral direction of crankshaft will change to longitudinal direction during hot engine running.

Moreover, several parameters affect the bore distortion in the engines as shown in Fishbone diagram (see Figure 1.2). In the diagram, the sub parameters

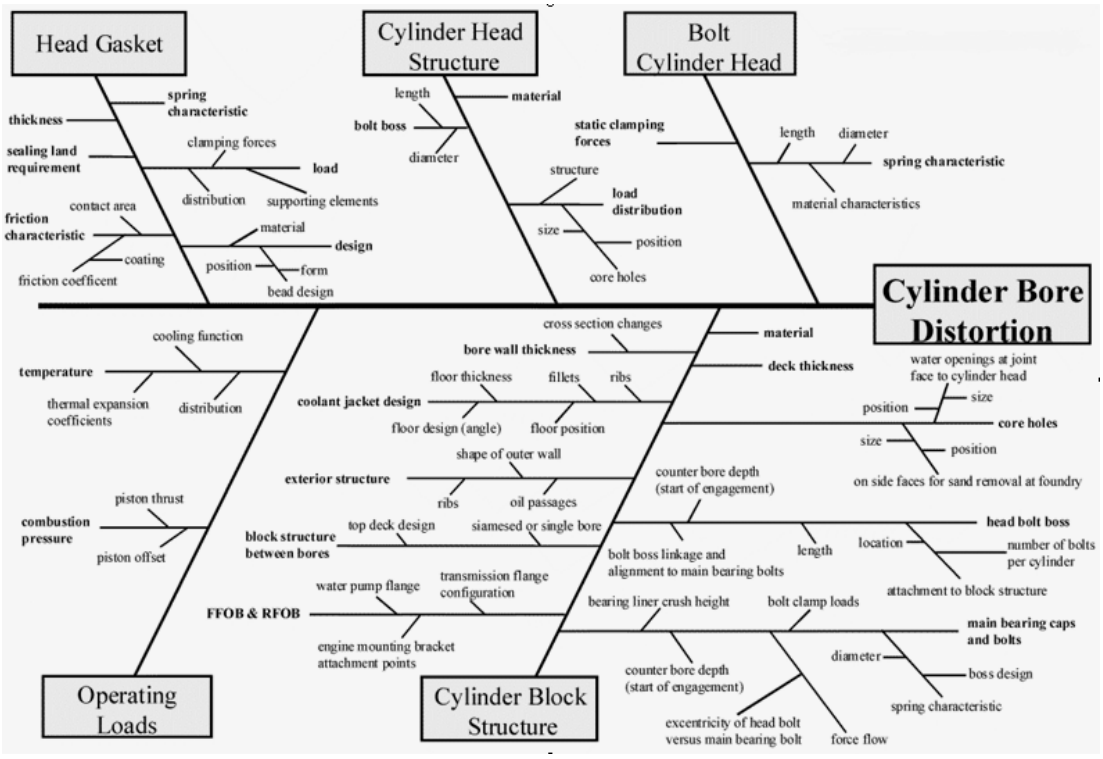

Figure 1.2 : Fishbone Diagram of the Cylinder Bore Distortion (Ford Handbook, 2001)

of main reasons which cause cylinder bore distortion, are showed schematically.

Many researches have been done for the cylinder bore distortion. Some of them are related with the bore distortion measurements. However, some of them are related with analytical studies.

Kakede and Chow (1993) investigated the using finite element analysis of cylinder boring process and the parameters, which affect the machining such as speed effect, source of distortion and number of inserts.

Abe and Suzuki (1995) developed a calculation method, which considered sliding effect of the cylinder head on the top deck of the cylinder block, based on a FEM model. In addition, they investigated the effect of bore distortion on lube oil consumption and they compared their results with the measured values, which were reported by Fujimoto (1991).

The effects of bore out-of-roundness on the performance of a piston-ring in a distorted bore are investigated by Ma et. al. (1995) analytically and they reported that the ring performance is influenced by bore distortion significantly.

Tomanik (1996) investigated the relationship between bore distortion and ring conformability and he proposed a semi-empirical criterion using the measurement values and analytical studies about bore distortion, which ring can conform.

One of the most extensive study on bore distortion was reported by Koch et. al. (1998). They studied oil consumption both experimentally and analytically. They set up a FEM model in order to analyze bore distortion and compared the results with the measured values. Also, they identified the parameters which affect bore distortion, are

- Influence of thread engagement
- Influence of water jacket design
- Influence of cold start condition
- Influence of temperature load at different operating states
- Influence of cylinder head gasket stiffness
- Influence of cylinder block material

Moreover, they reported the Fourier analysis calculation, which analyzes the bore distortion as different order amplitudes.

Maassen et. al. (2001) investigated the bore distortion with analytical and empirical methods for prediction, verification and optimization in addition to study of Koch et. al. (1998).

Bardizmashvilli et. al., (2004) wrote a code in MATLAB for representing the bore distortion maximum amplitudes of bore distortion orders in order to examine the ring conformability. Then, they compared the results, which are taken from the code written in MATLAB with FEM data. In that study, they also investigated the different approaches of Fourier harmonic, which are represented by Geotze (1988), Dunaevsky (1990) and Tomanik (1996).

Later, Sato et. al. (2006) established a bore distortion FEM model in order to analyze friction by piston secondary motion simulation in consideration of cylinder bore distortion. After that, McClure and Tian (2008) investigated the piston secondary motion, considering the bore distortion deformation according the static and dynamic FEM analysis results.

1.2.1 Cylinder Bore Distortion FEM Analysis Methodology

FEM calculations represent an effective tool that is being employed to an increasing extent in the field of engine development. In many cases, it is not possible to specify the required input data and parameters with the necessary accuracy. It is, therefore, essential to obtain the assistance of measurement results. After validating measurement and calculation, the influence of modifications to optimize the engine design can be examined in a realistic manner via FEM calculations. The FEM model that is used can be developed by measuring experience in future projects. This approach means that fewer tests and test components are required. As a consequence of the development time can be decreased.. (Koch et. al. 1998)

It is very difficult to measure the bore distortion during engine working conditions. So, Finite Element Analysis is used with some assumptions of working conditions in order to calculate the bore distortion.

These assumptions are shown in Figure 1.3

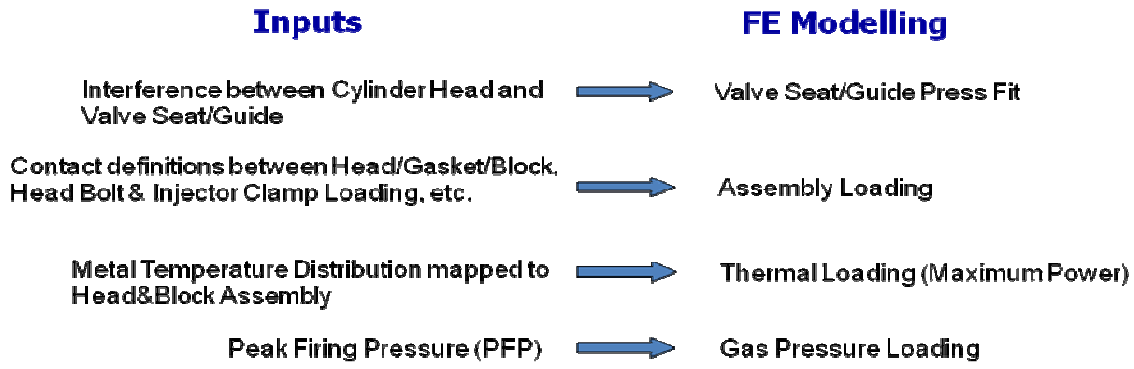

Figure 1.3 : FEM Analysis Assumptions

Figure 1.4 shows the example FEM model of the bore distortion analysis. Block, Head, Gasket and Head Bolts are used in the model. In order to connect the movement of the components non-linear contact elements are used in ABAQUS which is assumed as friction and pressure parameters. Other details with FEM model are described in section 4.2

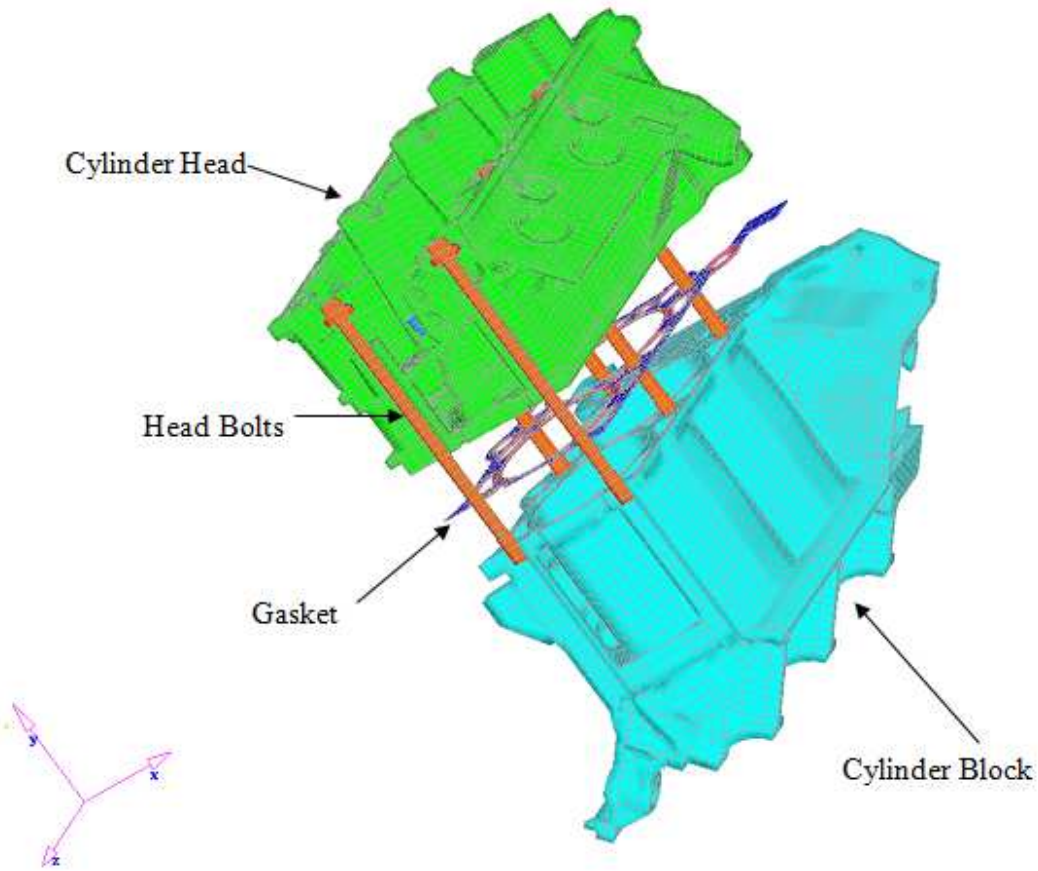

Figure 1.4 : Example FEM Model (Ford Handbook, 2001)

A great amount of research has been made for bore distortion analysis methodology. Abe and Suzuki (1995) developed a FEM model which includes non-linear element model (see Figure 1.5). However, their model were not includes contact elements and solid bolt model which are the important input parameters in order to analyze the distortion caused by assembly loads. Instead of contact elements amongst head, gasket and block, friction coefficients were used.

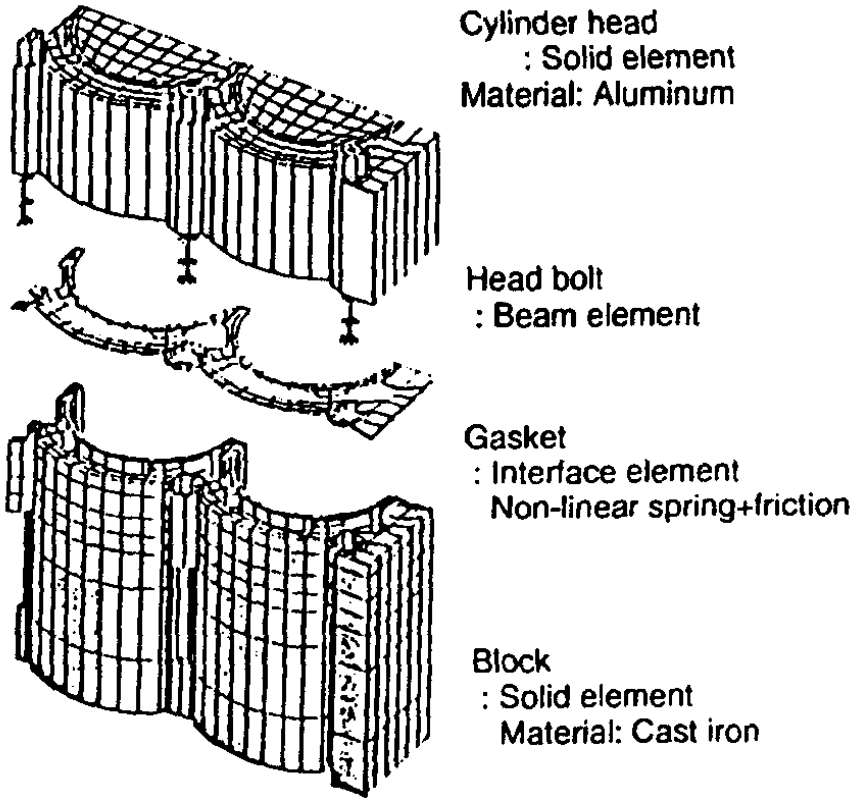

Figure 1.5 : FEM Model (Abe and Suzuki, 1995)

Koch et. al. (1998) and Maassen et. al. (2001) established a FEM model, which includes not only head, gasket and block models, but also main bearing shells, and bed plate model. (see Figure 1.6) However, these models of components cause increased in analysis time, unnecessarily. On the other hand, absence of bolts is another deficiency of FEM model.

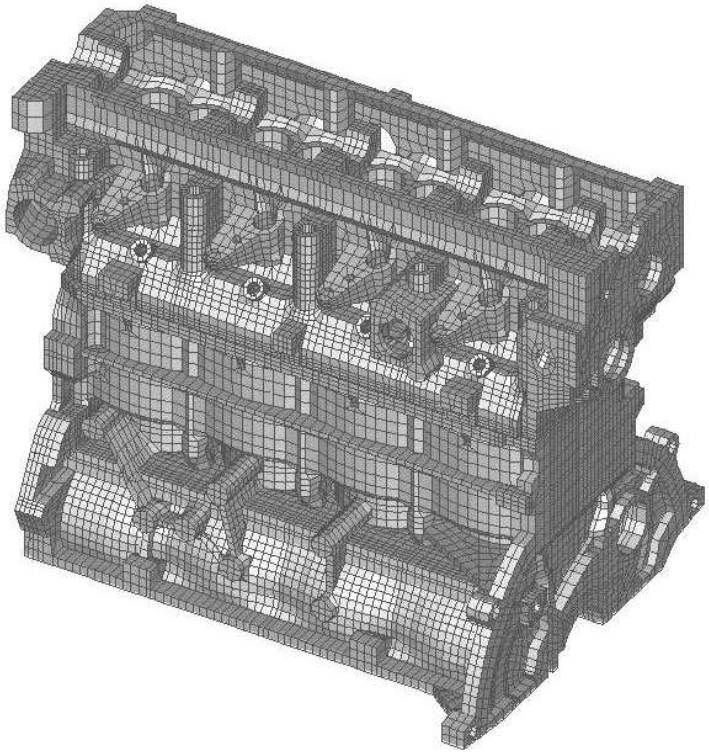

Figure 1.6 : FEM Model (Koch et. al., 1998)

Sato et. al. (2006) developed a FEM model, which is more accurate than done before. (see Figure 1.7). However, absence of interference between cylinder head and valve/seat guide is lack of model.

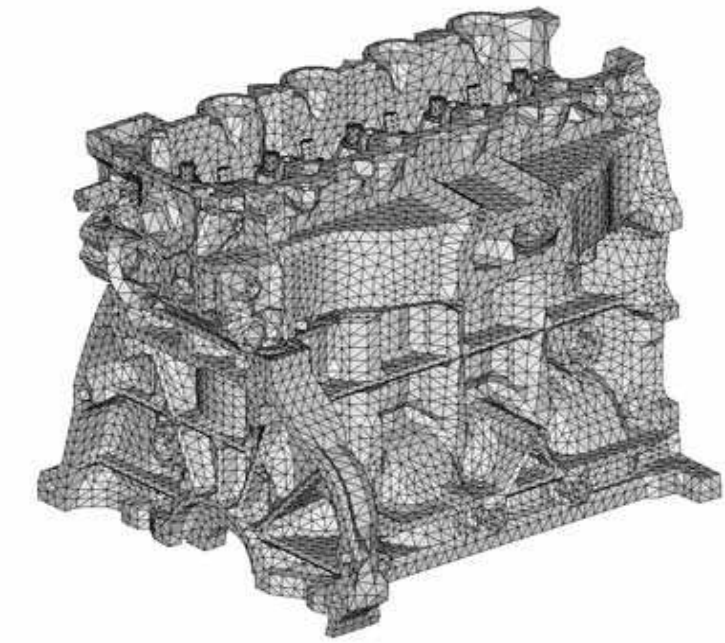

Figure 1.7 : FEM Model (Sato et. al., 2006)

1.2.2 Post Processing of Cylinder Bore Distortion Analysis

In practice, it is normal that the cylinder liner is not perfectly cylindrical and of nominal bore size along its entire length. The bore distortion causes loss of conformity between the piston rings and cylinder liner. Limited piston ring follow-up performance, in particular caused by bore deformation, causes an increase in the lubricating oil consumption.

The non-circularity of the cylinder bore can be described by a Fourier series. (Tomanik 1996) (see Figure 1.8)

$$\Delta r = A_0 + A_1 \cos(q) + A_2 \cos(2\,q) + \ldots + A_i \cos(i\,q)$$

$$+ B_1 \sin(q) + B_2 \sin(2\,q) + \ldots + B_i \sin(i\,q) \qquad \textbf{(1.1)}$$

where

Δr: radial deviation from the circle

Ai, Bi: Fourier coefficients

q: angular position

i: order of deformation

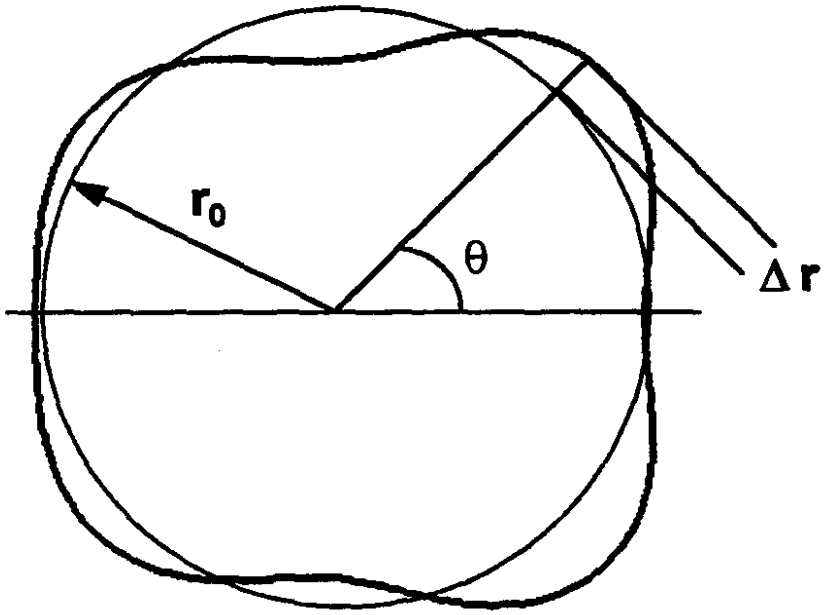

Figure 1.8 : Deformed Bore Cross Sections (Tomanik, 1996)

Bore distortions from the nominal radius r_0 with a Fourier series can also represented by orders.(see Figure 1.9) Letting $\xi(\phi)$ denote the measured bore shape (where ϕ is the polar angle), $\xi(\phi)$ is approximated by

$$\xi(\phi) \approx r_0 + \sum_{k=1}^{N} A_k \cos(k(\phi + \delta_k)) \qquad \textbf{(2.2)}$$

where k is the *order* and δ_k is *phase angle*. (Bardizmashvilli et. al., 2004)

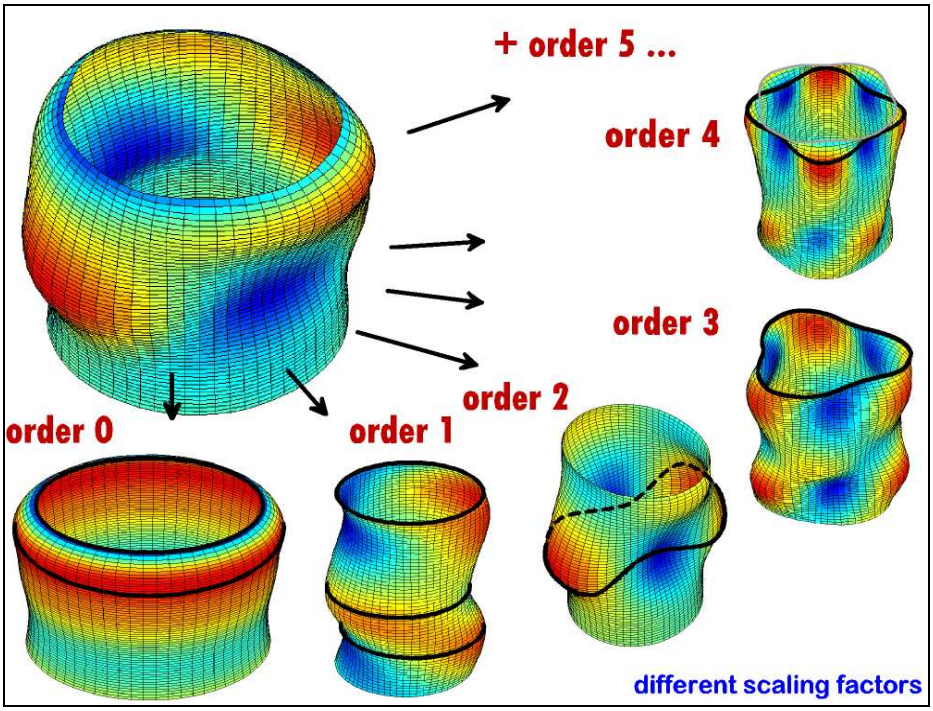

Figure 1.9 : Bore Distortion Orders (Ford Handbook, 2001)

There are several reasons for the non-circularity of the cylinder bore. The cylinder liners are machined to a level of accuracy specified in terms of tolerances. The allowed difference between maximum and minimum diameter of the cylinder bore may be from 10 to 100 times the thickness of the oil film between piston rings and the liner. Therefore, the deviation from circularity within the manufacturing tolerances is likely to have a significant outcome on the performance of the piston assembly. The zero and first order bore distortions (see Figure 1.9) are a function of the size and location tolerances of the cylinder bore (Chittenden and Priest, 1993).

The assembling of the head-block can cause deformations on the cylinder liner. An example of this is the tightening of the cylinder head bolts. According to Chittenden and Priest (1993), if a fourth-order distortion (see Figure 1.9) is a major component in a distorted cylinder bore of a particular engine, the tightening of the four cylinder head bolts of this engine is the reason. The clamping of the cylinder liner between the cylinder head and the support at the lower end of the liner in the engine block, results in an outward deformation of the cylinder liner´s inner surface (Reipert and Voigt, 2001). Inadequate cooling or over-cooling of a specific region of the cylinder may cause expansion differences around the circumference of the cylinder and along its length, which leads to distortion of the cylinder bore (Chittenden and Priest, 1993). The magnitude of the thermal expansion is by far larger than the deformation caused by the clamping of the bolts (Reipert and Voigt, 2001).

The gas pressure acts on the cylinder wall in a restricted area. Distortion of the cylinder liner due to the combustion pressure is significant only in highly rated diesel engines with thin-walled wet liners (Chittenden and Priest, 1993).

The maximum deformation by clamping, by thermal expansion and by gas pressure is observed at the upper edge of the cylinder (Reipert and Voigt, 2001). The ring conformability is reduced significantly with an increase in the order of bore distortion. Complicated ring geometries with several non-conformed regions arise from a combination of multiple-order bore distortions. (Ma et.al., 1997, Chittenden and Priest, 1993).

1.3 Effect of Bore Distortion on Lube Oil Consumption

In case of less bore distortion, the engine will consume a small amount of oil. Also, cylinder wear and ring wear are both increased. Smaller amount of distortion provides less friction and therefore improves fuel economy.

First researches for the effect of bore distortion are studied with experimental methods. Some researchers neglected the bore deformation when they were investigated the oil consumption. Later, liner deformation was assumed as an effective parameter for LOC and was investigated by Schneider et. al. (1993).

Schneider et. al. (1993)., investigated the out-of roundness for the different cylinder bores in an engine as a parameter study of under different bolt torques and showed the effects of the parameters on oil consumption.

Ma et. al.(1995) investigated the basic evaluation of the effect of bore distortion and ring lateral displacement on the performance of a single ring. They showed that the predicted performance characteristics of the ring are noticeably affected by bore out-of roundness and ring lateral displacement. The important issue that they found is cylinder bore distortion and ring lateral movement affect the net oil transport, upward and downward oil flows that may be great significance in practical circumstances where oil on the combustion chamber side of the compression ring may be burnt, evaporated or else be degraded.

The cylinder bore deformations which are caused by thermal loads, were investigated by Abe and Suzuki (1995) as an analytical study and they showed the effect of thermal distortion on the ring conformability and importance of establishing countermeasures against thermal distortions to reduce oil consumption.

Hitosugi et. al. (1996) performed an experimental study in order to investigate the effects of bore distortion orders on LOC. Moreover, this is the unique study which aims the focusing on the effects of different orders. They made second, third and fourth order deformed liners, which are tested for investigating the LOC and showed that in the fourth order deformed profile, the LOC is found higher.

Ma (1998) developed a computational model of piston-ring pack lubrication, which includes the effect of many important factors such as bore distortion, ring conformability and lubricant shear-thinning. The following points can be obtained from the paper: With a distorted cylinder bore, increasing the radial widths of the rings will have a favorable effect on the frictional losses of the ring pack, which result in a more significant increase in the oil transported into the combustion chamber that may cause higher oil consumption. Although, the bore distortion can reduce the ring pack power loss, it will dramatically increase the net upward oil transport rate, particularly for the larger degrees of bore distortion.

According to Liu and Tian (2005), bore distortion is found to have an important influence on the oil transport. Due to the reduced conformability of the top ring caused by the bore distortion, a relatively large amount of oil is left on the liner by

the top ring during the intake stroke. Under the impact of increasing gas pressure acting on the back, the top ring can carry some oil to the upper region of liner, and even up-scraping of oil is observed. Both up and down-scraping of oil by the top ring are found to increase with the amplitude of bore distortion.

1.4 Objective of Thesis

The main focus of this study is to first explore, than quantify the effects of cylinder bore distortion on diesel engine oil consumption, while other significant parameters such as load (or brake mean effective pressure), oil temperature and speed are kept constant.

Firstly, finite element analysis was performed for the piston in order to find the stiffness calculation and its methodology in ABAQUS. Then, non-linear cylinder bore distortion analysis was performed under operation conditions, both hot and cold assembly cases. According to results, which were performed in ABAQUS, a code is written in MATLAB in order to investigate distorted bore profile and Fourier coefficients of the distortion, which gives the orders of the distorted bore. Besides, an oil consumption model has been established by using AVL EXCITE PR software and various parameters in the model has been modified especially piston stiffness characteristics in order to obtain best results. In addition to distorted liner profile, straight liner, order 0 shape liner, order 1 shape liner, order 2 shape liner, order 3 shape liner and at least order 4 shape liner are used for the investigated parameters and entered the liner profile in AVL EXCITE PR. Finally, the mechanisms behind observed variability on oil consumption are analyzed with the help of available analytical model.

This thesis report consists of 4 sections including the introduction. In section 1, a literature survey is given, also comprising of oil consumption mechanisms, bore distortion. Basic oil consumption sources and driving mechanisms are presented with previously published work. Bore distortion is explained with various calculation approaches; especially FEM Analysis and its post-processing are presented. At the end of the section 1, previous work the effects of bore distortion on LOC is presented together with experimental and theoretical research. Section 2 includes general information about the AVL EXCITE PR, which is used for analytical investigations in this study. Basic principles, governing equations and common assumptions

employed in the calculation models are presented. In Section 3, piston stiffness calculation, bore distortion FEM analysis and oil consumption model are explained. Section 4 is the main focus of the thesis which concentrates on the effects of bore distortion on diesel engine oil consumption. The findings from the analytical model are compared with different liner case results and necessary explanations are made clarifying the differences, explaining the trends and underlying mechanisms.

2. THEORY

Healthy assessments and conclusions can only be made with deep understanding and enough knowledge about the used computer code. Therefore, this section is dedicated to general information about main principles, approaches and assumptions of AVL EXCITE PR.

The software consists of three modules, Piston Movement Module, Ring Movement Module and Lube Oil Consumption Module. Ring Movement and Lube Oil Consumption Modules will be explained on separately in the same order. **(**AVL EXCITE PR Theory, 2009a):

2.1 Piston Ring Movement Module

AVL EXCITE PR- Module Piston Ring Dynamics was developed in order to be able to analyze effects of design modifications of piston and piston rings in view of low LOC, blow-by and friction values. For the determination of the dynamic loads upon the rings, AVL EXCITE PR -Module Piston Ring Dynamics considers forces and moments due to inertia, friction and the flow of gas from the combustion chamber through the inter-ring volumes into the sump. If the influence of piston slap on ring dynamics should be taken into account, the program uses the results from piston slap calculation as input, which is pre-calculated for either a mono piston or an articulated piston (AVL EXCITE PR - Module Piston Movement**)**. From these results, ring dynamics are influenced by both the piston radial and tilting motions.

The Piston Ring Dynamics Module calculates the dynamic components of motion of the single rings in a thrust - anti-thrust plane. The simulation also gives values for blow-by, inter-ring pressures and oil film thickness between the rings and liner over crank angle.

The main characteristics of the Software AVL EXCITE PR - Module Piston Ring Dynamics can be listed as follows:

1. Rings are modeled as condensed masses. The contact between the thrust and anti-thrust sides is given by a beam model, which is for pressure compensation. In addition, twisting is considered.
2. Inter-ring regions, which are defined by the piston and ring dimensions were considered as volumes. These volumes were used for computing the gas flow through rings and they are connected because of the opening of ring end gaps and actual orientation of the rings in grooves.
3. Gas flow behind rings and ring-groove flank clearances are regarded as possible. Pressure distribution in the clearance is calculated according to the liner and ring contours, so that the oil film between ring running surface and liner was taken into account.

2.1.1 General Assumptions in Piston Ring Dynamics Calculation

The following assumptions are made for calculation of piston ring dynamics (AVL EXCITE PR Theory, 2009a):

1. The calculation is simultaneously done at TS (thrust side) and ATS (anti thrust side), the mutual influence being taken into by the consideration of gas flow through the ring groove and geometric considerations.
2. Rings are assumed as single masses.
3. The radial mass forces of the rings are disused.
4. The equation of motion in radial direction is not solved explicitly; there will only be a calculation as to whether the ring is lifted from the liner wall.
5. The radial friction force between ring flanks and piston ring groove is calculated by means of the Friction Function according to Stribeck.
6. The calculation of the gas flow and pressure is quasi stationary (constant conditions in each time step) being done by a system of chambers and throttling points. Flow processes are considered as being isothermal. The max. velocity of flow is limited to the sound velocity at the throttling points.
7. There is no any pressure drop in the piston top land, the combustion pressure acts above the top ring. Below and behind the oil ring, the crankcase pressure is active.

8. The gas pressure distribution in the flank clearance between ring and groove is calculated by assuming the pressure gradient as being indirectly proportional to the current clearance.

2.1.2 Governing Equations of Ring Dynamics

The forces acting on a piston ring are shown in Figure 2.1. AVL EXCITE PR uses the equations for the ring dynamics, which are written below.

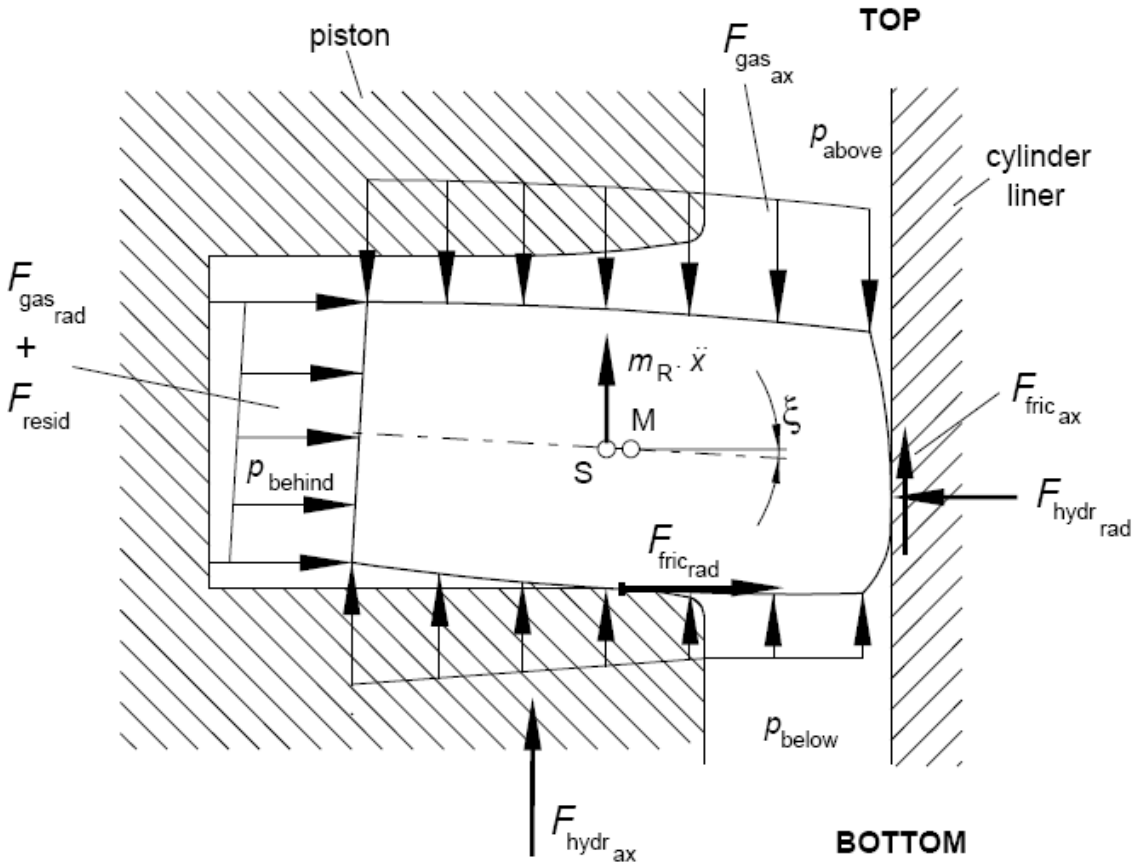

Figure 2.1 : Forces Acting on Piston Ring (AVL EXCITE PR Theory, 2009a)

In axial direction:

In order to control whether the ring is in contact with the groove flank, contact force between the ring and groove is calculated as:

$$F_{contact,ax} = F_{inertia,ax} + F_{fric,ax} + F_{gas,ax} + F_{bend} \qquad \textbf{(2.1)}$$

If $F_{contact,ax} > 0 \Rightarrow$ There is contact with the piston and ring does the same motion as the piston, i.e.:

$$x_{ring} = x_{piston} \tag{2.2}$$

If $F_{contact,ax} < 0 \Rightarrow$ The ring lifts from groove flank, hence the dynamics equation has to be solved:

$$m_{ring} \cdot \ddot{x}_{ring} = \sum F = F_{fric,ax} + F_{gas,ax} + F_{hydr,ax} + F_{bend} \tag{2.3}$$

Where the symbols refer to the following:

m_r : Mass of piston ring

$F_{fric,ax}$: Axial friction force between liner and ring surface

$F_{gas,ax}$: Axial gas force

$F_{hydr,ax}$: Damping caused by the oil filling of the groove

F_{bend} : Bending force caused by the interaction between TS and ATS

In radial direction:

The contact force between the ring and liner is calculated as:

$$F_{contact,rad} = F_{gas,rad} + F_{tension} + F_{fric,rad} \tag{2.4}$$

If $F_{contact,rad} \leq 0 \Rightarrow$ ring lifts from the liner. In this case, the equation of motion is not solved explicitly.

Where the symbols refer to:

$F_{tension}$: Force caused by the tension of the ring

$F_{gas,rad}$: Gas force

$F_{fric,rad}$: Friction force between ring and ring groove

$F_{hydr,rad}$: Force caused by the hydrodynamic gap between liner and ring running surface (including radial damping force)

2.1.3 Gas Flow Through the Ring Pack

One of the main important issues in ring dynamics calculation is that ring dynamics and gas dynamics in the ring pack depend on each other. Because of being main drivers of ring motion, inertial forces and gas forces have to be evaluated correctly.

In order to calculate the gas forces acting upon rings, the pressure resulting from the gas flow have to be known. For this, AVL EXCITE PR divides the entire ring package into chambers (volumes behind and between the rings), which are connected one to another by throttling points (see Figure 2.2).

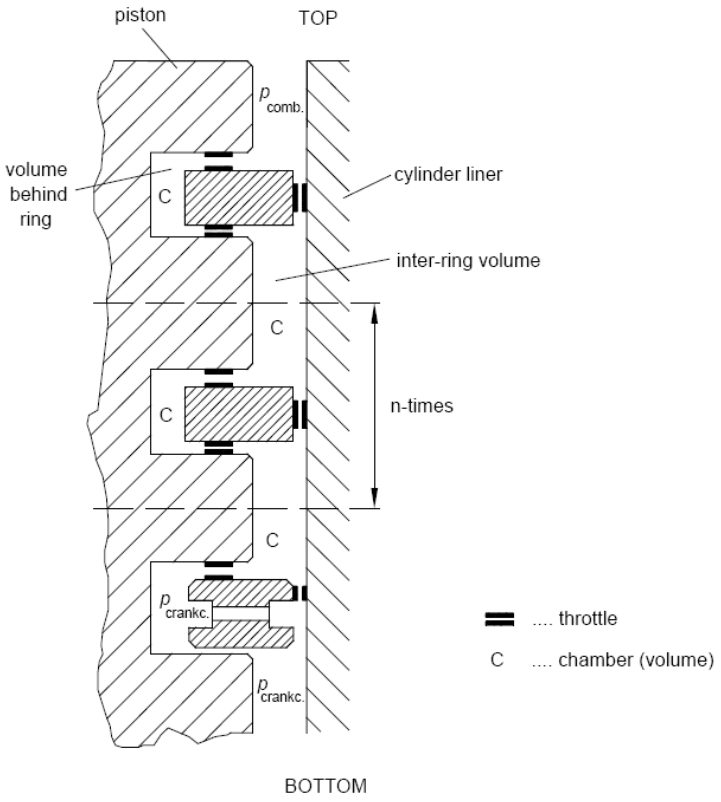

Figure 2.2 : Gas Flow Model for Entire Ring Package (AVL EXCITE PR Theory, 2009a)

Starting upon the known pressure p_{comb} on the piston top land and p_{crankc} below or behind the oil ring, the pressures in the chambers will be determined in a quasi-stationary way by means of a step-by-step calculation of the gas masses flowing through the throttling points.

The basic model used is the flow process from a chamber with the state quantities p_C, T_C, V_C into the surroundings or from a different chamber with the state quantities p_o,

T_o, V_o via a throttle with cross sectional area A and gas flow coefficient ψ. (see Figure 2.3):

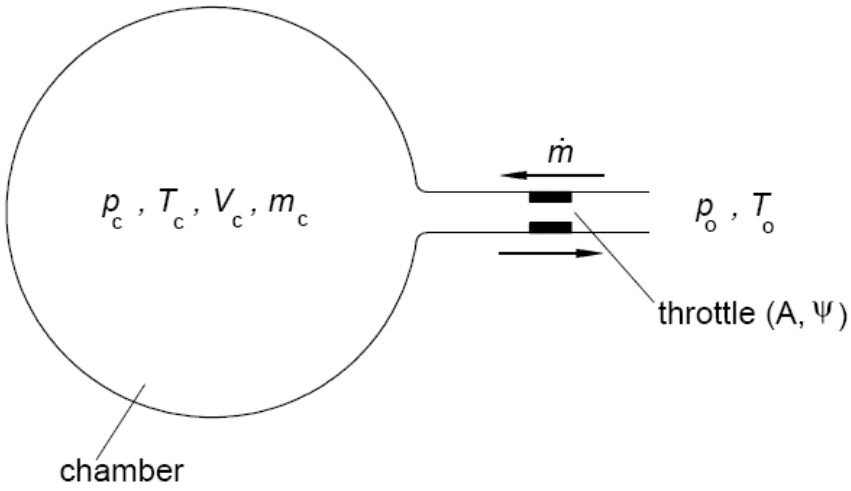

Figure 2.3 : Gas Exchange Process from a Chamber (AVL EXCITE PR Theory, 2009a)

AVL EXCITE PR uses the equations, which are written below for the gas exchange process from a chamber. Two important considerations for the flow process are that isothermal change in the state is assumed and maximum gas velocity is limited by the speed of sound in the throttle.

Mass flow: $$\dot{m} = A \cdot \psi \cdot p_c \cdot \sqrt{\frac{2}{R \cdot T_c}} \cdot \sqrt{\frac{k}{k-1} \cdot \left[\left(\frac{p_0}{p_c} \right)^{\frac{2}{\kappa}} - \left(\frac{p_0}{p_c} \right)^{\frac{k+1}{k}} \right]} \quad \textbf{(3.5)}$$

Rate of change of mass: $$\Delta m = \dot{m} \cdot \Delta t \quad \textbf{(3.6)}$$

Pressure in the chamber: $$p_c = \frac{R \cdot T_c}{V_c} \cdot (m + \Delta m) \quad \textbf{(3.7)}$$

Where the symbols refer to:

R	: Gas constant of combustion gas
k	: Isentropic exponent
Δt	: Time step
ψ	: Gas flow coefficient
A	: Cross sectional area

For the gas flow, the following throttling points are considered:

- Ring running surface (see Figure 2.4) including end gap (see Figure 2.5)

- Ring flanks (top and bottom side) (see Figure 2.4)

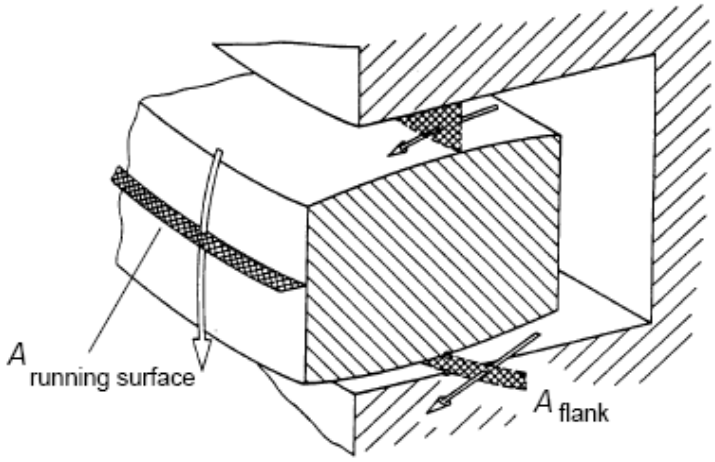

Figure 2.4 : Throttling Points and Discharge Areas at Ring Flanks (AVL EXCITE PR Theory, 2009a)

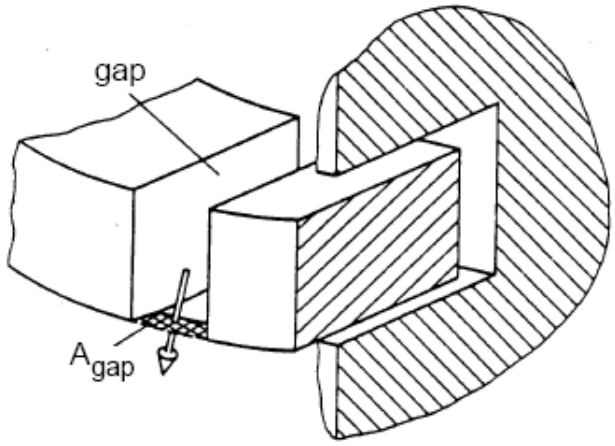

Figure 2.5 : Throttling Point and Discharge Area at End Gap (AVL EXCITE PR Theory, 2009a)

2.2 Lube Oil Consumption Module

The following oil consumption sources are considered in Lube Oil Consumption Module:

1. Evaporation of lube oil from liner wall
2. Oil throw-off of accumulated oil above the top ring due to inertia forces.
3. Oil blow through the end gap of the top ring into the combustion chamber due to a negative pressure gradient
4. Oil scraping at piston top land’s edge

2.2.1 Evaporation from Liner Wall

AVL EXCITE PR simulated the evaporation of lube oil from the cylinder bore wall considering diffusion process in a medium with flow velocity (see Figure 2.6)

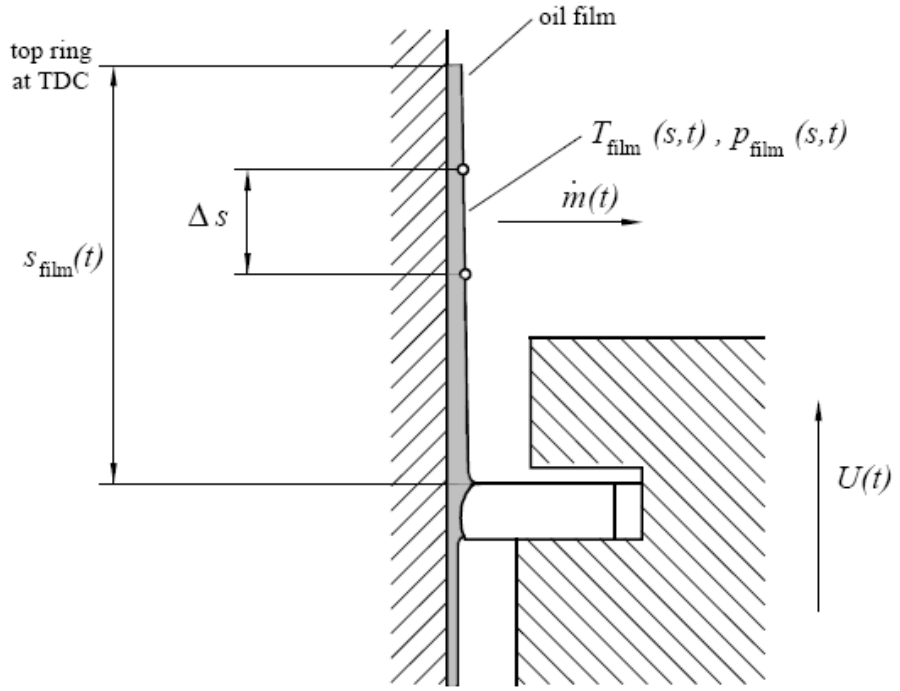

Figure 2.6 : Oil Mass Flux into Combustion Gas (AVL EXCITE PR Theory, 2009a)

The stationary convective material-exchange between lube oil and combustion gas is described by the following equation, which is used by AVL EXCITE PR. In this equation, the program calculates mass flow rate into boundary surface using the mass transfer coefficient and concentration of lube oil. The mass transfer coefficient is obtained by experimental studies.

$$\beta \cdot (c_{film} - c_{\infty}) = \dot{m} = -D \cdot \frac{dc}{dy} \qquad \textbf{(2.8)}$$

Where:

β : Mass transfer coefficient

c_{film} : Concentration of lube oil at film surface

c_{∞} : Concentration of lube oil in combustion chamber

D : Diffusion coefficent

$\dot{m}$: Mass flow rate into boundary surface

y : Coordinate perpendicular to boundary surface

Δs : Movement of the piston during time step Δt

s_{film} : Uncovered area of the oil film

For the calculation of the temperature T_{film} of the oil film surface, an oil vapor layer (100% oil) above the oil film is assumed as shown in Figure 2.7:

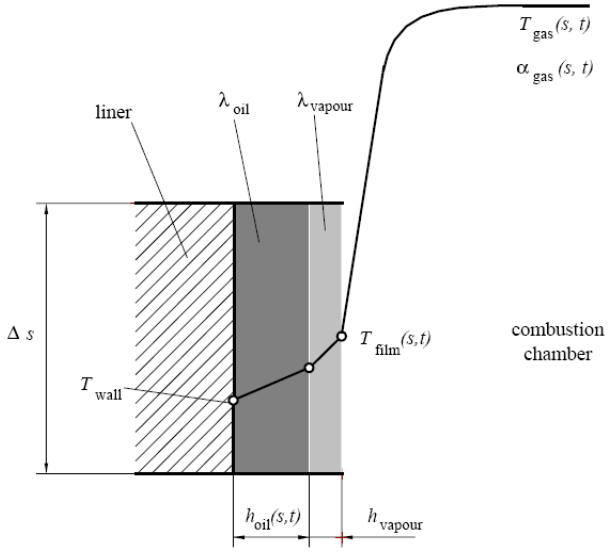

Figure 2.7 : Temperature Distribution from Liner Wall to Combustion Gas (AVL EXCITE PR Theory, 2009a)

The thickness of the oil film h_{oil} is specified by the piston ring dynamics calculation.

2.2.2 Oil Throw-off from Top Compression Ring

The flow rate of oil above the first piston ring and the piston stroke velocity rates are taken into account to calculate the amount off thrown-off oil. For determining the thrown-off oil quantity, the level of latent oil volume left between the piston top land and liner wall is considered as well as the piston acceleration. Oil volume above the first ring may vary depending on the following transport mechanisms.

2.2.2.1 Oil transport mechanisms onto top ring

1. The oil scraping of top ring - Calculated by the difference in left oil film thickness during the upwards and the downwards motion of the top ring

2. Oil flow through the ring gap into the second land (decreasing the accumulated oil) - Due to positive pressure gradient (combustion pressure greater than 1st interring pressure) oil accumulated above the first ring will flow down the gap into the 2nd land. The oil flow due to a negative pressure gradient into the combustion chamber is assumed as instantaneous loss of the oil.
3. Oil flow through the ring groove - The oil flow from the area behind the ring to the area above the ring is caused by the squeezed oil, if the ring moves relative to the piston (axial "pumping" of the ring) and by the flow due to the pressure gradient as shown in Figure 2.8.

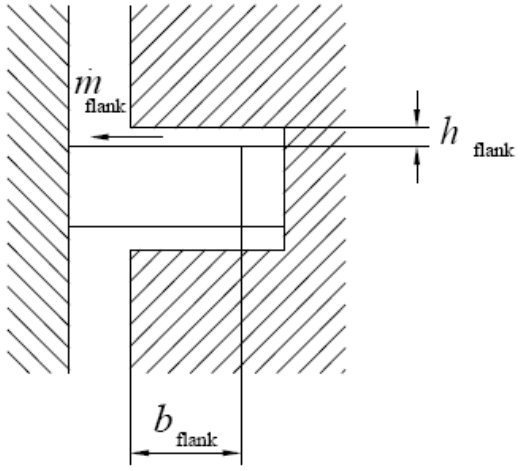

Figure 2.8 : Oil Transport through Ring Groove (AVL EXCITE PR Theory, 2009a)

2.2.2.2 Calculation of thrown-off volume

To observe the behavior of the thrown-off quantity of the accumulated oil between piston top land and liner wall, the process is simulated where the entire film is seperated into individual layers and acceleration between layers assumed constant. According to Newton, shear stresses are incurred at layers. If forces caused by these shear stresses between layers are overcome by the inertial forces acting on the piston ring, oil is squeezed through the gaps to the combustion chamber and extinguished as shown in Figure 2.9.

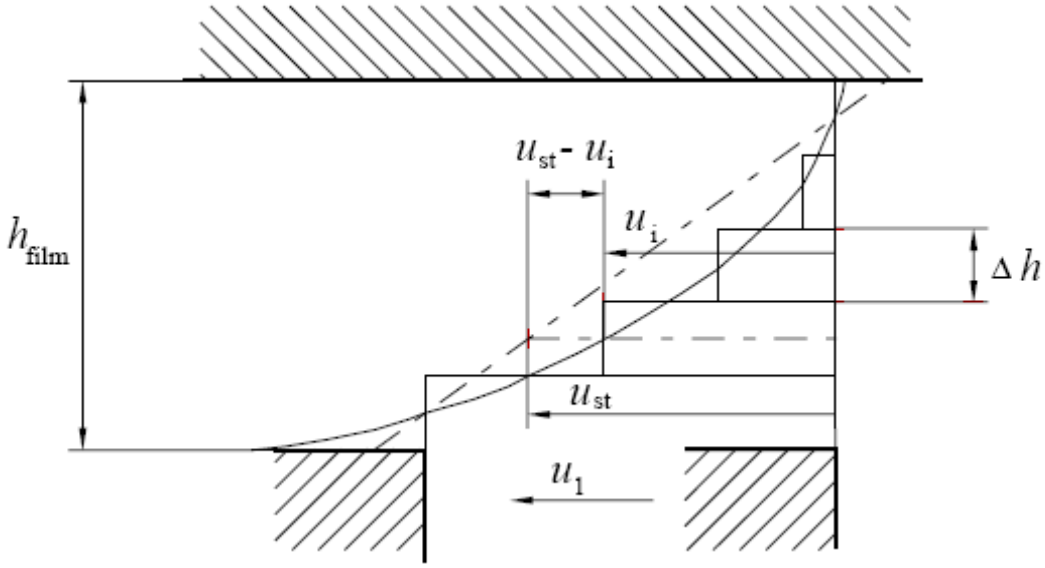

Figure 2.9 : Velocity Distribution in Discrete Layers of Oil Film (AVL EXCITE PR Theory, 2009a)

Finally, the thrown-off oil volume can be calculated by AVL EXCITE PR as follows:

$$V_{throw-off} = (u_m - u_{st,m}) \cdot h_{film} \cdot d_{film} \cdot \pi \cdot \Delta t \quad \textbf{(2.9)}$$

In this equation, program calculates thrown-off oil volume using the stationary velocity and geometric properties of the oil film.

Where the symbols refer to:

$$u_m = \frac{\sum u_i}{i} \quad \textbf{(2.10)}$$

$$u_{st,m} = \frac{a_0 \cdot \Delta t}{2} \quad \textbf{(2.11)}$$

a_0 : Acceleration at the beginning of motion

h_{film} : Height of oil film between top land and liner

d_{film} : Diameter of oil film

2.2.3 Oil Blow Through Top Ring End Gap

The pressure gradient over the top ring determines the direction of oil flow. Using this gradient oil run through the end gap into the combustion chamber is computed by AVL EXCITE PR. Negative pressure gradient over the top ring indicates that combustion pressure is less than the pressure at 2nd land which causes oil to run

through the end gap. This effect causes an instantaneous oil loss irrelevant to inertial forces.

2.2.4 Top Land Scraping

The piston's lateral movement and tilting motion together with geometric conditions are the main parameters, which are considered by AVL EXCITE PR in order to calculate the scraped amount of oil.

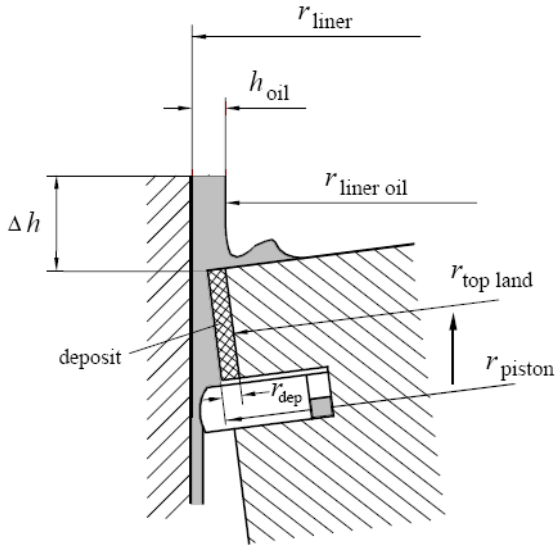

Figure 2.10 : Top Land Scraping Geometric Considerations (AVL EXCITE PR Theory, 2009a)

3. METHODOLOGY

3.1 Piston Stiffness Calculation

In order to predict oil consumption, the input parameters should be entered as realistic as possible. While piston moves inside the liner, a radial elasticity is considered along the piston height as well as along the angular positions. The elasticity is considered by means of a stiffness matrix, enabling contact forces between piston and liner to be calculated for deformations arising during piston movement.

The stiffness matrix was generated by the pre-processing in the Piston Movement Module. As input for the pre-processing, the deformations in the piston cross sections versus increasing load are required. These deformations can be determined either by calculation (Finite Element Analysis) or by direct measurement.

3.1.1 Piston Deformation Measurement

In case of direct measurement for determining piston deformation, a test rig has been established by AVL EXCITE, which is showed in Figure 3.1. Depending on the load, the contact area between the piston and the liner is changed due to the changing piston and liner deformations. Generally, the angle of contact between piston and liner in circumferential direction increases with increasing load. This case causes the usual digressive rigidity of pistons against load.

Therefore, the geometry and the stiffness of the support in the test rig and the piston contour affect the measured deformations.

The radial deformations on the piston surfaces against piston load have to be measured for the AVL EXCITE PR.

Time consuming by measuring all areas in the piston can be reduced by the fact that practically no deformations occur near the skirt with loads in the area of the piston lands and, vice versa, loads applied at the skirt’s cross sections the area at the ring lands will not be deformed. (see Figure 3.1)

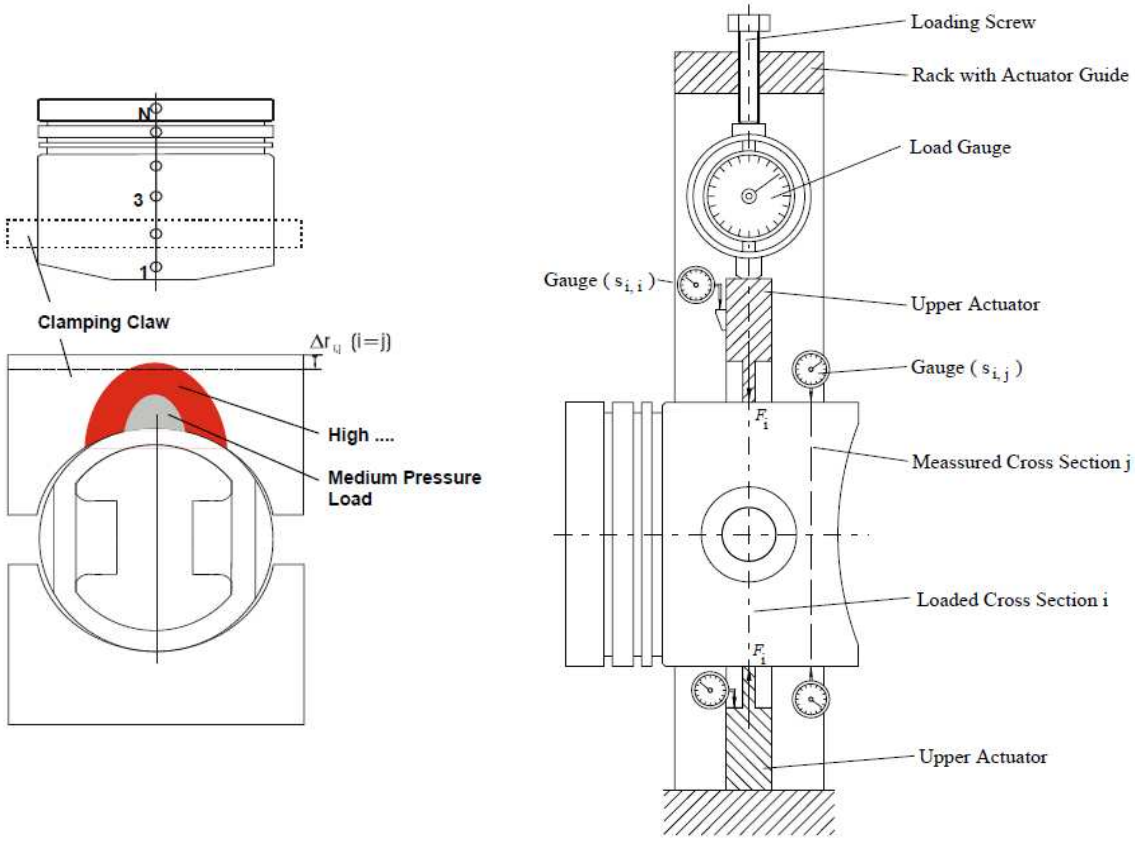

Figure 3.1 : Piston Stiffness Measurement Test Rig (AVL EXCITE PR Theory, 2009a)

3.1.2 The FEM Representation of Test Rig

The test rig is not suitable for this project because it is expensive and time-consuming method for one time. So, the FEM model is needed for calculating piston deformations.

In order to calculate correct stiffness results rapidly, the FEM model of the piston stiffness measurement test rig was established in ABAQUS linear static analysis.

There are 2 steps for it.

1- The FEM model which is for correlating the Test Rig.

2- Simplified second FEM model in order to obtain results, rapidly,

In step 1, a FEM model which includes a rigid clamping claw model and piston model. For the mesh models, 3-D second order tetrahedral elements are used. Between claw and piston, contact elements are used in order to obtain exact pressure area. (see Figure 3.2)

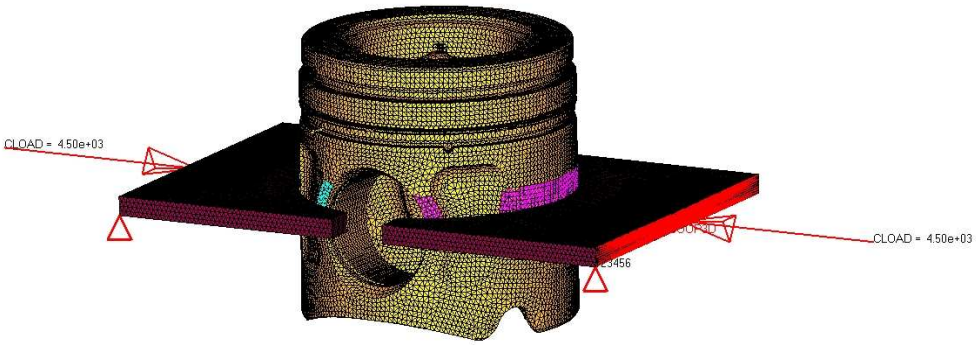

a) Isometric view

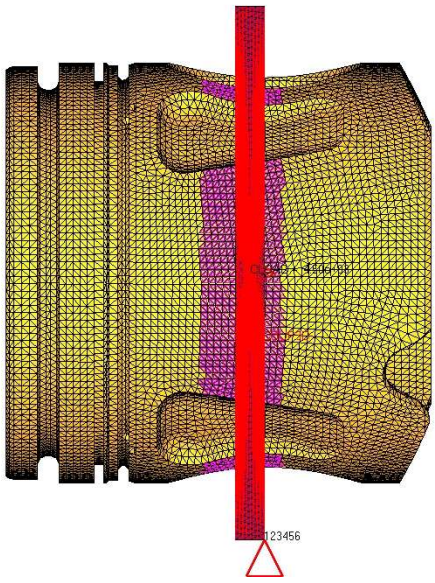

b) Side view

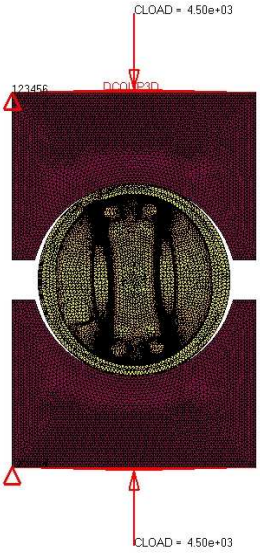

c) Bottom view

Figure 3.2 : FEM Model of the Test Rig

Boundary conditions are the forces, which are distributed along the top sides of claw. This FEM model has to be re-established for all points on the piston. Therefore, it means that the neccesity of much time for the total analysis.

In step 2, Because of necessity much time for the calculating stiffness in step 1, a simplified FEM model has to be done. (see Figure 3.3) The important points for the simplification are the boundary conditions. Thus, pin bearing locations are constrained in X, Y, Z directions. Besides, top area of the piston crown is constrained in Z direction. In addition, the force is applied the contact area as shown in the Figure 3.3

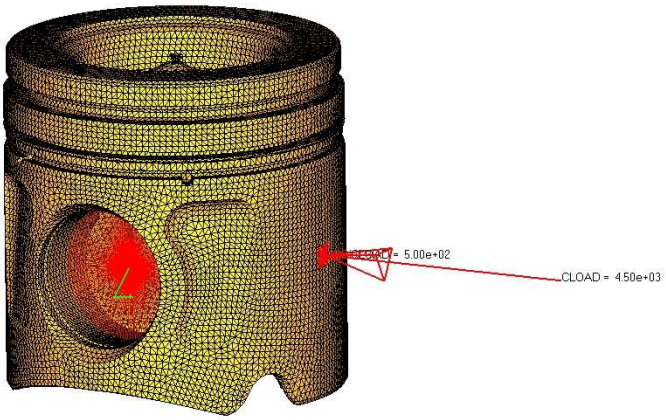

Figure 3.3 : Simplified FEM Model

In the FEM model, second order tetrahedral elements are used for the psiton. In addition, rigid body elements are used for the constrained nodes. (see Figure 3.3)

The compared results are shown in Figure 3.4 and Figure 3.5. In Figure 3.4, the stress results are shown. The distribution of stress area is similar to each other.

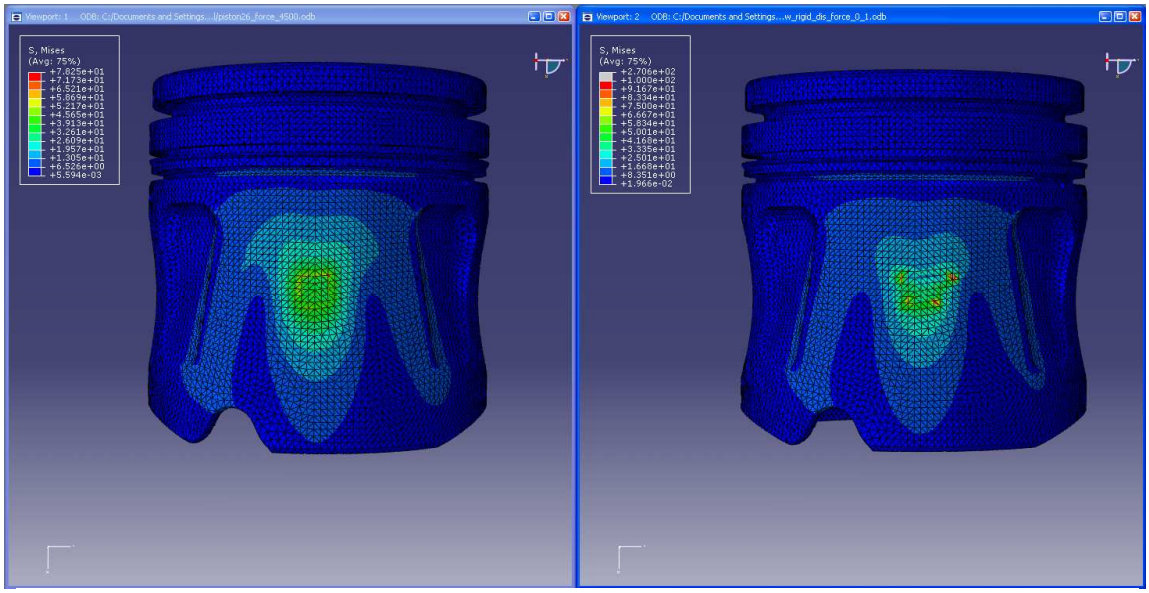

a) Simplified FEM Model b) Fem Model of Test Rig

Figure 3.4 : Stress Results

In Figure 3.5, the deformations of the nodes are compared as shown. Moreover, the values of the displacements in the center area are very close the each other

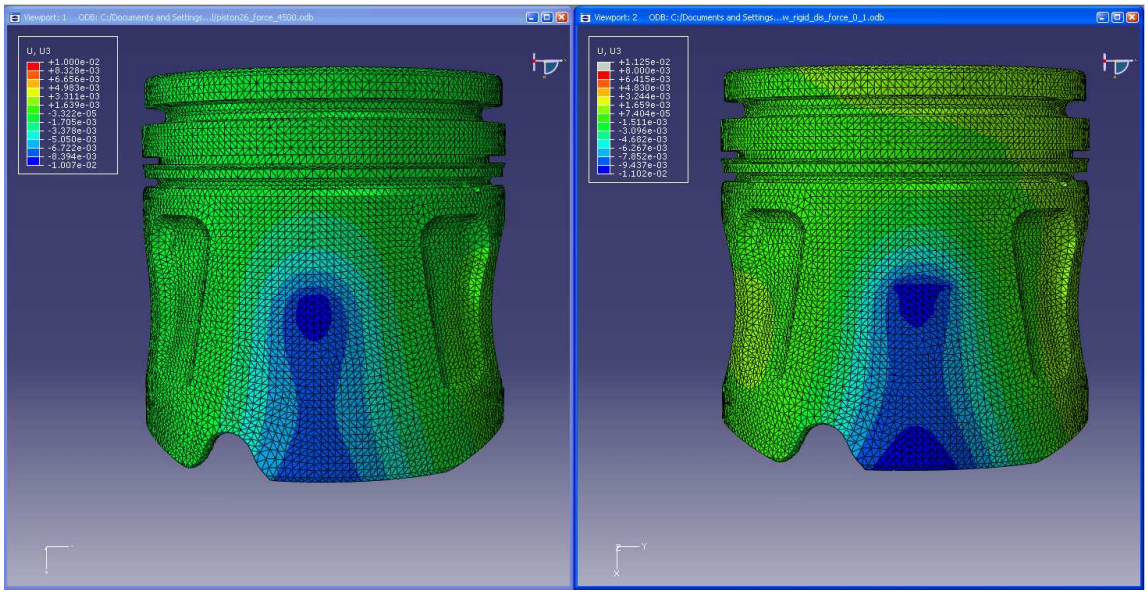

a) Simplified FEM Model b) FEM Model of Test Rig

Figure 3.5 : Displacements Results

3.1.3 Piston Stiffness Calculation

The piston stiffness matrix was calculated in a preprocessing part of EXCITE Piston & Rings - Module Piston Movement. The nonlinear stiffness behavior is approximated by a third order polynomial function. (AVL EXCITE PR Theory, 2009a)

$$F_i = \sum_j A_{ij} \cdot s_{i,j}^3 + \sum_j B_{ij} \cdot s_{i,j} \qquad \textbf{(4.1)}$$

Forces F_i in measuring points i depend on the elastic deformations $s_{i,j}$ at all points j = 1...n defined along the piston surface. The coefficients A_{ij} and B_{ij} of the stiffness matrices are determined by a set of deformations in all points due to the different loads at each point. (see Figure 3.6a)

So, the FEM analysis is established similar to Figure 3.6a whose details are explained in section 3.1.2, is shown in Figure 3.6b.

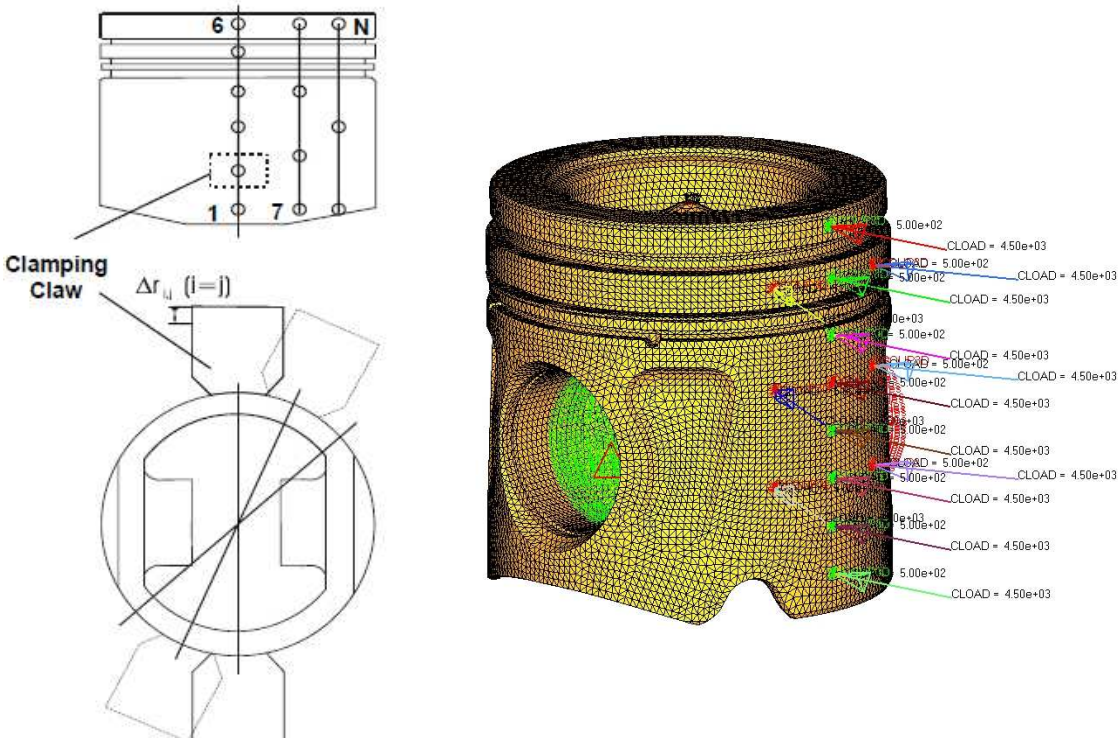

a) Measured Points b) FEM Analysis Model

Figure 3.6 : Piston Stiffness Analysis

2 different loads were applied to the points which are the measured deformation at the same time. These are 500 N and 4500 N. The effect of clamping is simulated by constraining the pin locations and top crown of the piston.

The results are written as a text file format which EXCITE Piston & Rings - Module Piston Movement can read it.

3.2 Cylinder Bore Distortion Analysis

This section describes a finite element analysis method, which was used to predict cylinder block bore distortion. The model includes cylinder head, valve seat inserts, head gasket, cylinder block, and head bolts. In addition, cam carrier, cam carrier bolts, injectors and injector clamps are also added to model in order to obtain good results. (see Figure 3.7) Soft springs are used as an aid for convergence. The analysis simulates assembly of these components and takes care of interactions among them. Bore distortion is post-processed based on displacement results from the analysis. Cylinder bore distortion results consist of roundness, cylindricity, and Fourier coefficients calculated at different depth of cylinder bores. These results are used to solve problems related to piston slap, oil consumption and piston blow-by.

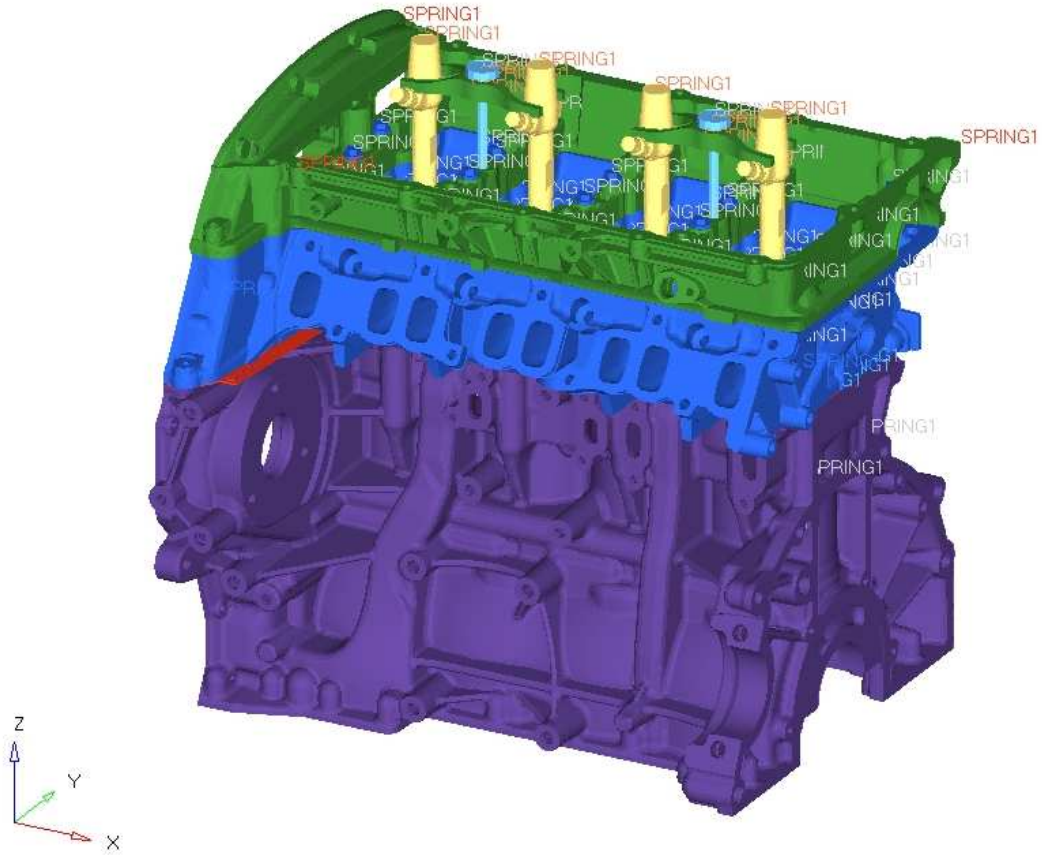

Figure 3.7 : FEM Model of Bore Distortion Analysis in Shaded View

3.2.1 FEM Models of the Analysis

Software, which is called Hypermesh, was used for pre-processing section. Cylinder Block, Cylinder Head, Cam Carrier, Injectors, Clamps and valve seats were modeled with second order tetrahedral elements. (see Figure 3.8) In addition, bolts were modeled with hexahedral elements. Gasket was also modeled with ABAQUS GK3D8 and GK3D6 gasket elements, which means also hexahedral and pentahedral elements in order to include thermal loading. The gasket model includes one layer of gasket elements with different initial contact gaps defined at areas with different initial thickness. Figure 3.9 shows the gasket model with different embossment areas represented by different colors.

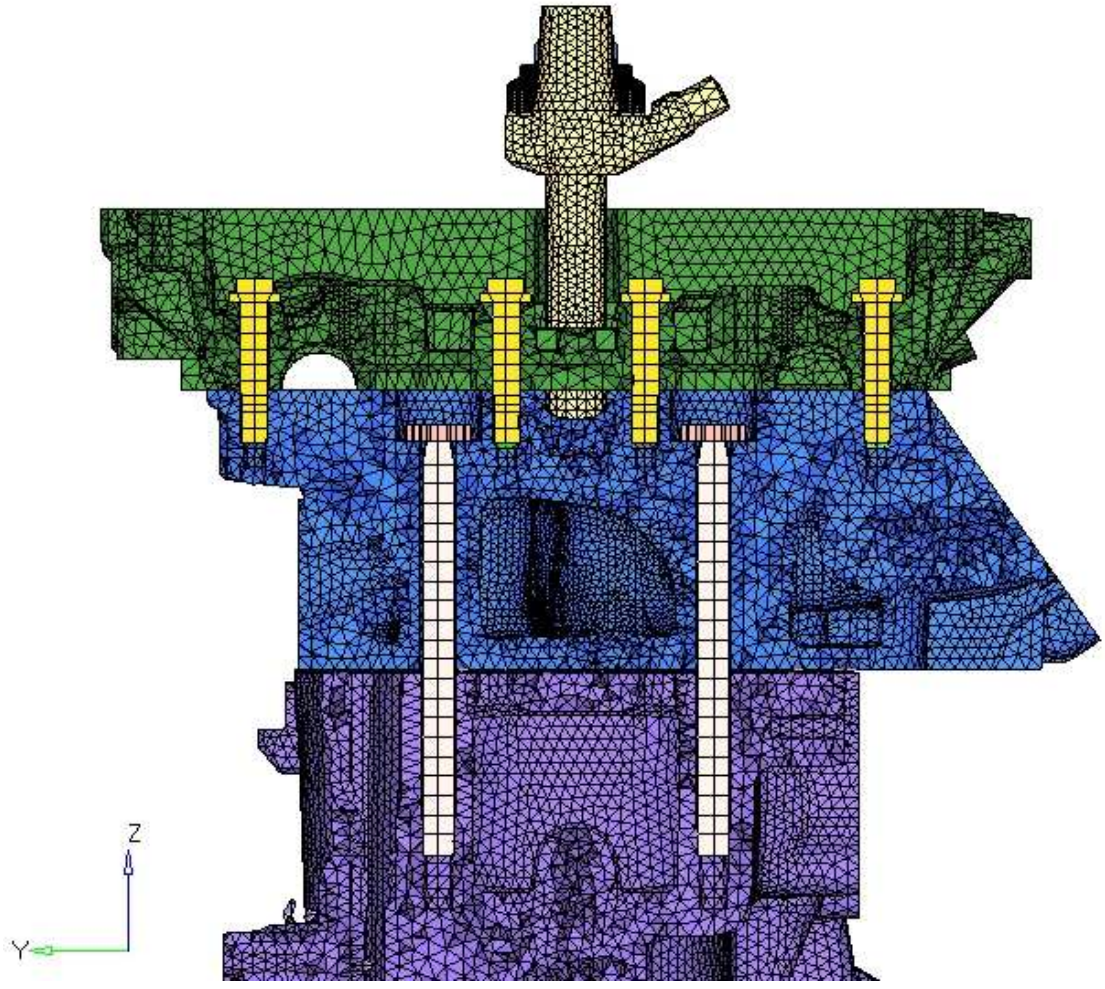

Figure 3.8 : Element Types Used in FEM Model

Since this analysis includes nonlinear contact simulation between head gasket, head, and block. (see Figure 3.10) Moreover, between bolts and holes, contact elements were also used in order to supply the pre-tension loads, it cost much more CPU time than ordinary linear elastic analysis. Contact interference conditions are shown in Table 3.1.

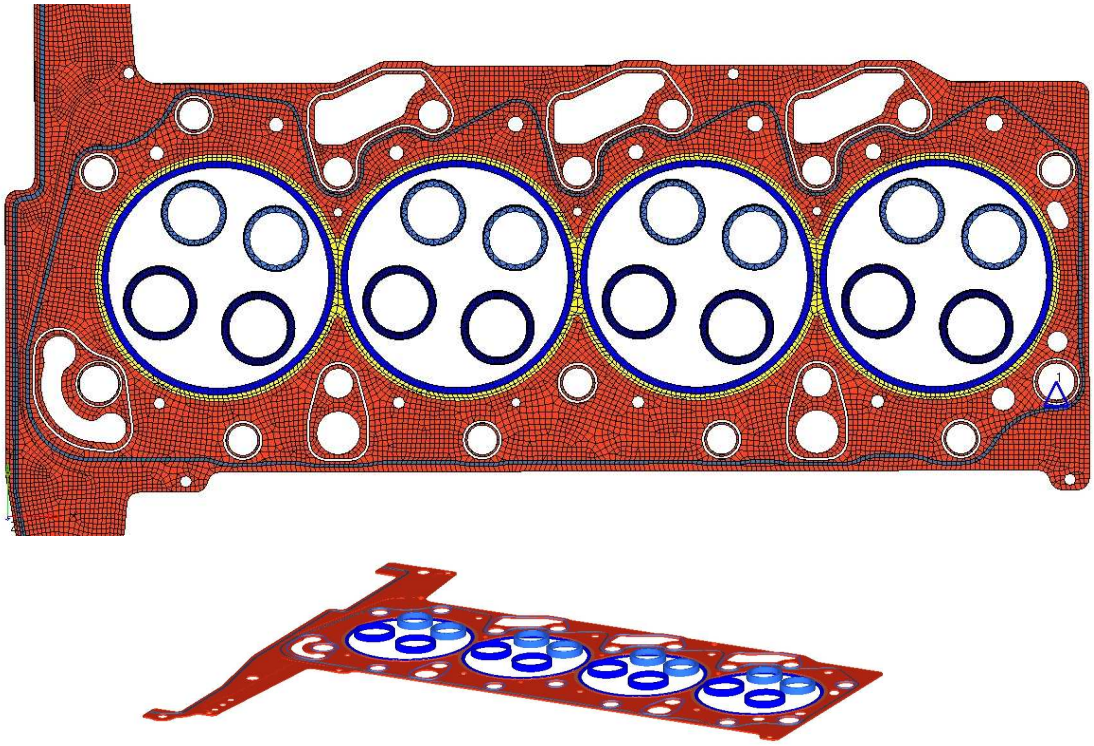

Figure 3.9 : Gasket and Valve Seats FEM Model in Shaded View

It can be said for contact mechanism, when two solid bodies touch, force is transmitted across their common surface. In some cases, only forces normal to the contact surfaces are transmitted. If friction is present, a limited amount of force tangential to the contact surfaces also can be transmitted. Frictional force results in shear stress along the contact surfaces.

General objective of contacts is to determine contacting areas and transmitted stress.

Contact has a severely discontinuous form of nonlinearity. Either a constraint must be applied (that the surfaces cannot interpenetrate) or the constraint is ignored.

Table 3.1: Contact Interface Conditions Between Each Components

Block-Gasket	Head-Gasket	V Seat-Head (Side)	V Seat-Head (Bottom)	Bolt Top-Component	Bolt-Block Thread Area
No Separa-tion	No Separa-tion	Tied	Tied	Tied	Tied

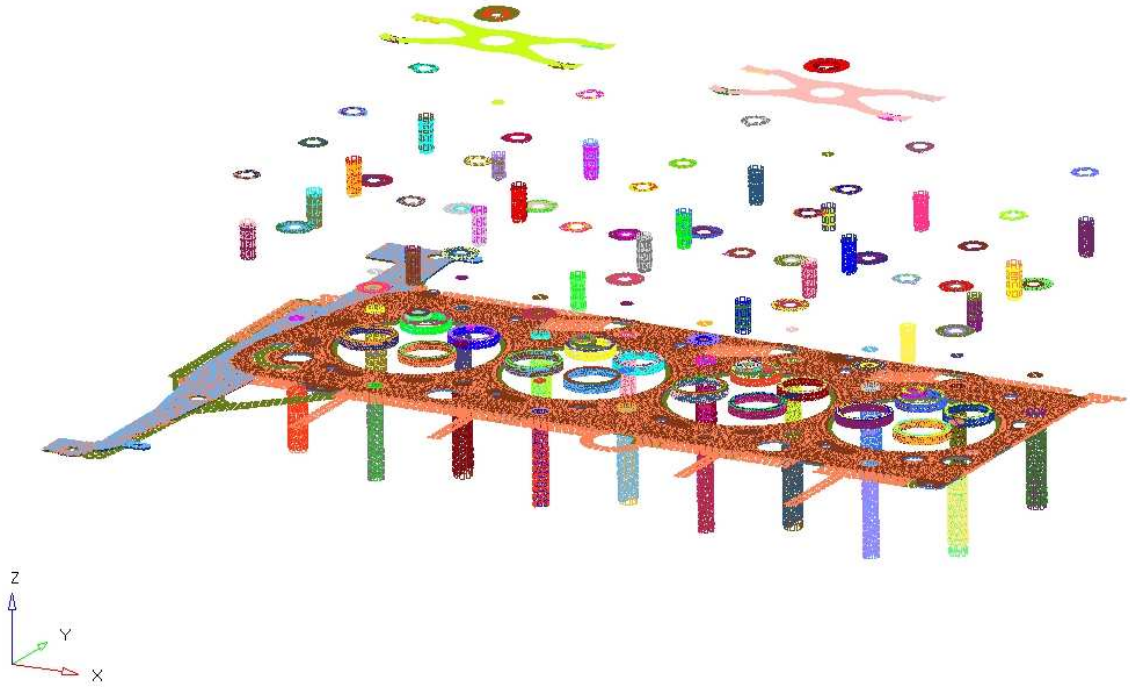

Figure 3.10 : Contact Elements Used in FEM Model

3.2.2 Material Properties

The properties listed below were used for the analysis.

- Linear elastic material properties for each component
- Elastic-plastic curve for head bolt.
- Gasket bead pressure-closure curves under loading from test data. (see Figure 3.11)

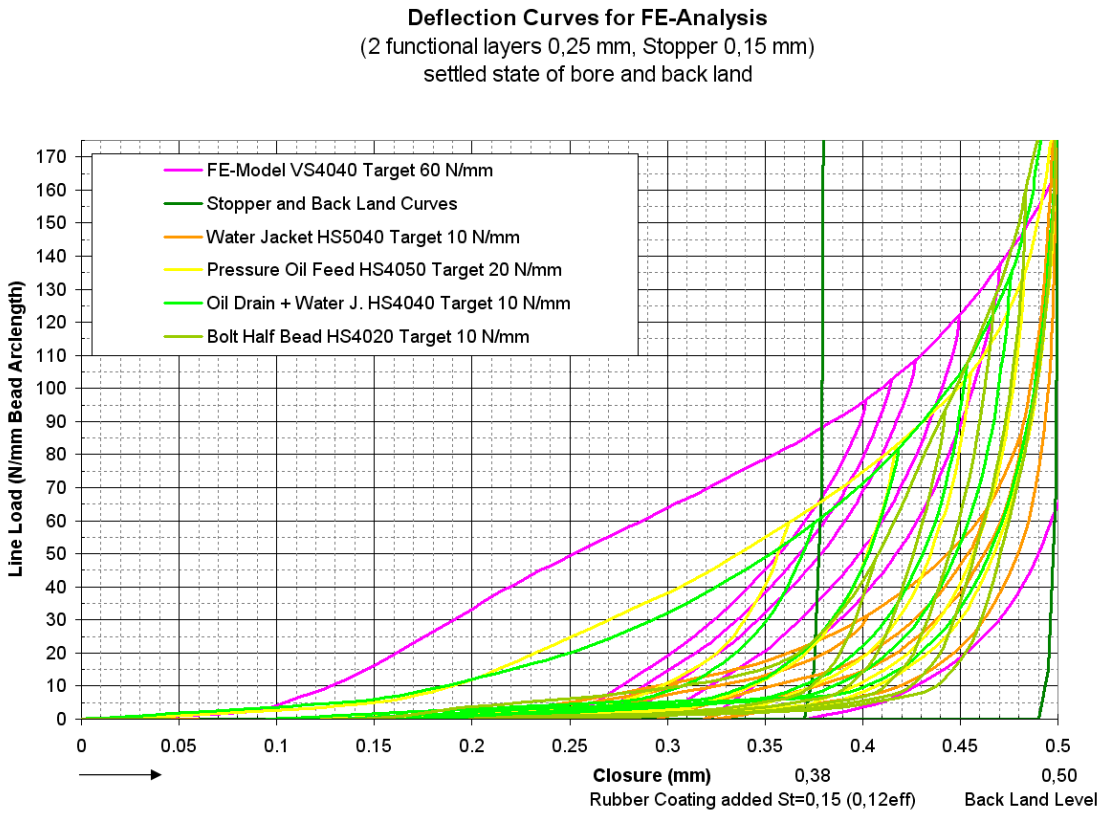

Figure 3.11 : Gasket Bead Pressure-Closure Curve

3.2.3 Boundary Conditions

Boundary conditions of the analysis can be shown as listed in the Figure 3.12.

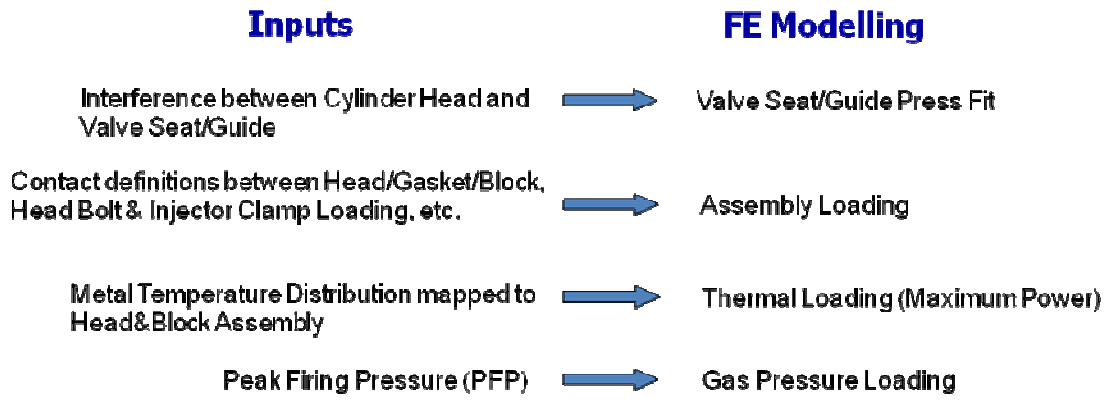

Figure 3.12 : Load Types Used in Analysis

Bolt and clamp loads were applied by using ABAQUS pretension commands. A surface located at bolt shank area was defined as pretension surface. For each pretension surface, a reference node without geometry definition needs to be

associated. Clamp load was applied on this reference node. Detailed assembly loads input are given in Appendix A.1.

Thermal loading was mapped to geometry as a displacement. Heat flux and temperature results from Computational Fluid Dynamics program whose name is STAR-CCM were taken as inputs, which are shown in Figure 3.13. Thermal analysis was done in ABAQUS whose results are shown in Figure 3.14 for cylinder bores.

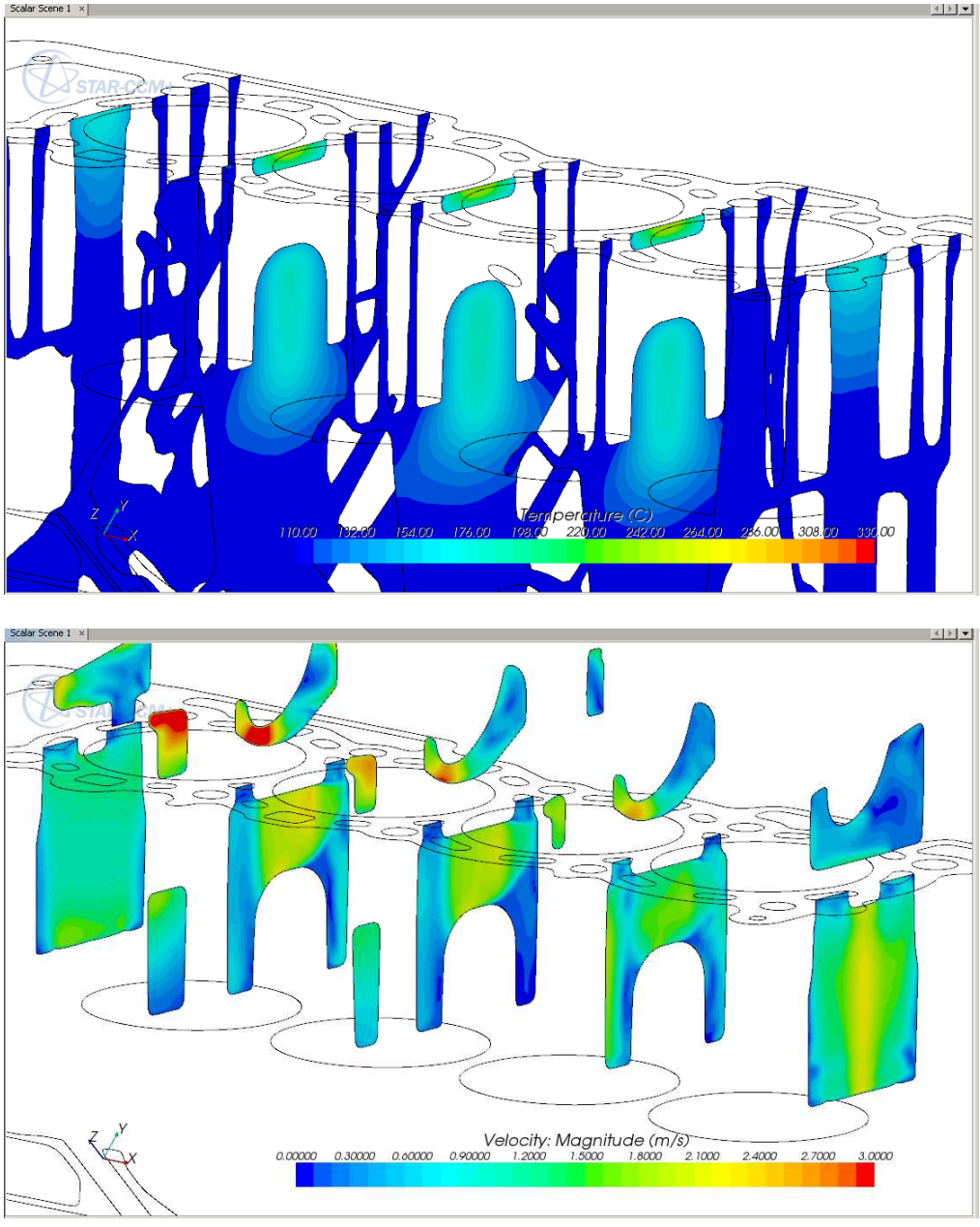

Figure 3.13 : CFD Results (Temperature and Flow Velocity) [°C and m/s]

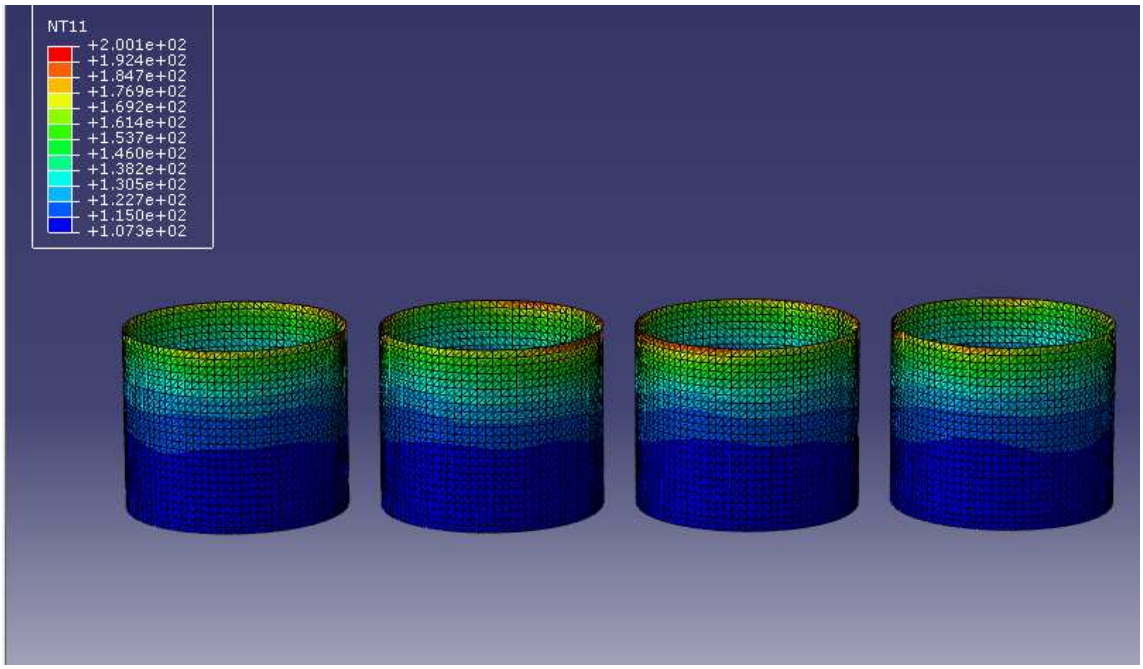

Figure 3.14 : Thermal Loading for Cylinder Bores [°C]

Constrained areas are the bottom side of the cylinder block in X, Y, Z directions. Other rigid body motions were removed. Soft springs were used as an aid for convergence. The triangles shown in the Figure 3.15, which are the constrained nodes

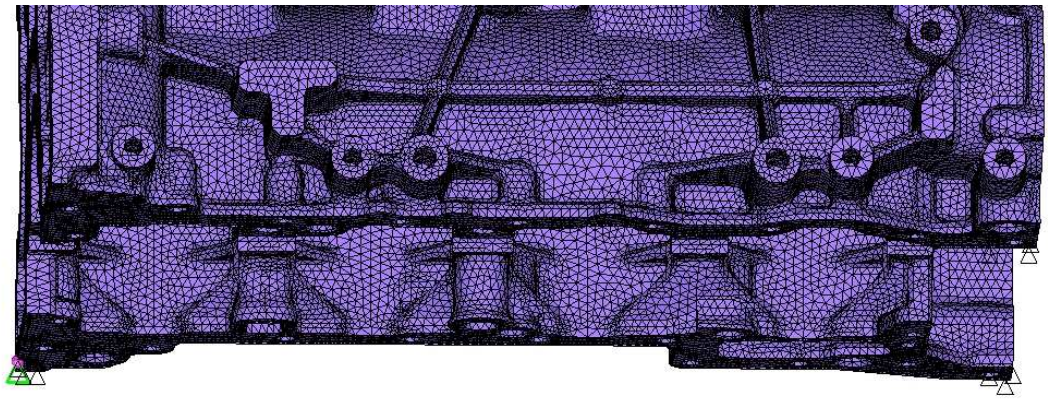

Figure 3.15 : Constrained Nodes in Bottom Side of Cylinder Block

3.2.4 Results of Bore Distortion Analysis

Bore Distortion analysis is non-linear static analysis solved in ABAQUS. The displacement results are shown for the cylinder block in Figure 3.16 and 3.17.

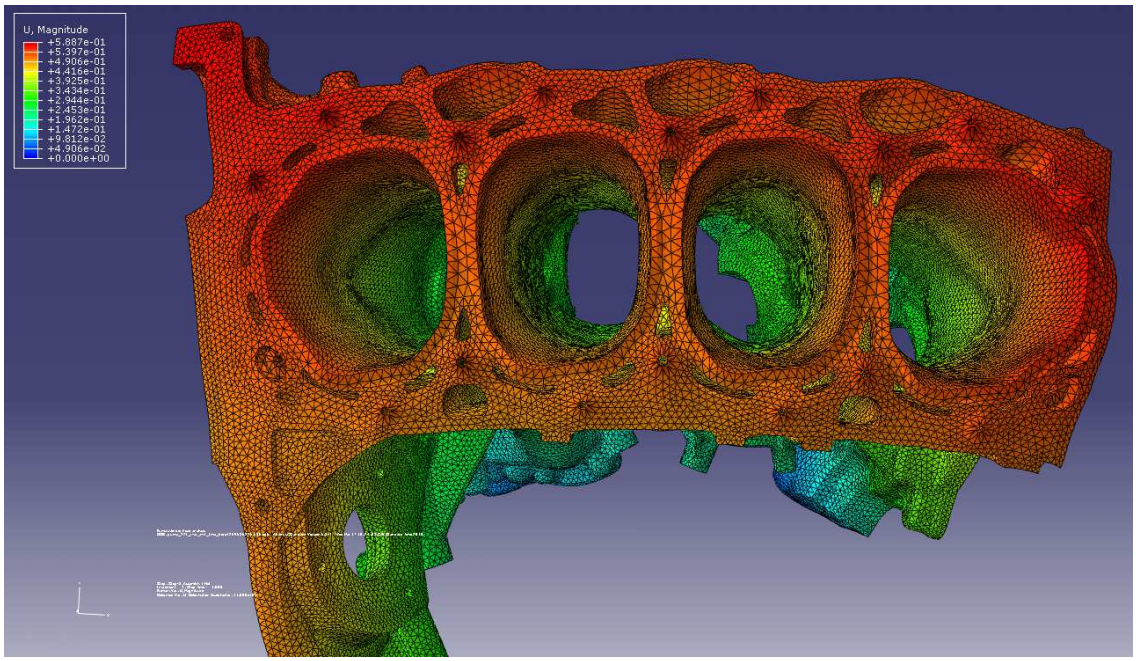

Figure 3.16 : Displacement Results Top View of the Block (scaled 1000 times) [mm]

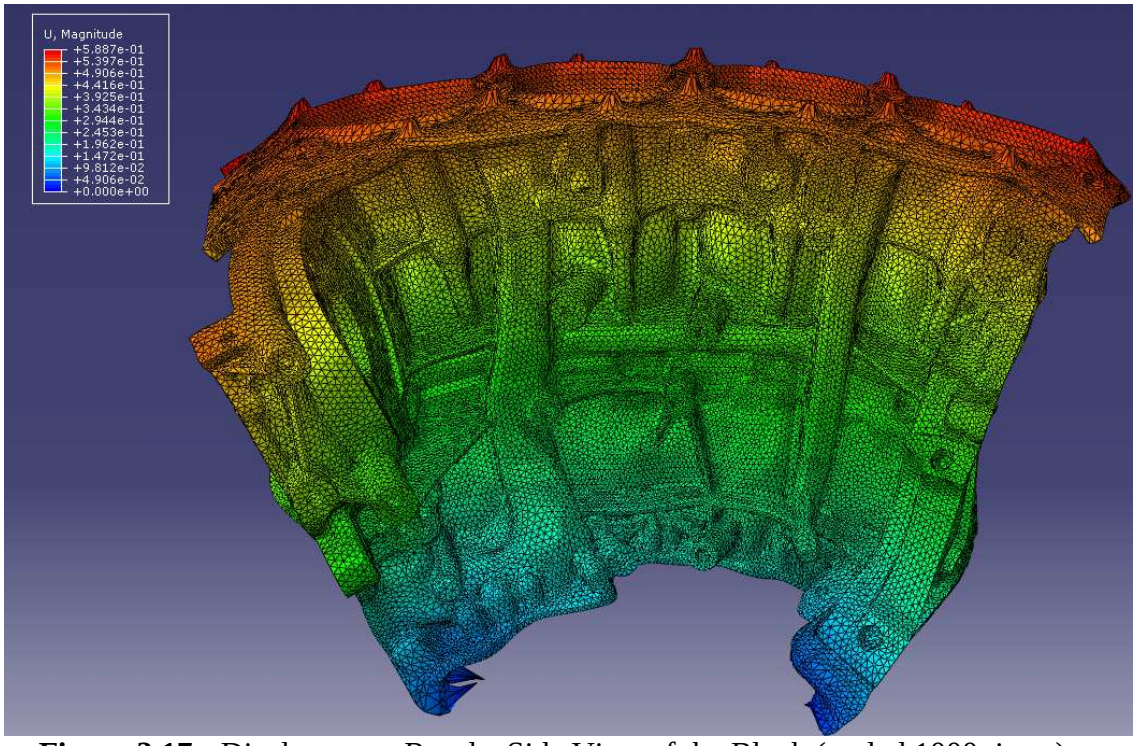

Figure 3.17 : Displacement Results Side View of the Block (scaled 1000 times) [mm]

The deformations around the bolts between head and block are obviously shown. Moreover, thermal results, which are shown in Figure 3.14 shows the temperatures, increase from bottom to top of the cylinder. Thus, the deformations are effected from thermal behavior of the cylinder block. Besides, assembly loads due to pre-tension loads of the bolt clamps also effect the increased deformations at top of the block.

The fourth cylinder was selected for the oil consumption analysis in order to investigate the effect of bore distortions on lube oil consumption and blow-by.

Figure 3.18 shows the details of this cylinder.

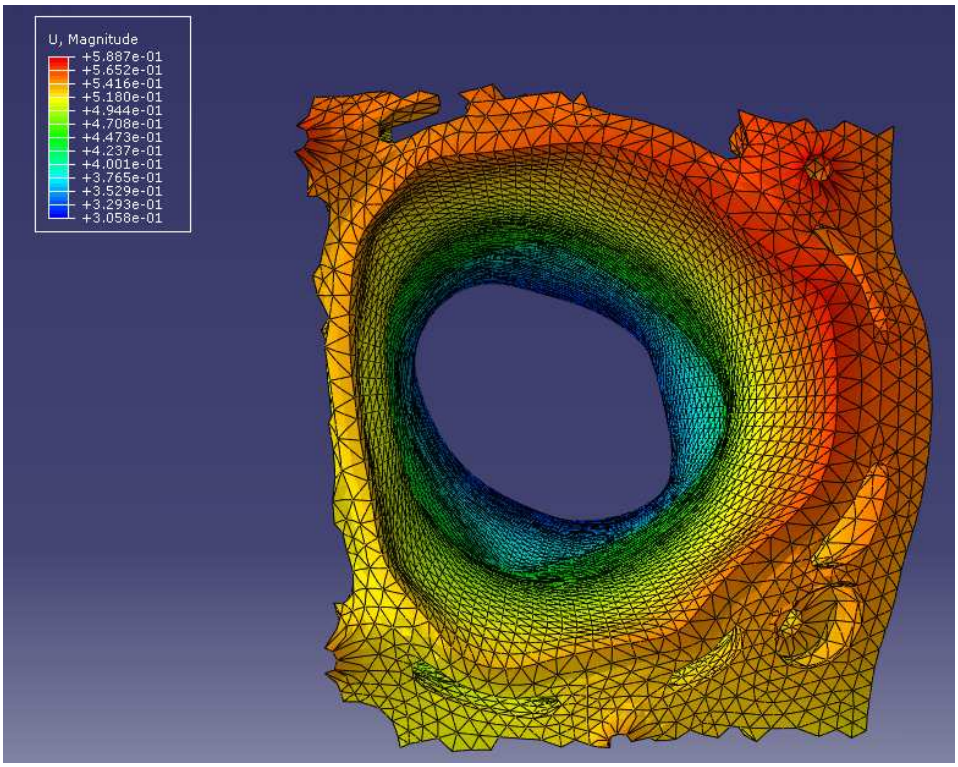

a) Top View of the Cylinder

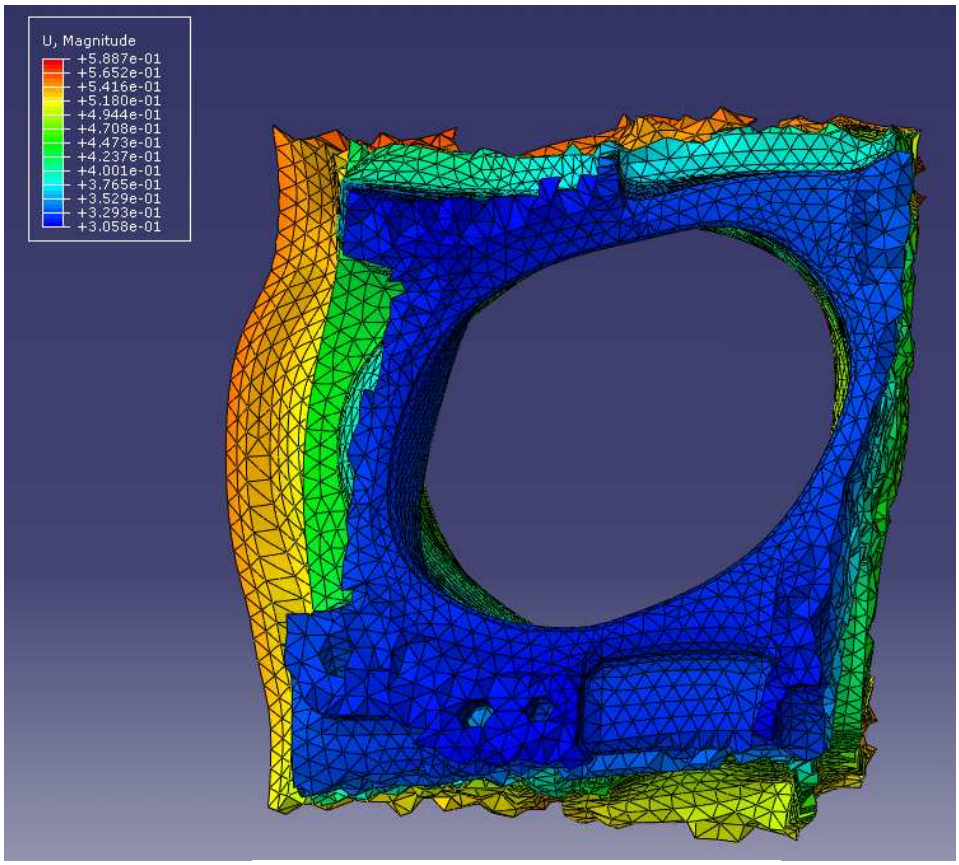

b) Bottom View of the Cylinder

Figure 3.18 : Displacement Results for the Selected Cylinder (scaled 1000 times) [mm]

3.2.5 Post-Processing of the Bore Distortion Analysis

The post-processing of the bore distortion analysis is designed to estimate the deformation of a cylindrical surface of a cylinder bore under certain loading and boundary conditions with respect to a best-fit reference cylinder. Out-of roundness and Fourier coefficients are used for the post-processing, which is mentioned in the section 1.2.2.

The deformation results of the nodes on the bore profile were written in an ABAQUS *.dat file which was used as an input for the code written in MATLAB in order to obtain distorted profile in cylindrical coordinates and Fourier coefficients of orders. The details of the code are given in Appendix A.2.

Bore distortion analysis was repeated in order to obtain both hot and cold assembly conditions. The distorted profile shapes are shown in Figure 3.19 and 3.20

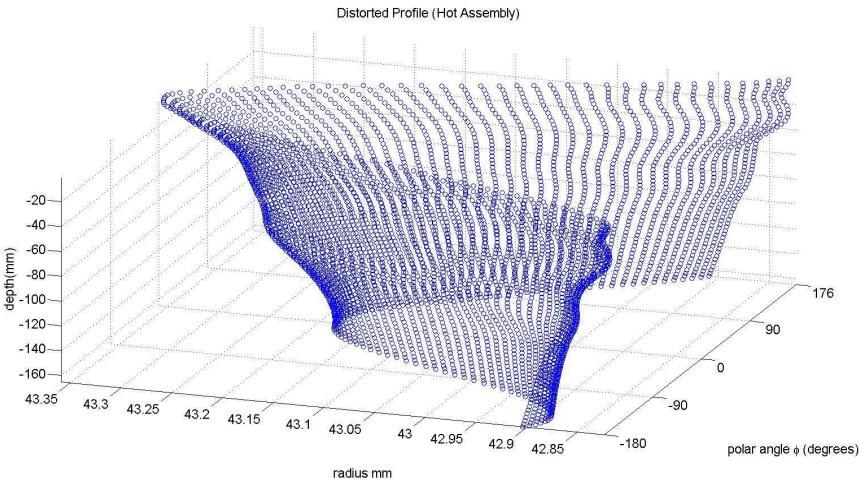

a) Hot Assembly Condition

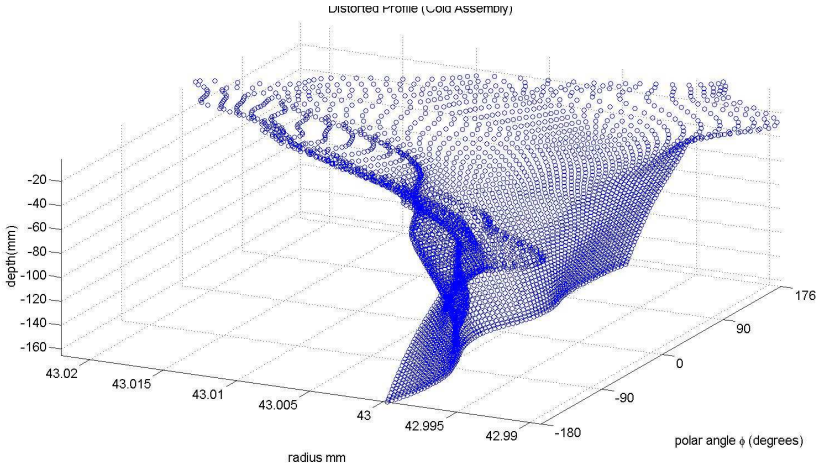

b) Cold Assembly Condition

Figure 3.19 : Distorted Bore Profile

The nominal radius is 43 mm of the cylinder. In hot assembly conditions, the effect of thermal loads is shown more at top of cylinder than the bottom sides. In addition, pre-tension loads are more effective at the top side.

Besides, the effect of pre-tension loads shows its effect much in cold assembly conditions between top and bottom side of the cylinder.

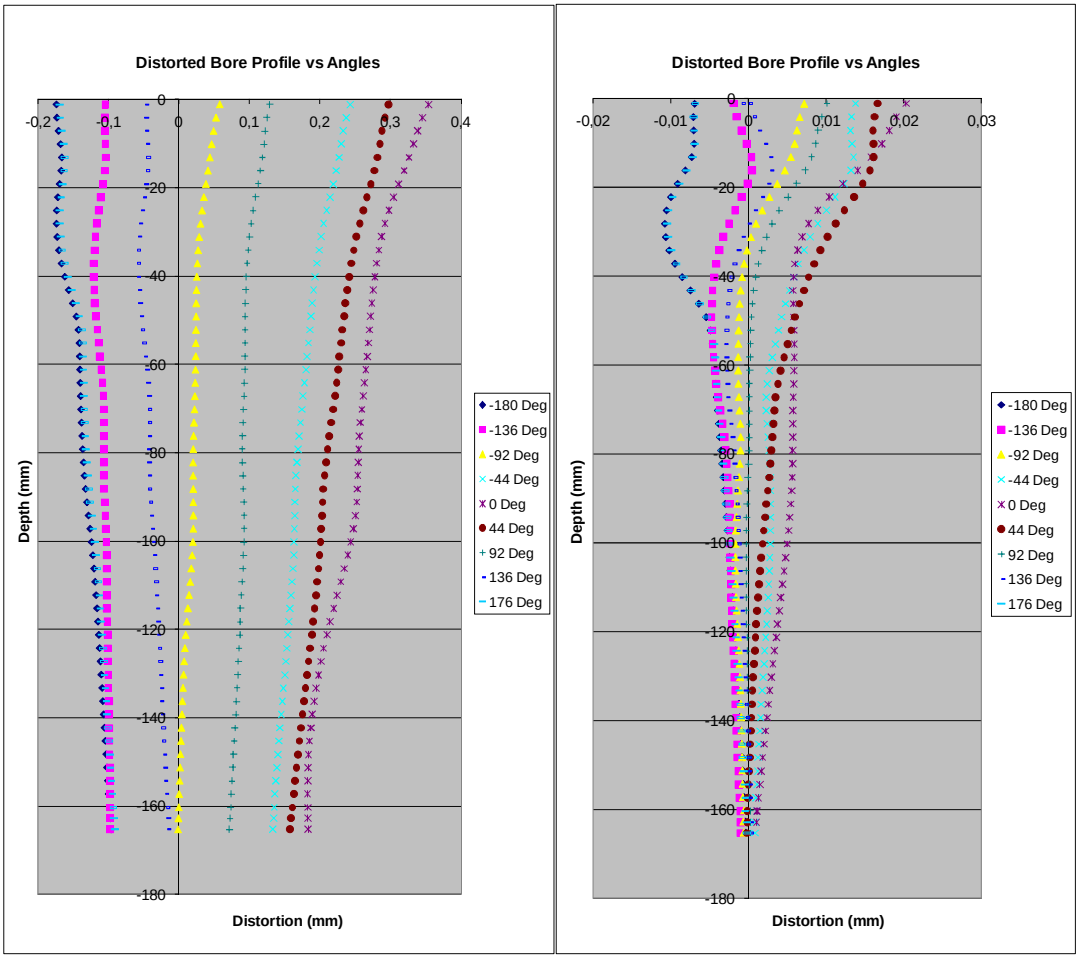

b) Hot Assembly Condition b) Cold Assembly Conditon

Figure 3.20 : Distortions vs Polar Angles

Maximum distortions are 350 microns for the hot assembly condition and 20 microns for the cold assembly condition. Somewhere, distortions are negative because of other the distortion of the other cylinders which is called an eccentricity of the center. Especially, because of the investigating the fourth cylinder of block, this case is important for the distortion.

The Fourier coefficients were calculated with the equation below. Letting $\xi(\phi)$ denote the measured bore shape (where ϕ is the polar angle), $\xi(\phi)$ is approximated by

$$\xi(\phi) \approx r_0 + \sum_{k=1}^{N} A_k \cos(k(\phi + \delta_k)) \qquad \textbf{(3.2)}$$

where *k* is the *order* and δ_k is *phase angle*. (Bardizmashvilli et. al., 2004). The magnitudes of the orders are shown in Figure 3.21 and 3.22 for each condition.

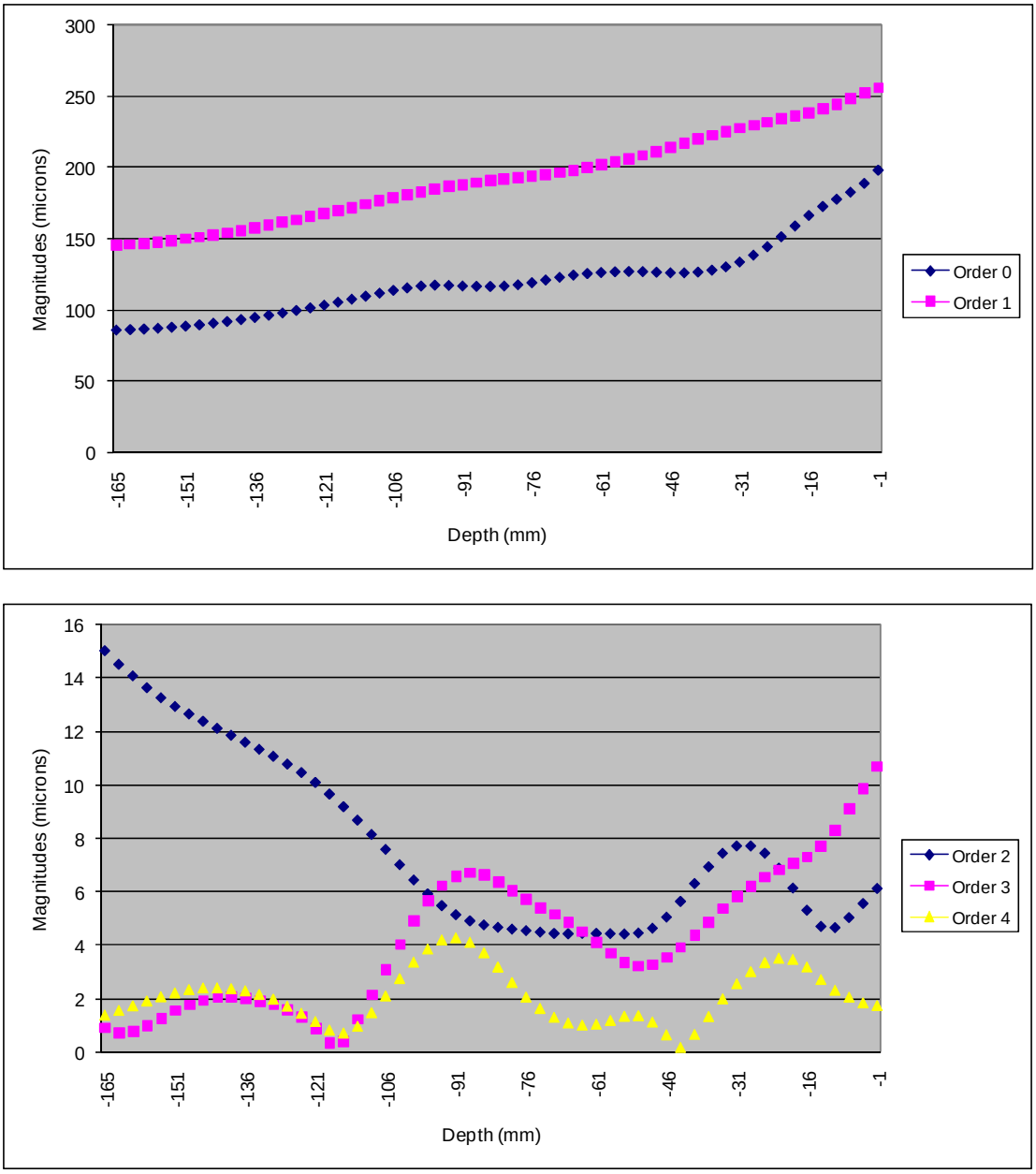

Figure 3.21 : Magnitudes of Orders for Hot Assembly Conditions

From the graphics, it is obviously seen that order 0 and order 1 are the dominant orders as it was predicted. Besides, amongst the other orders at the topside, order 3 is dominant. On the other hand, at the bottom side order 2 is dominant. Because of the selecting fourth cylinder, order 1, which is thought an eccentricity of the center, is the most dominant order amongst them.

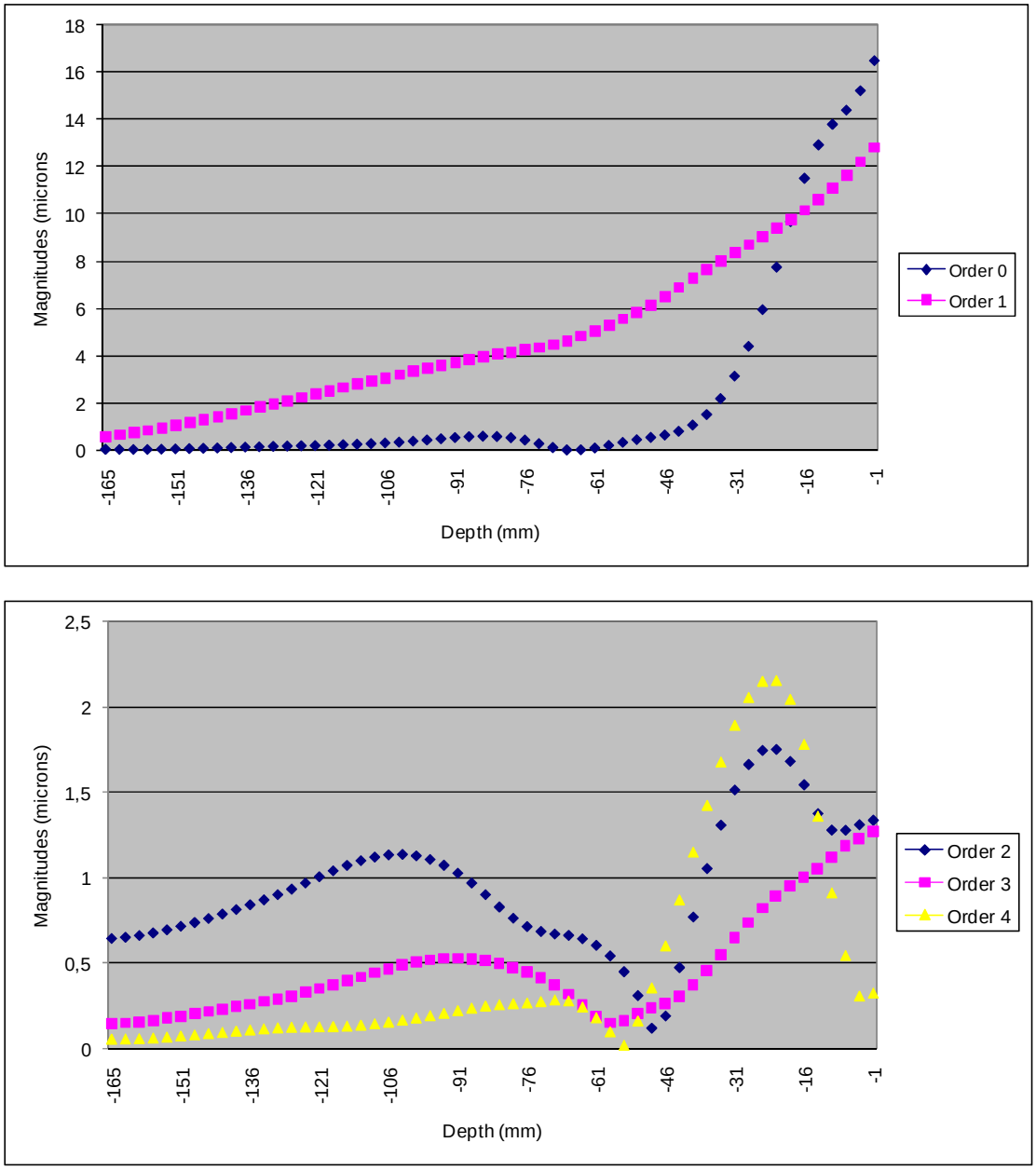

Figure 3.22 : Magnitudes of Orders for Cold Assembly Conditions

In contrast, in the case of cold assembly conditions order 1 is the dominant order as mentioned before, but not as dominant as hot assembly conditions. Moreover, order 4, which is caused by pre-tension loads, is dominant somewhere at the top side in cold assembly conditions.

3.3 AVL EXCITE PR Oil Consumption Model

A piston dynamics, ring dynamics and oil consumption model for I4 2.2 L engine was established using AVL EXCITE PR simulation code. The model includes the piston, piston pin, liner, conrod, and piston rings as shown in Figure 3.23.

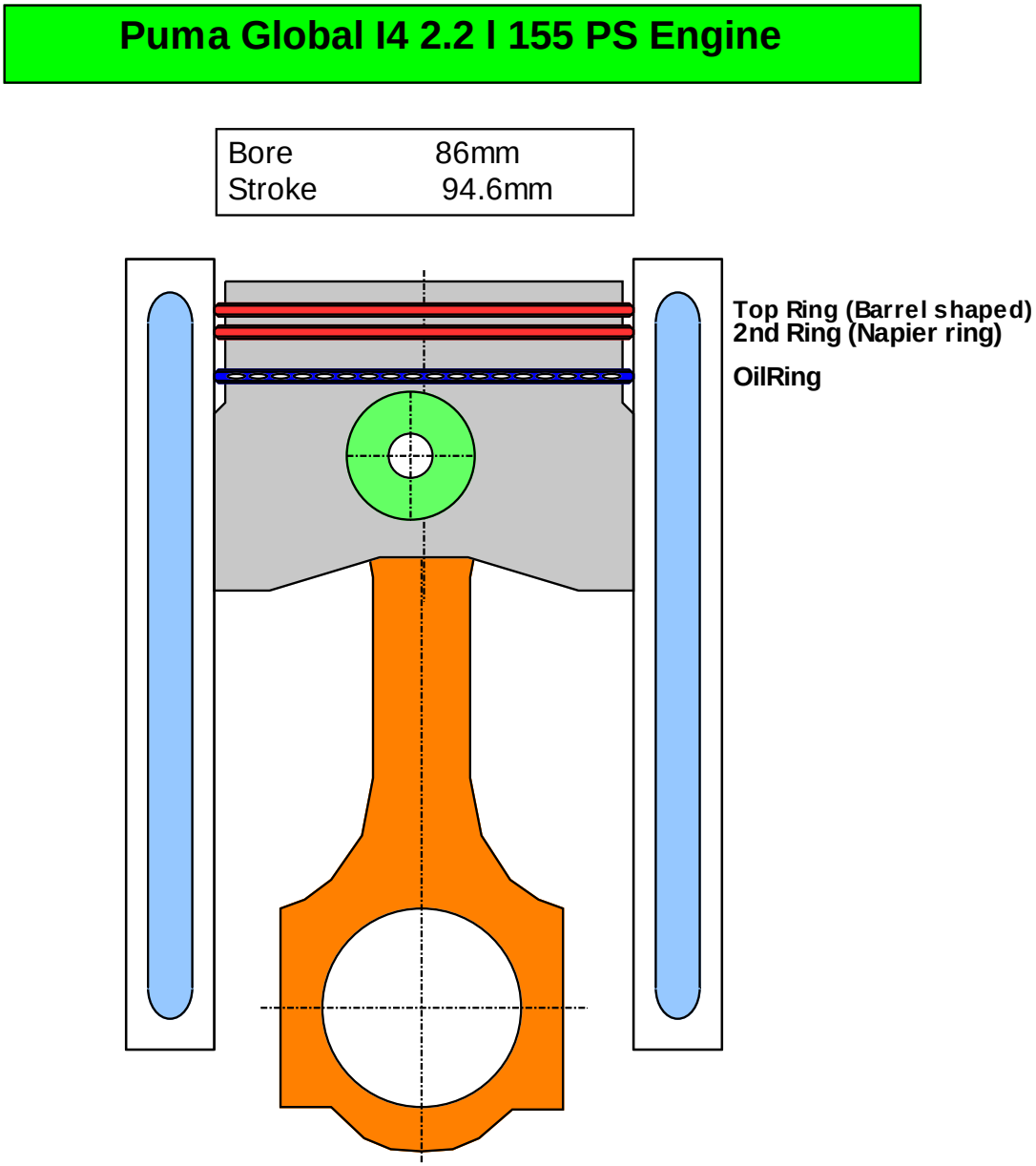

Figure 3.23 : Piston Assembly Model

The general specifications of the engine under investigation are given in Table 3.2.

Table 3.2: General Specifications of 2.2 L Engine

Engine configuration:	4 Cylinder in-line
Fuel injection system:	Common Rail DI Diesel
Scavenging system:	Turbo-charged
Bore:	86 mm
Stroke:	164.4 mm
Swept volume:	2.198 L
Valve train:	OHV, 4 valves per cylinder

3.3.1 Piston, Liner and Cranktrain

The geometrical input data for the piston was used in cold state. Besides, axial piston temperature profile was entered the AVL EXCITE PR in order to obtain hot profile for the piston. Distorted bore profile, straight liner profile, second, third and fourth order distorted bore profile were used for liner geometrical data. The data of the piston is given in Appendix A.2.

The stiffness matrix of the piston was extracted by using the CAD model of the piston and finite element solver ABAQUS which is explained in section 3.1. First, the flexibility matrix of the piston was determined by finite element method, and then AVL EXCITE PR obtains the stiffness matrix by matrix inversion. The data of the stiffness matrix input file is given in Appendix A.3. The inertial properties of the piston pin are also included in piston properties.

The mass and moment of inertia values are used for conrod and pin

3.3.2 Piston Rings and Ring Groove

The geometrical data of the piston rings in addition to estimations for their operating temperatures were used for the calculation. Therefore, the hot geometry of the rings and groove were calculated according to thermal expansion considerations. The data used for piston rings are shown in Appendix A.4.

The simulation was performed at 4000 RPM and full load. So, all the data are taken or calculated in this condition.

The thermodynamic data of combustion gas was calculated with software, which is named Wave, calculates 1-D CFD analysis. (see Figure 3.24)

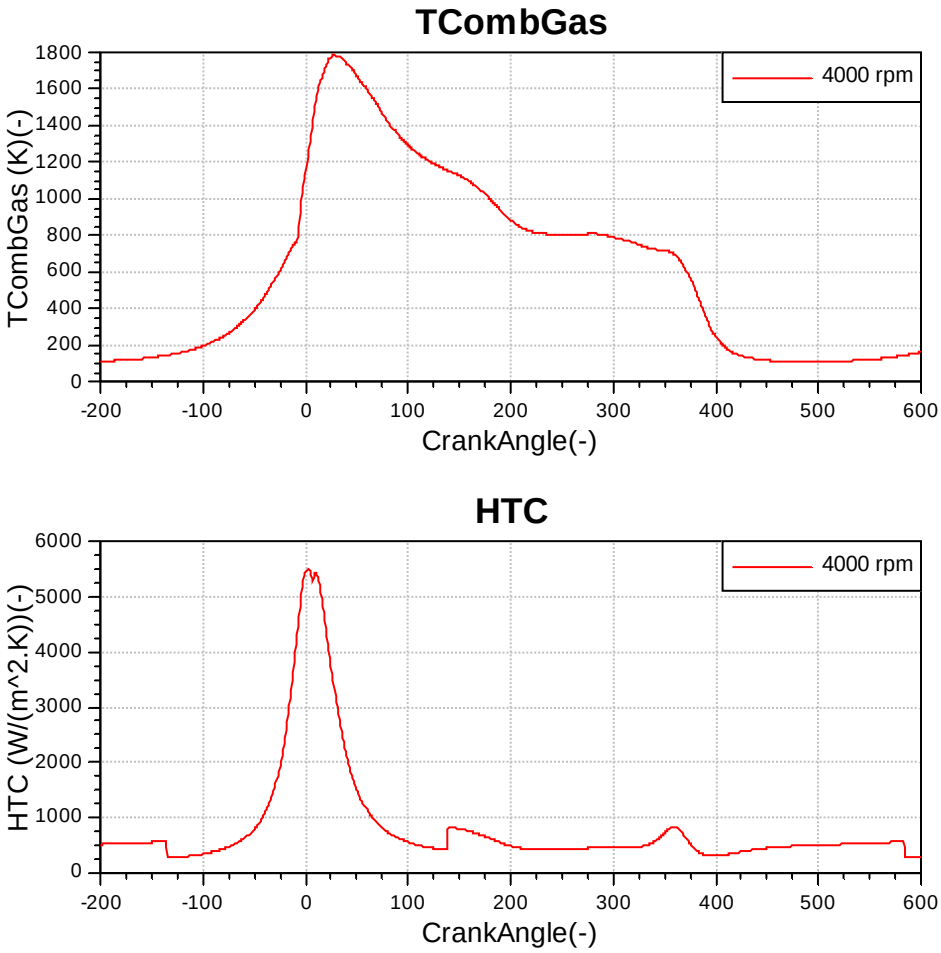

Figure 3.24 : The Thermodynamic Data

4. RESULTS AND DISCUSSIONS

Bore distortion is one of the main critical issues in diesel engine development. Excessive cylinder bore out-of-roundness can adversely affect the sealing functionality and durability of the piston-ring pack in an engine.

This study aims to point out and quantify the influence of bore distortion, especially orders of distortion mainly on oil consumption and blow-by. Although focus is placed on oil consumption, blow-by was also investigated which are strongly inter-related and blow-by trends provide a deeper understanding of mechanisms behind oil consumption.

In this section, the effect of bore distortion on oil consumption and blow-by characteristics of Puma 2.2 L diesel engine was investigated for 4000 RPM and full load condition. The pressure curve is given in Figure 4.1

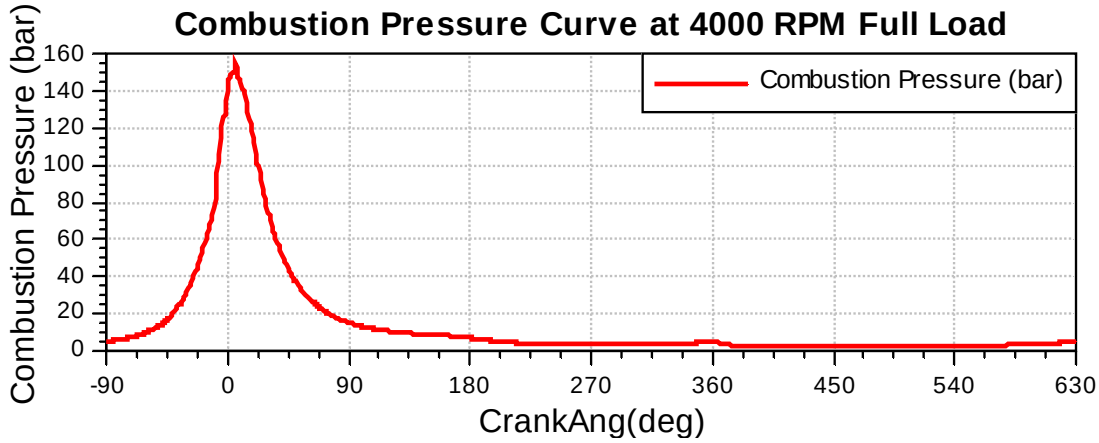

Figure 4.1 : Combustion Pressure Excitation Curve

4.1 Input Liner Data Cases

7 different liner cases are used for the analysis.

1) Straight Liner
2) Distorted Liner (see Figure 4.2 a)
3) Order 0 Shape Liner (see Figure 4.2 b)
4) Order 1 Shape Liner (see Figure 4.2 c)
5) Order 2 Shape Liner (see Figure 4.2 d)
6) Order 3 Shape Liner (see Figure 4.2 e)
7) Order 4 Shape Liner (see Figure 4.2 f)

Hot assembly conditions were used for the distorted liner. AVL EXCITE PR enables to use the Fourier coefficients. Thus, each order was entered as its amplitude and phase coefficients. No deformation was assumed for the straight liner.

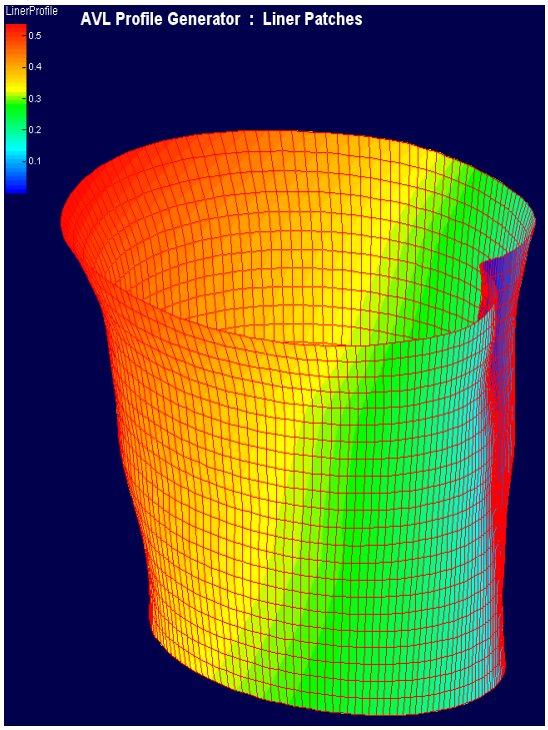

a) Distorted Profile (Scaled 300)

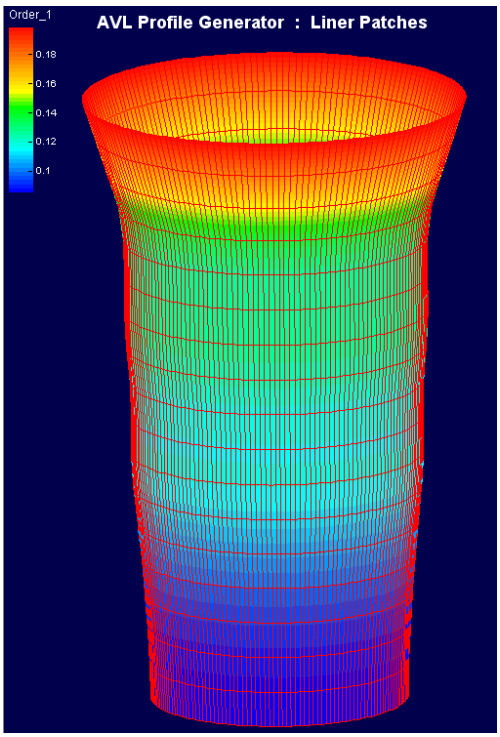

b) Order 0 Profile (Scaled 150)

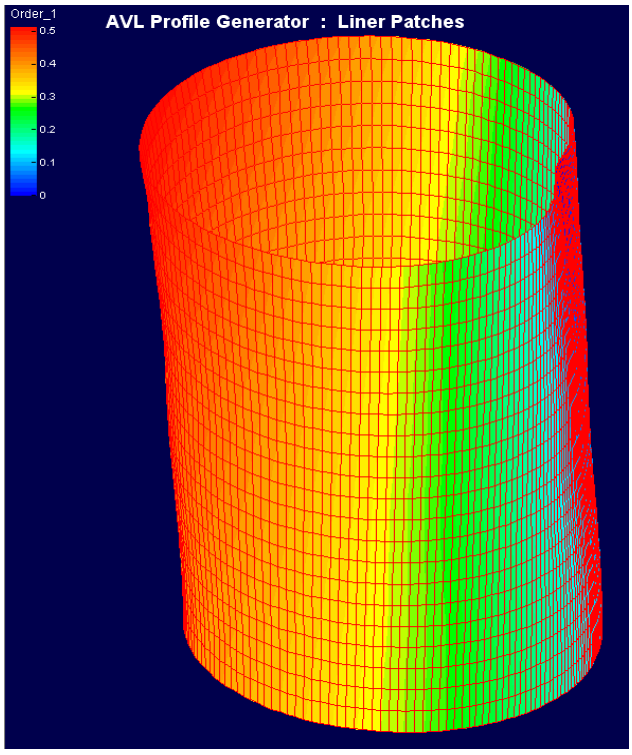

c) Order 1 Profile (Scaled 150)

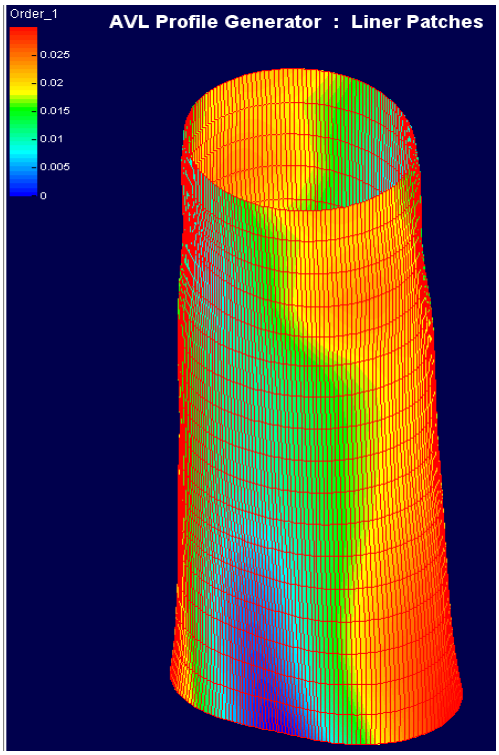

d) Order 2 Profile (Scaled 400)

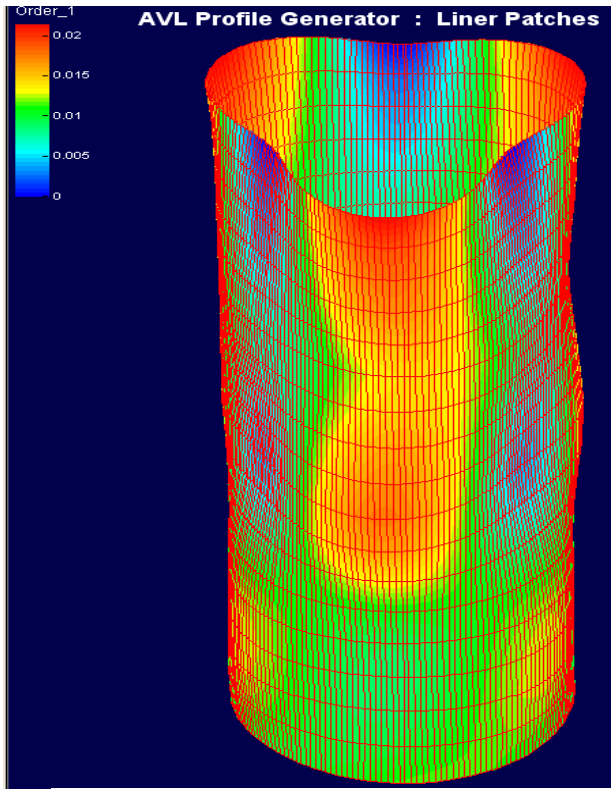

e) Order 3 Profile (Scaled 500)

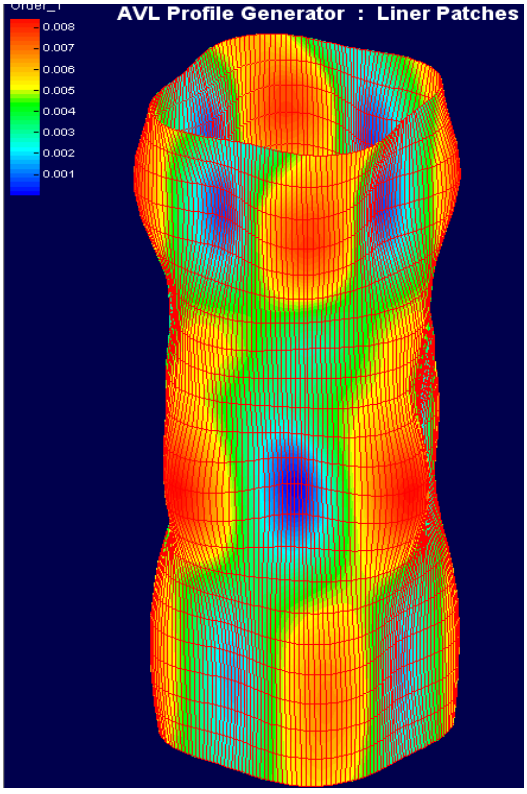

f) Order 4 Profile (Scaled 1500)

Figure 4.2 : Liner Cases Used in AVL EXCITE PR

4.1.1 Results for Straight Liner vs. Distorted Liner Conditions

The LOC by oil evaporation according the CA graph is shown in Figure 4.3. There was no significant difference between straight liner and distorted liner on oil evaporation. Because, the liner and oil temperatures are the main factors for the oil evaporation which are the same for both cases.

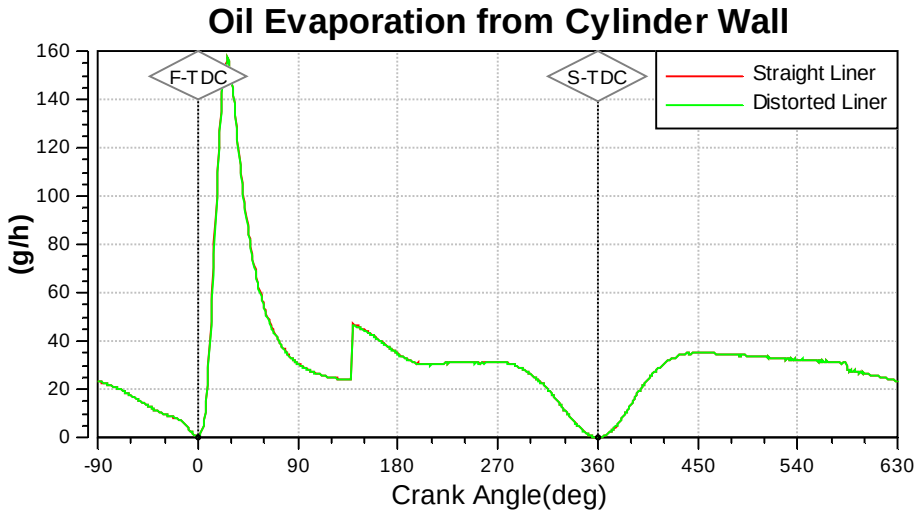

Figure 4.3 : LOC by Oil Evaporation for Case 1

The LOC by Reverse Blow-by according to CA graph is shown in Figure 4.4 with logarithmic scale. It is obviously seen that there is a significant difference between two cases. Distorted shape of the bore causes this difference. It is also seen that, the oil blow is larger in exhaust and intake sections of the piston movement where the gas flows occur.

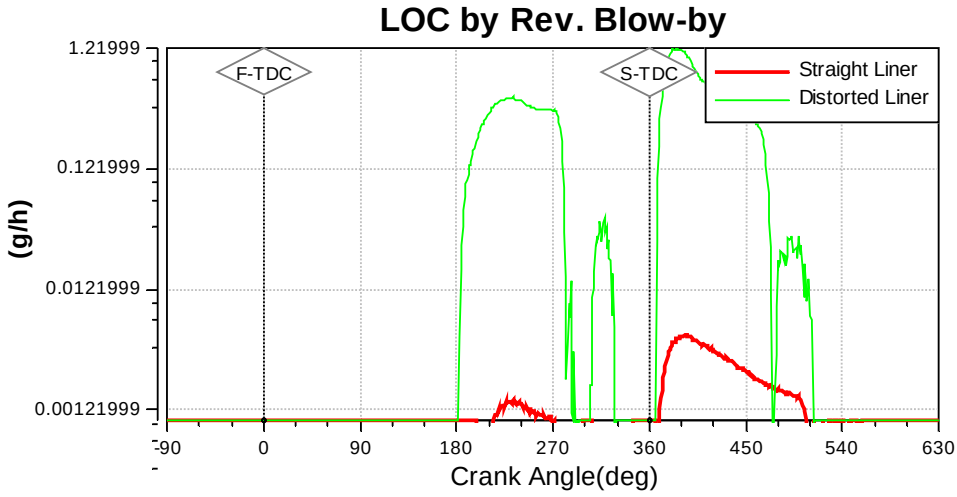

Figure 4.4 : LOC by Rev. Blow-by (Logarithmic Scale) for Case 1

The LOC by “Throw-Off” according to CA graph is shown in Figure 4.5. The value of the straight liner case is higher than the distorted liner case. The acceleration and deceleration effects are the main parameters for the throw-off, which is seen clearly from the graph. In distorted liner, distortion does not permit the oil to travel to top land, upwards. Therefore, the amount of oil, which is consumed, is more in straight liner case.

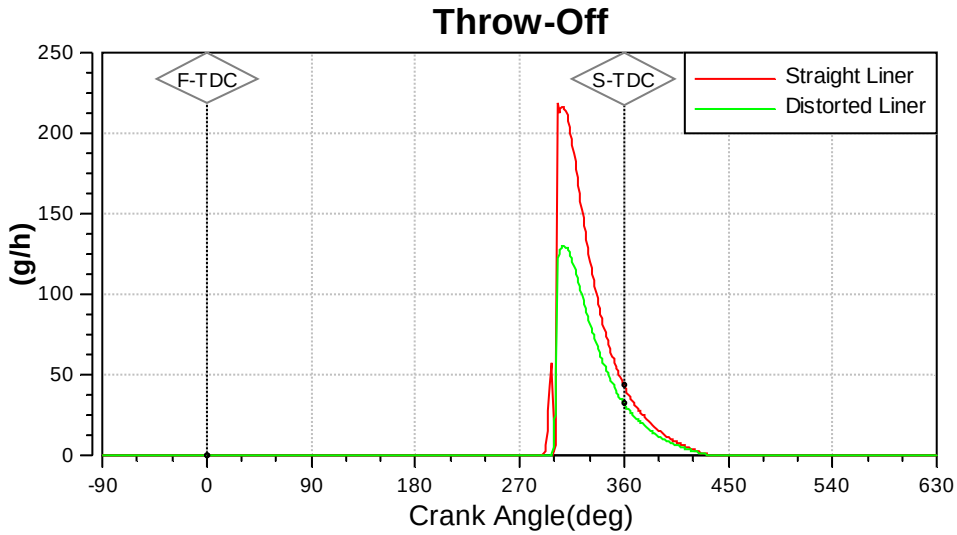

Figure 4.5 : LOC by Throw-Off for Case 1

Blow-by is a small amount of unburned fuel and oil, which escape around the piston rings and enter the crankcase during the engine operation. The blow-by according to CA graph is shown in Figure 4.6. The Blow-by amount in distorted liner case is more than straight liner case.

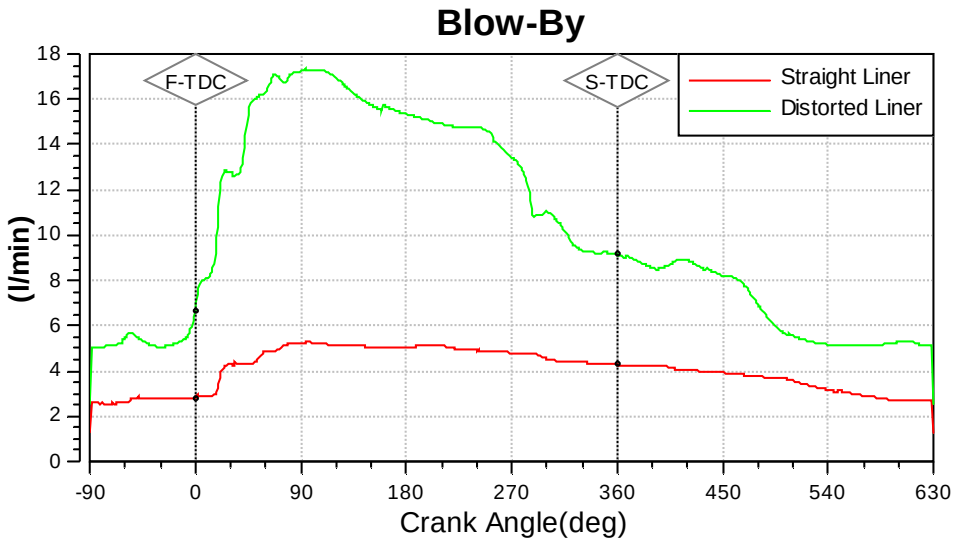

Figure 4.6 : Blow-By for Case 1

4.1.2 Results for Order 0 vs. Order 1 Shape Liners Conditions

Order 0 and Order 1 Liner Cases were investigated together because of having high magnitudes according to other orders. Oil evaporation graph according to CA is shown in Figure 4.7. The amount of oil evaporation is closer for two conditions because of having same initial liner temperatures. Moreover, all liner conditions have same oil properties and the concentration of oil at the surface has similar values because of having high deformations for order 0 and order 1. Thus, oil evaporation values are closer each other.

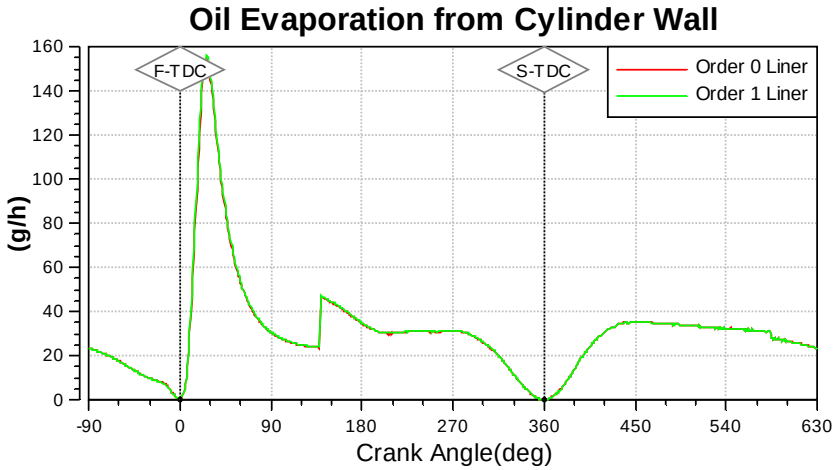

Figure 4.7 : LOC by Oil Evaporation for Case 2

Oil blow graph for the order 0 and order 1 liner cases is shown in Figure 4.8. Because of the shape of the order 0, the amount of oil blow is too much. Besides, this shape of order 0 lets the oil blows to combustion chamber, easily.

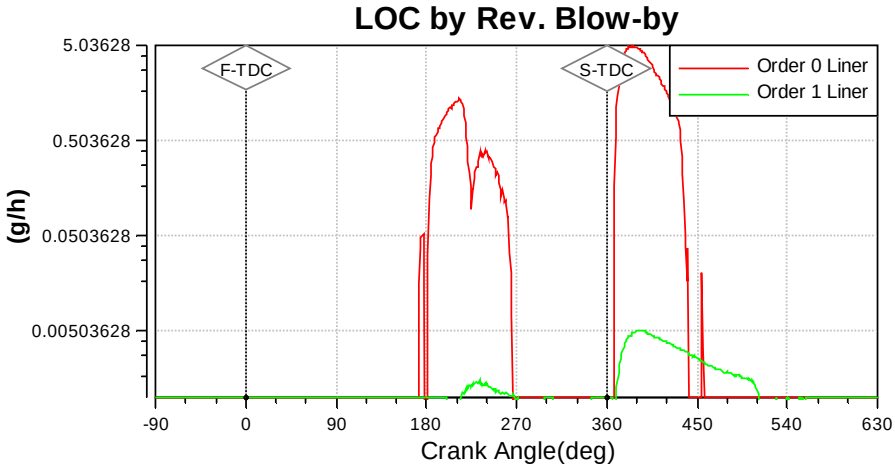

Figure 4.8 : LOC by Rev. Blow-by (Logarithmic Scale) for Case 2

Also this shape of order 0 causes the increasing of throw-off against order 1 shape liner.(see Figure 4.9). Oil travel to combustion chamber in the throw-off mechanism can easily occur because diameter in order 0 shape liner increases homogenous at the top side of the liner where acceleration and deceleration happen upwards.

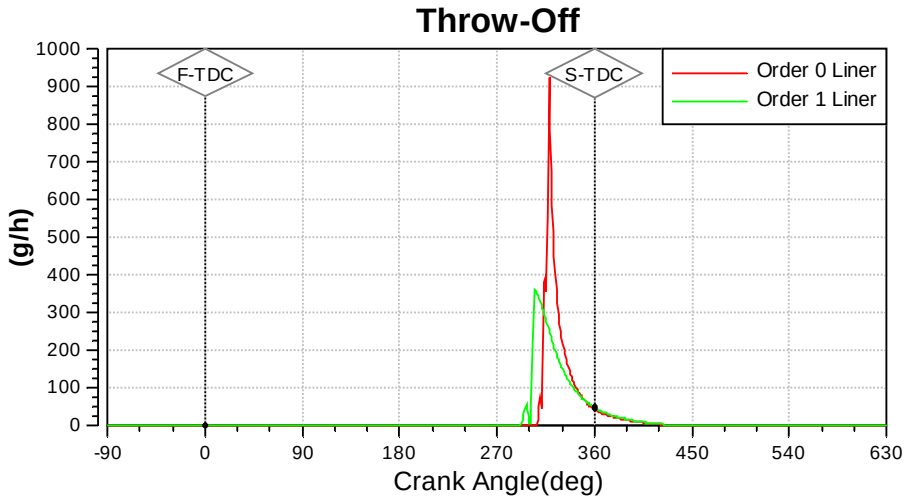

Figure 4.9 : LOC by Throw-Off for Case 2

Blow-by is affected from the liner shape which is shown in Figure 4.10, obviously. Moreover, order 0 shape liner condition has a high amount of blow-by according to order1 liner shape.

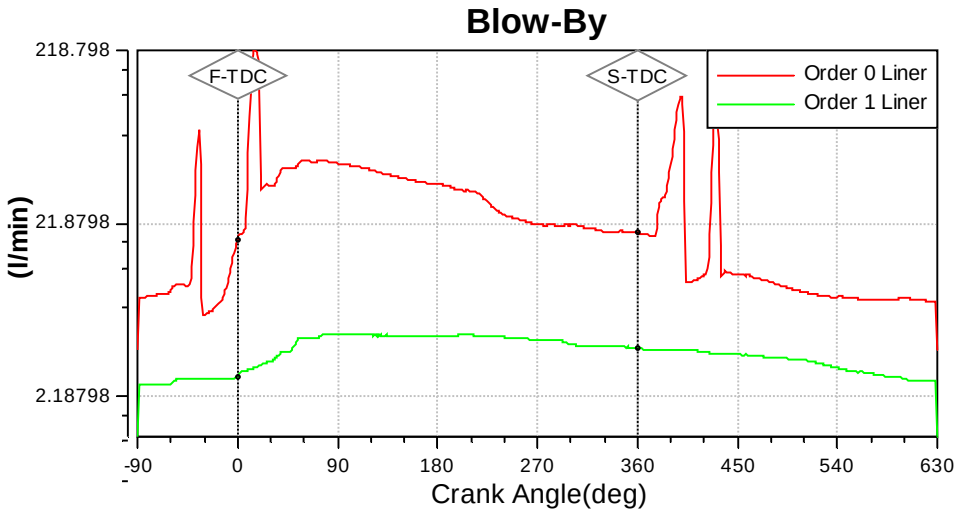

Figure 4.10 : Blow-By (Logarithmic Scale) for Case 2

4.1.3 Results for Order 2 vs. Order 3 vs. Order 4 Shape Liners Conditions

Oil evaporation graph for order 2, order 3 and order 4 liners is shown in Figure 4.11. According to graph, oil evaporation curves are the same for all conditions. One of the main reasons for the same results is the calculation method of the AVL EXCITE PR. Because, one of the important factors is concentration of lube oil at film surface which does not change amongst order 2, order 3 and order 4 shape liners

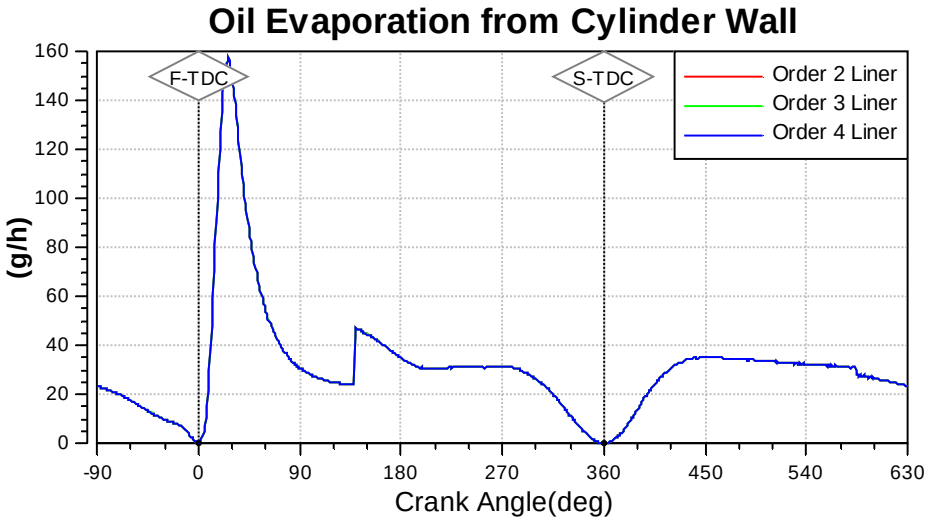

Figure 4.11 : LOC by Oil Evaporation for Case 3

LOC by Rev. Blow-by graph is shown in Figure 4.12. Oil blow amount for order 4 liner is higher than the others. Ring does not conform the liner at the valley sides. Thus, four-lobe shape of order 4 causes the blowing of oil in to the combustion chamber. Moreover, Order 3 liner curve is higher than order 2 liner.

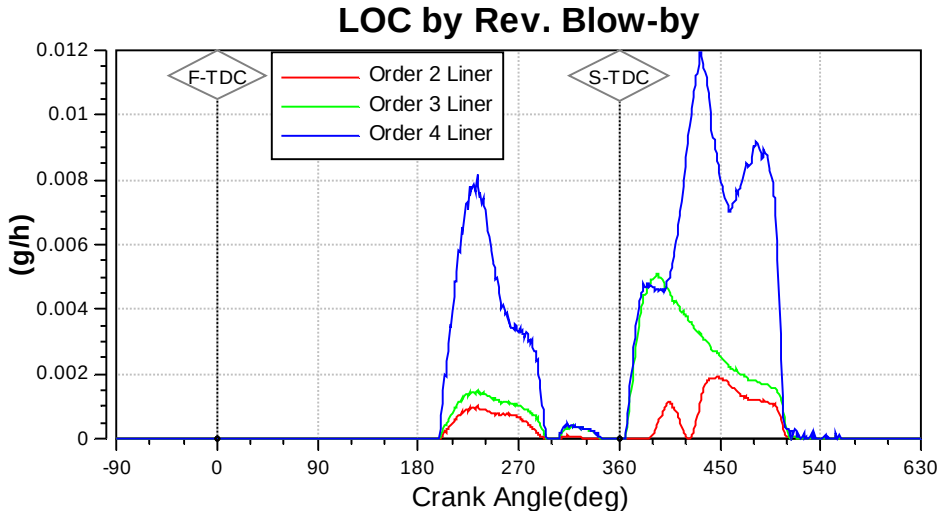

Figure 4.12 : LOC by Rev. Blow-by (Logarithmic Scale) for Case 3

On the other hand, throw-off curve for order 2 liner case is higher than the other cases. Throw-off curves of order 3 and order 4 liner cases are very close to each other. (see Figure 4.13)

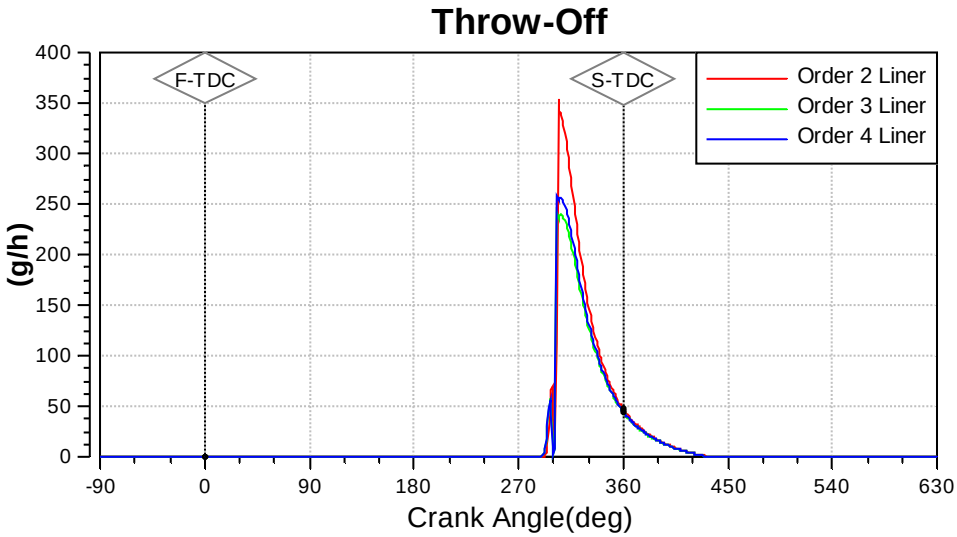

Figure 4.13 : LOC by Throw-Off for Case 3

Blow-by result is shown in Figure 4.14. It is clearly seen from the graph, there is no significant difference between different order cases.

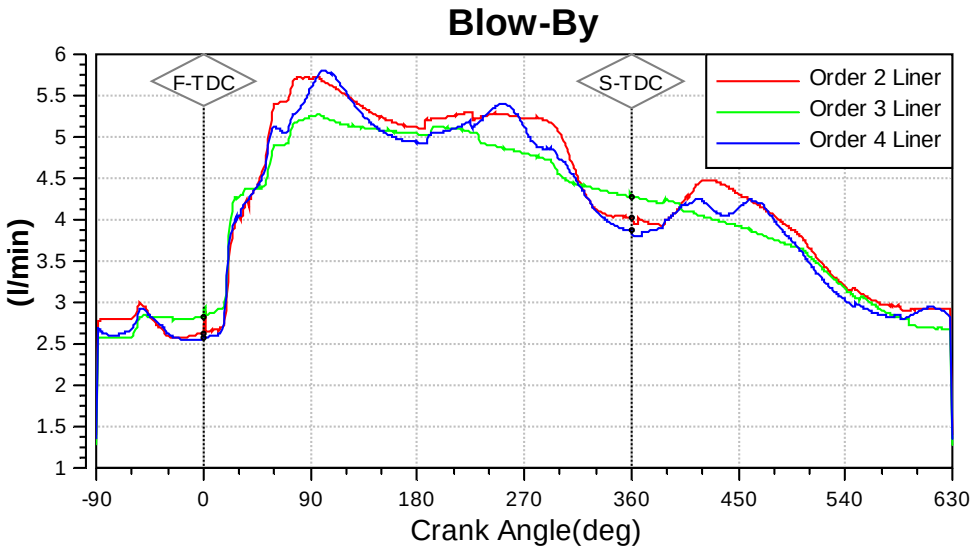

Figure 4.14 : Blow-By for Case 3

4.1.4 Comparing Results for All Conditions

The amount of oil evaporation is closer for all conditions because of having same initial liner temperatures. Another reason for the same results is the calculation method of the AVL EXCITE PR. Because, one of the important factors is concentration of lube oil at film surface which does not change amongst order 2, order 3 and order 4 shape liners. (see Figure 4.15)

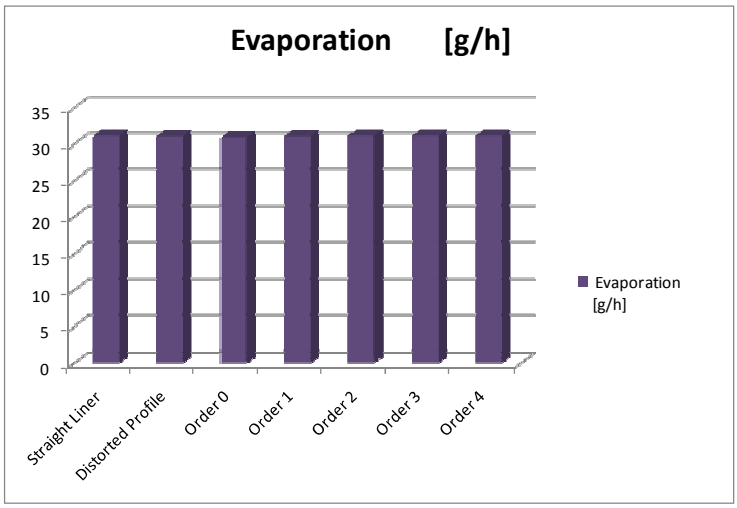

Figure 4.15 : Comparison of Oil Evaporation Values

The highest difference between LOC mechanisms is seen in Oil-Blow. In case of Order 0 and Distorted Liner cases, amount of oil-blow is very high. Because, diameter of the order 0 shape liner increases homogenous at the top side of the liner. This shape of order 0 permits the oil blows to combustion chamber at the ring gaps. So, the chart is seen in logarithmic view. (see Figure 4.16)

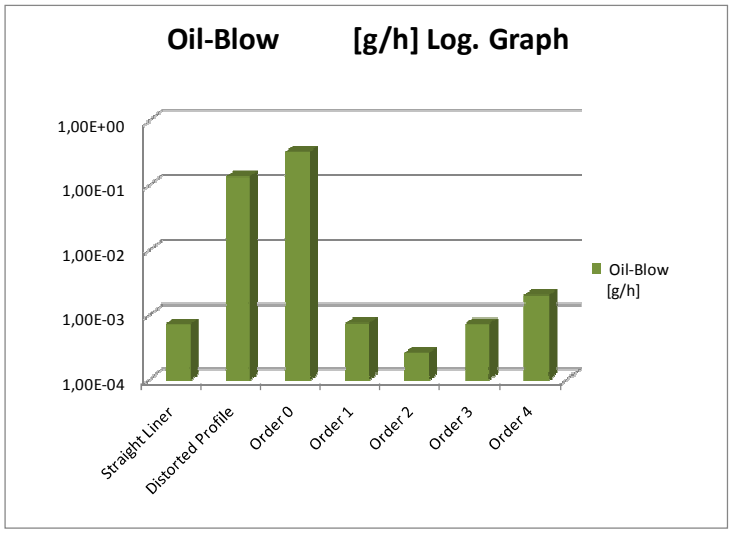

Figure 4.16 : Comparison of Oil-Blow Values

For the distorted profile case throw-off value is smaller than the other cases. On the other hand, order 0 liner case is the worst. Oil travel to combustion chamber in the throw-off mechanism can easily occur because diameter in order 0 shape liner increases homogenous at the top side of the liner where acceleration and deceleration happen upwards. In addition, in straight liner condition, diameter of the liner is equal at all frames. Therefore, this shape of liner permits the oil travel in to combustion chamber in acceleration and deceleration, which is the reason of throw-off mechanism. (see Figure 4.17)

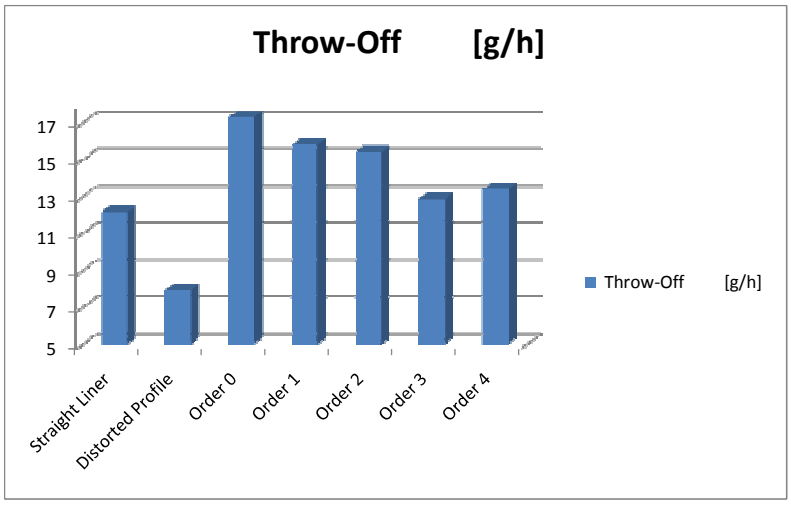

Figure 4.17 : Comparison of Throw-Off Values

Because of the piston design, the piston crown is not interact with liner. Therefore, the LOC by oil scraping was found zero for all cases. (see Figure 4.18)

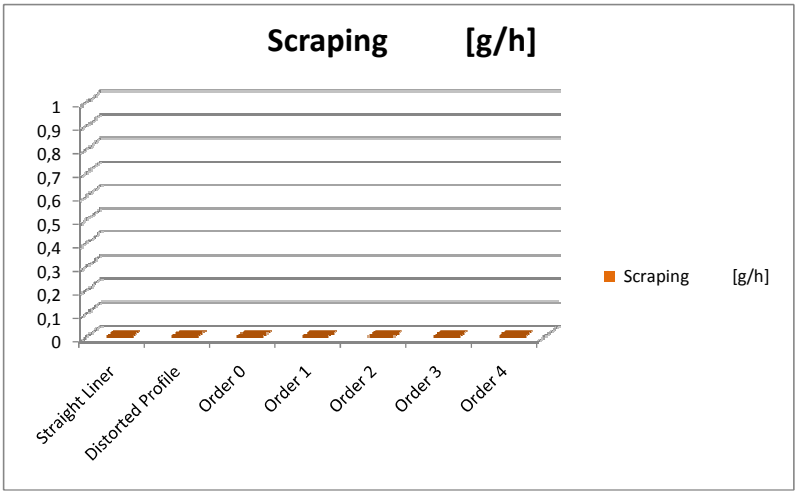

Figure 4.18 : Comparison of Oil Scraping Values

The total LOC for the cylinder is shown in Figure 4.19. Effect of orders on LOC is clearly seen. Oil evaporation is the most effective mechanism in defining total lube oil consumption. On the other hand, the determining factor is the throw-off mechanism. Because, oil evaporation values are similar for all conditions and oil blow values are too low. The minimum LOC was found for the distorted liner shape because of having low LOC by throw-off values against to other liner shapes.

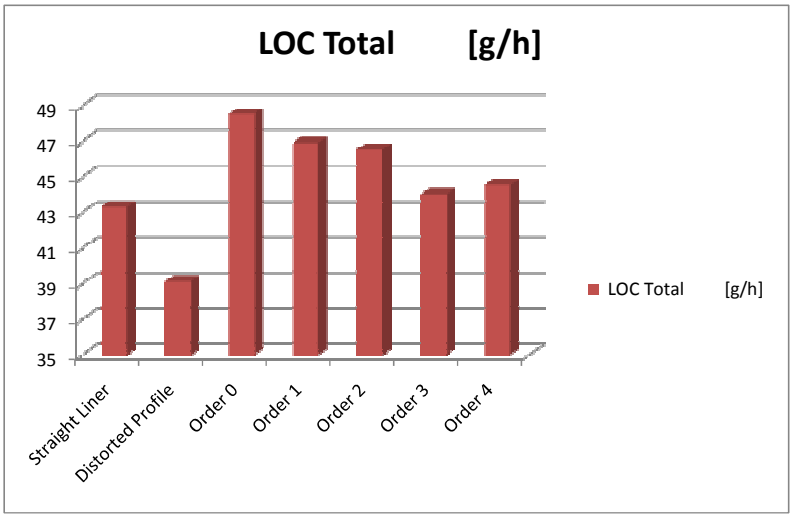

Figure 4.19 : Comparison of Total LOC

On the other hand, for the blow-by amounts, distorted liner case is more than the other cases except from the order 0 shape liner. Because, diameter of the order 0 shape liner increases homogenous at the top side of the liner. This shape of order 0 permits the gas blows to crankshaft at the ring gaps. (see Figure 4.20)

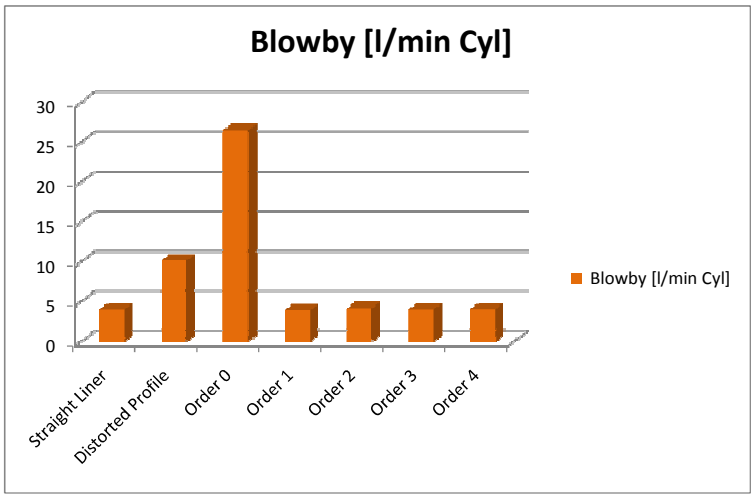

Figure 4.20 : Comparison of Blow-by Values

5. CONCLUSION AND FUTURE RECCOMENDATIONS

In this thesis, the effect of cylinder bore distortion on engine oil consumption is assessed using computerized models. First of all, a theoretical model was constructed for lube oil consumption of 2.2 L diesel engine using AVL EXCITE PR. Then, an analysis for calculating the piston stiffness was done with the purpose of providing the optimum conditions for the oil consumption analysis. The analysis results were entered in AVL EXCITE PR with the appropriate format for assigning the stiffness data of the piston.

In order to investigate the bore distortion on LOC, different distorted bore profile data are entered in the AVL EXCITE PR. Cylinder bore distortion FEM analysis was performed in ABAQUS. Distortion results in Cartesian coordinates were written in a text file, which was post-processed by a code written in MATLAB. As a result of this, the distorted profile in polar coordinates and Fourier coefficients were calculated via MATLAB for the order investigation. Distorted profile and orders from 0 to 4 were used as different liner inputs for investigating the oil consumption analysis.

3 cases were investigated for the bore distortion effect. Straight liner and distorted liner are the first case; Order 0 shape liner and order 1 shape liner are the second case; Order 2, order 3 and order 4 shape liners are the third case for investigating the all oil consumption mechanisms and blow-by. Finally, all different shape liners were investigated together for total oil consumption. From the results, the following conclusions were derived.

- Order 0 shape liner was found as the worst case for the oil blow and throw-off LOC mechanisms and blow-by. Because, diameter of the order 0 shape liner increases homogenous at the top side of the liner. This shape of order 0 permits the oil blows to combustion chamber at the ring gaps.

- Oil travel to combustion chamber in the throw-off mechanism can easily occur because diameter of the order 0 shape liner increases homogenous at the top side of the liner where acceleration and deceleration happen upwards.
- Also, this shape of order 0 permits the gas blows to crankshaft at the ring gaps.
- In straight liner condition, diameter of the liner is equal at all frames. Therefore, this shape of liner permits the oil travel in to combustion chamber in acceleration and deceleration, which is the reason of throw-off mechanism.
- Because of the piston design, the piston crown is not interact with liner. Therefore, the LOC by oil scraping is found zero for all cases.
- In case of distorted shape liner, LOC by oil blow and blow-by amount is higher than the amount found in case of straight liner.
- In case of order 2 liner shape has a higher amount of LOC than the case of order 3 and order 4 liner shapes. Besides, for the case of order 4 liner shape, amount of LOC is quite similar to case of order 3 liner case.
- In general, Oil evaporation is the most effective mechanism in defining total lube oil consumption. On the other hand, the determining factor is the throw-off mechanism. Because, oil evaporation values are similar for all conditions and oil blow values are too low. The minimum LOC was found for the distorted liner shape because of having low LOC by throw-off values against to other liner shapes.
- So, according to theoretical study, it can be said that the bore distortion has a significant influence on LOC and blow-by.

In this study, the fourth cylinder of an “in-line” type four-cylinder engine is selected for the investigation cylinder bore distortion and LOC. Study can be completed with selecting different cylinders of other “in-line” or “v” type engines.

In addition, different calculation methods and assumptions of LOC can be used for the future studies.

REFERENCES

Abe S. and Suzuki M., 1995. Analysis of cylinder bore distortion during engine operation, *SAE Paper*, 950541

Andersson, P., Tamminen J., and Sandstöm C., 2002. Piston Ring Tribology, *VTT TIEDOTTEITA – Research Notes* 2178

Audette, W.E. and Wong,V.W., 1999. A Model For Estimating Oil Vaporization From The Cylinder Liner As A Contributing Mechanism to Engine Oil Consumption**,** *SAE Paper,* 1999-01-1520.

AVL EXCITE PR Theory, 2009. AVL List GmbH.

Bardzimashvili, T., Kelly, J., Romelashvili, H., Sledd, W., and Geist, B., 2005. A Multiple Order Conformability Model for Uniform Cross-Section Piston Rings, *SAE Paper*, 2005-1-1643.

Chittenden R. J. and Priest M., 1993. Analysis of the piston assemply, bore distortion and uture developments, *Taylor, C.M. (ed.). Engine Tribology. Elsevier, 1993,Tribology series,* 26, pp. 241–270.

Dunaevsky V. V., 1990. Analysis of distortions of cylinder and conformability of piston rings, *Tribology Transactions,* Vol. 33, No. 1, pp. 33-40

Ford Handbook, 2001. Cylinder Bore Distortion.

Froelund, K., and Ertan, Y., 2004. Impact of Engine Oil Consumption on Particulate Emissions, *http://www.osd.org.tr/17.pdf*

Fujimoto H., Yoshihara Y., Goto T., Furuhama S., 1991. Measurement of Cylinder Bore Deformation During Actual Operating Engines, *SAE Paper*, 910042.

Gerhard, C., Almeida M.C.L., Palermo J.L.G., 1992. Oil Consumption Improvement in a D.I. Diesel, *SAE Paper,* 921490.

Greenwood, J. A., and Tripp, J. H., 1971, The Contact of Two Nominally Flat Surfaces, *Proc. Inst. Mech. Engrs*., Vol. 185, p. 625.

Goetze AG, 1989. *Piston Ring Manual*, Burscheid, D-5093

Hitosugi H., Nagoshi K., Komada M., and Furuhama S., 1996. Study on Mechanism of Lubricating Oil Consumption Caused by Cylinder Bore Deformation. *SAE Paper,* 960305.

Inagaki, H., Saito, A., Murakami, M., and Konomi, T., 1995. Development of Two-Dimensional Oil Film Thickness Distribution Measuring System**,** *SAE Paper,* 952346.

Kakede N. and Chow J., 1993. Finite Element Analysis of Engine Bore Distortions During Boring Operations, *ASME Journal of Engineering for Industry***,** Vol. 115, pp. 379-384.

Koch F., Decker P., Gülpen R., Quadflieg F., Loeprecht M., 1998. Cylinder Liner Deformation Analysis – Measurements and Calculations, *SAE Paper*, 980567.

Ma, M.-T., 1998. A sensitivity analysis of the influences of the design and operational parameters on frictional losses of ring packs in an internal combustion engine, *Dawson, D. et. al. (ed.).Tribology for Energy Conservation. Elsevier, 1998*, pp. 367–379.

Ma, M.-T., Smith, E.H. and **Sherrington, I.,** 1995. Effects of Bore Out-of-Roundness on the Predicted Performance of Piston Rings in Internal Combustion Engines. *Dawson, D. et. al. (ed.). Lubricants and Lubrication. Elsevier, 1995*, pp. 367–379.

Ma, M-T., Sherrington, I., Smith, E.H. and Grice, N., 1997. Development of a detailed model for piston-ring lubrication in IC engines with circular and non-circular cylinder Bores. *Tribology International*, 30(1997a)11, pp. 779–788.

Maassen F., Koch F., Schwaderlapp M., Ortjohann T. and Dohmen J., 2001. Analytical and Empirical Methods for Optimization of Cylinder Liner Bore Distortion, *SAE Paper*, 2001-01-0569.

McClure F. and Tian T., 2008. A Simplified Piston Secondary Motion Model Considering the Dynamic and Static Deformation of Piston Skirt and Cylinder Bore in Internal Combustion Engines, *SAE Paper*, 2008-01-1612.

Liu L. and Tian T., 1995. Modeling Piston Ring-Pack Lubrication With Consideration of Ring Structural Response. *SAE Paper*, 2005-01-1641.

Loenne K, Ziemba R., 1988. The GOETZE Cylinder Distortion Measurement System and the Possibilities of Reducing Cylinder Distortions, *SAE Paper*, 89361.

Patir, N., and Cheng, H. S., 1979, Application of Average Flow Model to Lubrication Between Rough Sliding Surfaces, *ASME Journal of Lubricaton Technology*, Vol. 101, pp. 220-230.

Reipert P. and Voigt M., 2001. Simulation of the Piston/Cylinder Behavior for DieselEngines. *SAE Paper*, 2001-01-0563.

Sato K., Fujii K., Ito M. and Koda S., 2006. Application to Engine Development of Friction Analysis by Piston Secondary Motion Simulation in Consideration of Cylinder Block Bore Distortion, *SAE Paper*, 2006-01-0428.

Scania, 2009. 1d oil transport modeling through the Pistonring pack in A DI Diesel engine.

Schneider, E.W.,' Blossfeld, D.H., Lechman, D.C., Hill, R.F. and Reising, R.F., 1993. Effect of Cylinder Bore Out-of-Roundness on Piston Ring Rotation and Engine Oil Consumption, *SAE Paper*, 930796.

Thirouard, B., Tian, T., and Hart, D. P., 1998. Investigation of Oil Transport Mechanisms in the Piston Ring Pack of a Single Cylinder Diesel

Engine, Using Two Dimensional Laser Induced Fluorescence, *SAE Paper*, 982658.

Tomanik, 1996. Piston ring conformability in a distorted bore, *SAE Paper*, 960356.

Wahiduzzaman, S., Keribar, R. and Dursunkaya, Z., 1992. A Model for Evaporative Consumption of Lubricating Oil in Reciprocating Engines, *SAE Paper*, 922202.

Yılmaz, E., Tian, T., Wong, V.W. and Heywood, J.B., 2004. The Contribution of Different Oil Consumption Sources to Total Oil Consumption in a Spark Ignition Engine, *SAE Paper*, 2004-01-2909.

APPENDICES

APPENDIX A.1

```
***  INTERFERENCE COMMAND TO COMMENCE SHRINKAGE
**************************************************
**
** Intake Seat Press Fit  (Odd)
** Max. Diametrical Interference = 0.073mm
**
** Exhaust Seat Press Fit (Even)
** Max. Diametrical Interference = 0.073mm
**
*CONTACT  INTERFERENCE,  AMPLITUDE=AMP-RAMP,  TYPE=CONTACT
PAIR
head_intake_side1,seat_intake_side1, -0.0365
head_intake_side2,seat_intake_side2, -0.0365
head_intake_side3,seat_intake_side3, -0.0365
head_intake_side4,seat_intake_side4, -0.0365
head_intake_side5,seat_intake_side5, -0.0365
head_intake_side6,seat_intake_side6, -0.0365
head_intake_side7,seat_intake_side7, -0.0365
head_intake_side8,seat_intake_side8, -0.0365
head_exh_side1,seat_exh_side1, -0.0365
head_exh_side2,seat_exh_side2, -0.0365
head_exh_side3,seat_exh_side3, -0.0365
head_exh_side4,seat_exh_side4, -0.0365
head_exh_side5,seat_exh_side5, -0.0365
head_exh_side6,seat_exh_side6, -0.0365
head_exh_side7,seat_exh_side7, -0.0365
head_exh_side8,seat_exh_side8, -0.0365
**
**  HEAD BOLT AXIAL CLAMP LOAD AND INJECTOR
**    (pre-tension node set: head1 and head 2)
**  Axial clamp load at 55.0KN and 34.0KN
**
*CLOAD
head1, 1, 55.0E+3
head2, 1, 34.0E+3
injector_pre_tension, 1, 8.0E+3
**
*NODE PRINT, NSET= nset_pretension, FREQ=1
U1, RF1
*END STEP
**
**************************************************
**** STEP 3: Assembly
**************************************************
**
*STEP, AMPLITUDE=STEP, INC=50
Assembly
```

```
*STATIC
**
**Removing all soft springs
**
*MODEL CHANGE, REMOVE, TYPE=ELEMENT
RBM_BOLTS-X
RBM_BOLTS-Y
RBM_BOLTS-Z
RBM_INJECTOR-X
RBM_INJECTOR-Y
RBM_INJECTOR-Z
RBM_CAMCARRIER-X
RBM_CAMCARRIER-Y
RBM_CAMCARRIER-Z
RBM_HEAD-X
RBM_HEAD-Y
RBM_HEAD-Z
RBM_SEAT-X
RBM_SEAT-Y
RBM_SEAT-Z
*BOUNDARY, FIXED
head1, 1, 1
head2, 1, 1
injector_pre_tension, 1, 1
**
*CLOAD,OP=NEW
**
**  - .ODB field file
**
*OUTPUT, FIELD, FREQUENCY=999
*ELEMENT OUTPUT
S
*NODE OUTPUT
U, NT
*END STEP
```

APPENDIX A.2

```
% rm = known radius of bore/ring
% profile = bore profile (radius as a function of angle)
% angles = angles for which profile is known
clc
clear
layer=55
rm=43

%load data files here (reverse ordering)
A=importdata('grid.dat');
A = sortrows(A,1);
B=importdata('distorted_profile.dat ');
B = sortrows(B,1);
len = length(A);
C=[A,B]
C=sortrows(C,4)
%get grid locations and each component of displacement
x = C(1:len,2); y = C(1:len,3); z = C(1:len,4);
dx = C(1:len,6); dy = C(1:len,7); dz= C(1:len,8);

SP =1+(layer*90) num = 89;

boreX = x(SP:SP+num); boreY = y(SP:SP+num); boreZ = z(SP:SP+num);
dispX = dx(SP:SP + num); dispY = dy(SP:SP + num); dispZ= dz(SP:SP + num);
centX = XCent(1); centY = YCent(1); centZ = mean(boreZ);

%calculate radial component, through away the rest
for i=1:length(boreX)
   rv = [boreX(i)-centX, boreY(i)-centY];
   [angles1(i),grid(i)] = cart2pol(rv(1),rv(2));
   deltar(i)=cos(angles1(i))*dispX(i) + sin(angles1(i))*dispY(i);
end

%generate the profile (make sure angles are increasing)
prof = ([angles1;deltar])';
prof = sortrows(prof);

angles = (prof(:,1))';
profile = (prof(:,2))';


%FFT Calculations for Orders

Ntheta = 1024;                                  %fixed number of samples
theta = linspace(-pi,pi,Ntheta);
delta_theta = 2*pi/Ntheta;
Ncoeffs=4
```

```
theta_over = -pi:delta_theta:(pi + 5*delta_theta);              %define a temporary
vector that "wraps around" pi to –pi


pp =spline(angles,profile);
zeta_temp= ppval(pp,theta_over);
%overwrite here
zeta = zeros(size(theta));
zeta(1:Ntheta) = zeta_temp(1:Ntheta);
zeta(1:6)=zeta_temp(Ntheta:Ntheta +5);

zetahat =fft(zeta);
a0 = 2*zetahat(1)/Ntheta;  %DC component
for ik = 1:Ncoeffs
   ij = ik +1;       %index for fft

ak(ik) = 2.*(-1)^(ik).*real(zetahat(ij))/Ntheta;    %cosine terms
bk(ik) = 2.*(-1)^(ij).*imag(zetahat(ij))/Ntheta;     %sine terms
end
plot(angles,profile,'o',theta_over,zeta_temp)

coeff=[ak',bk']
%Ak=sqrt(ak.^2 + bk.^2);

%plot(Ak(2:8))
```

APPENDIX A.3

A.2.1 Piston and Liner Properties

Piston:

Piston Height:	74.8 mm
x – Center of Mass:	20.293 mm
y – Center of Mass:	0.3012 mm
Piston Mass:	0.5866 kg
Piston Moment of Inertia:	555.62 kgmm^2
Piston Profile:	Profile is defined in Meridian 0 deg and Meridian 90 deg. Figures A.1 and A.2

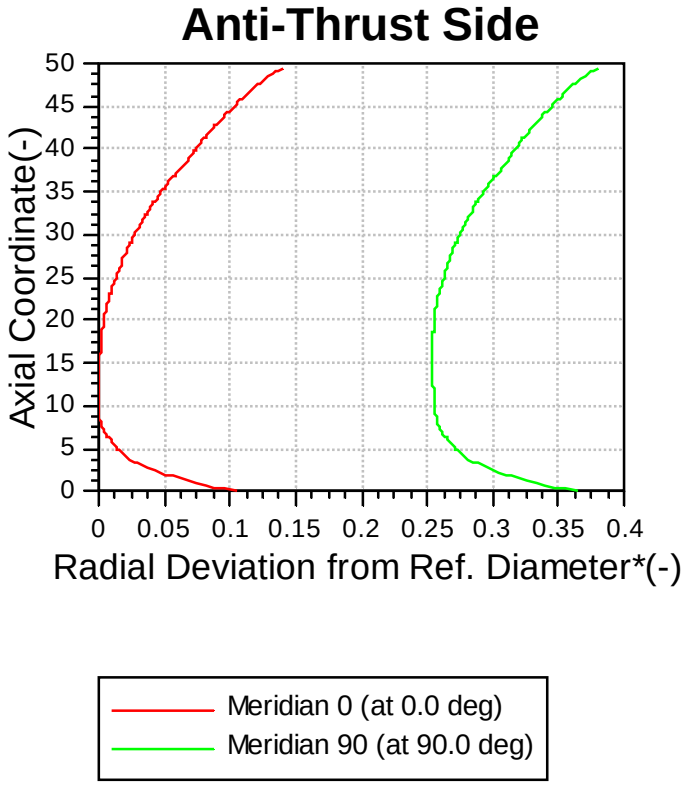

Figure A.1 : Piston Skirt Profile

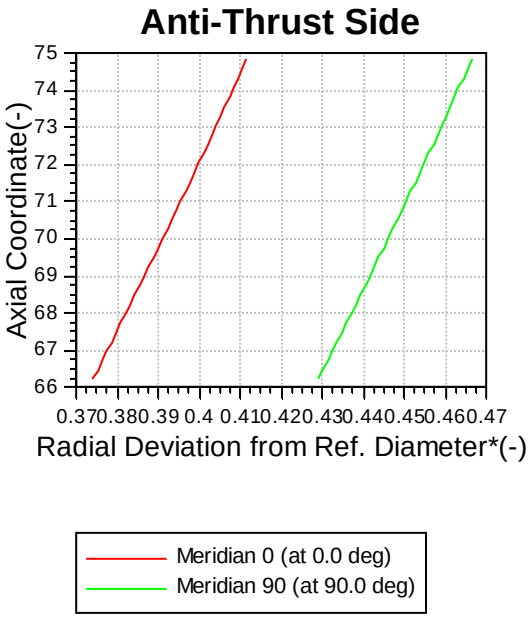

Figure A.2 : Piston Top Land Profile

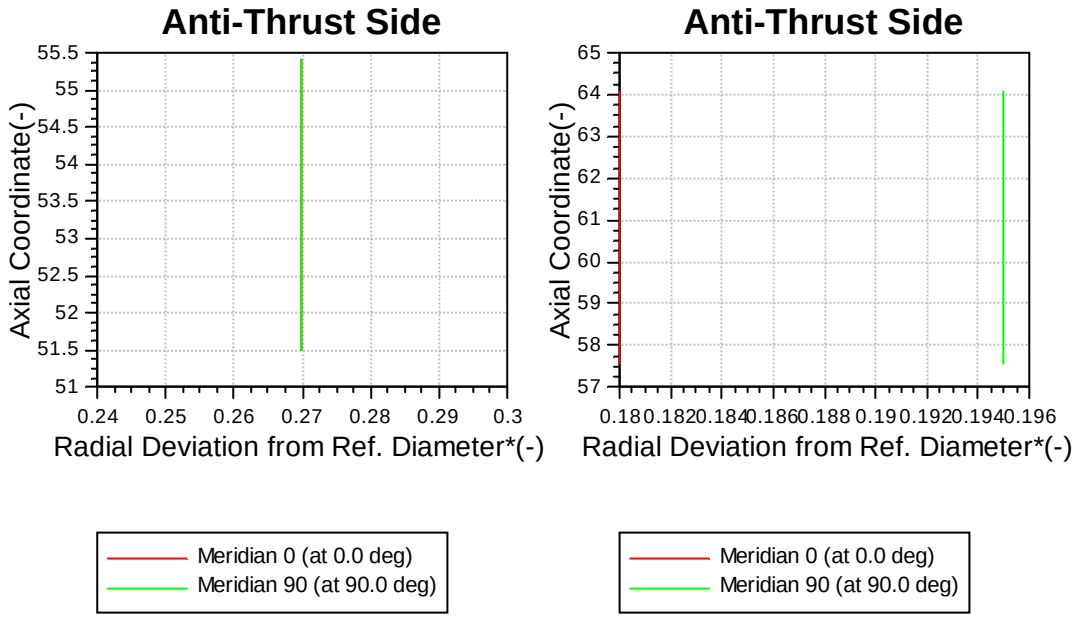

Figure A.3 : Piston Second and Third Land Profile

Liner:

Top Deck: 250.72 mm

Liner Height: 164.15 mm

Liner Profile: Several profiles are used for different analyses. They are figured in Section 5.1

Conrod:

x – Center of Mass:	49.59 mm
y – Center of Mass:	0 mm
Conrod Mass:	0.8711915 kg
Conrod Moment of Inertia:	4241.2401 $kgmm^2$
Big End Diameter:	56 mm
Small End Diameter:	30 mm

Piston Pin:

Pin Mass:	0.26476625 kg
Pin Moment of Inertia:	37.93 $kgmm^2$

A.2.2 Piston Rings and Ring Groove Properties

1. Ring (Barrel Shaped):

Ring Mass:	12.7 g
Center of Gravity:	0.0491 mm
Pre – Twist Angle:	0º
Tangential Force:	14.9 N
Ring End:	0.3 mm (variable)
Peripheral Edge:	0 mm
Summit Roughness:	0.55 μm
Radial Deviation:	-0.428 mm (above groove)
Radial Deviation:	-0.11 mm (below groove)
Groove Root Depth:	-4.35 mm
Distance from Piston Top:	9.69 mm
Groove Top Angle:	0º
Profile of Ring Face:	(Figure A.4)

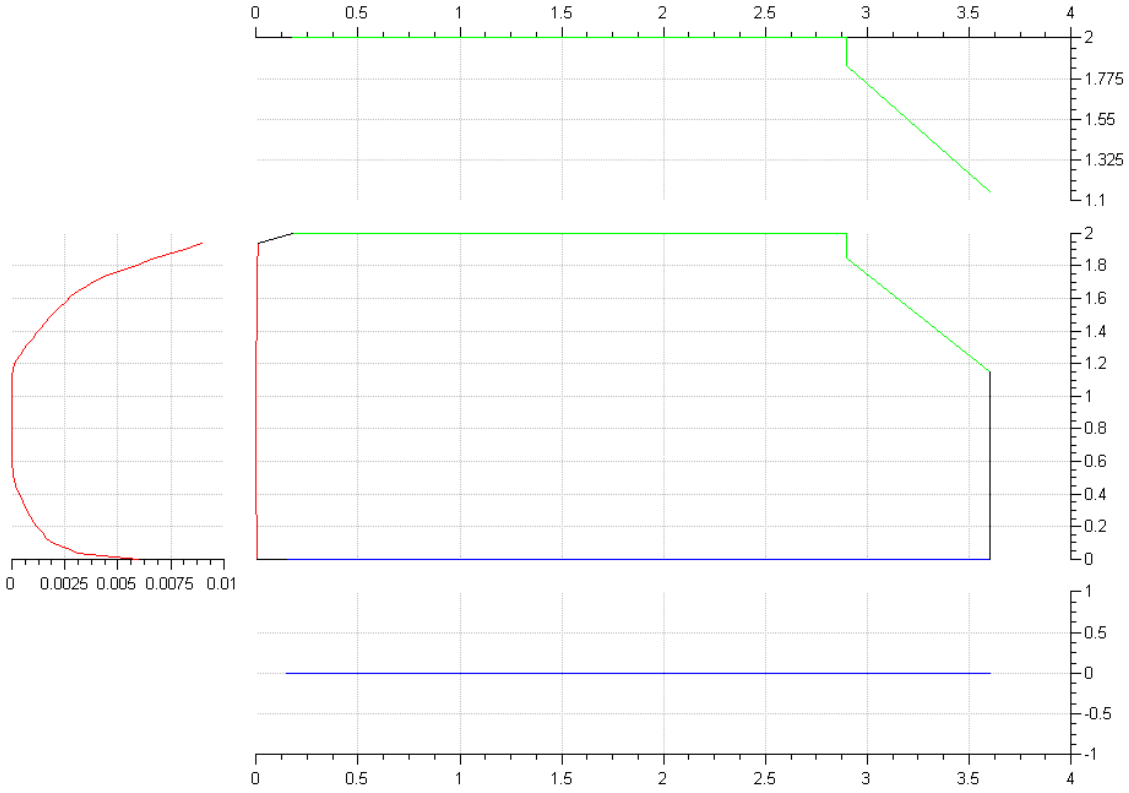

Figure A.4 : First Compression Ring Profile

2. Ring (Napier Ring):

Ring Mass:	12.5 g
Center of Gravity:	0.159 mm
Pre – Twist Angle:	0º
Tangential Force:	18.35 N
Ring End:	0.07 mm (variable)
Peripheral Edge:	0 mm
Summit Roughness:	0.55 µm
Radial Deviation:	-0.428 mm (above groove)
Radial Deviation:	-0.608 mm (below groove)
Groove Root Depth:	-4.35 mm
Distance from Piston Top:	18.34 mm
Groove Top Angle:	0º
Profile of Ring Face:	(Figure A.5)

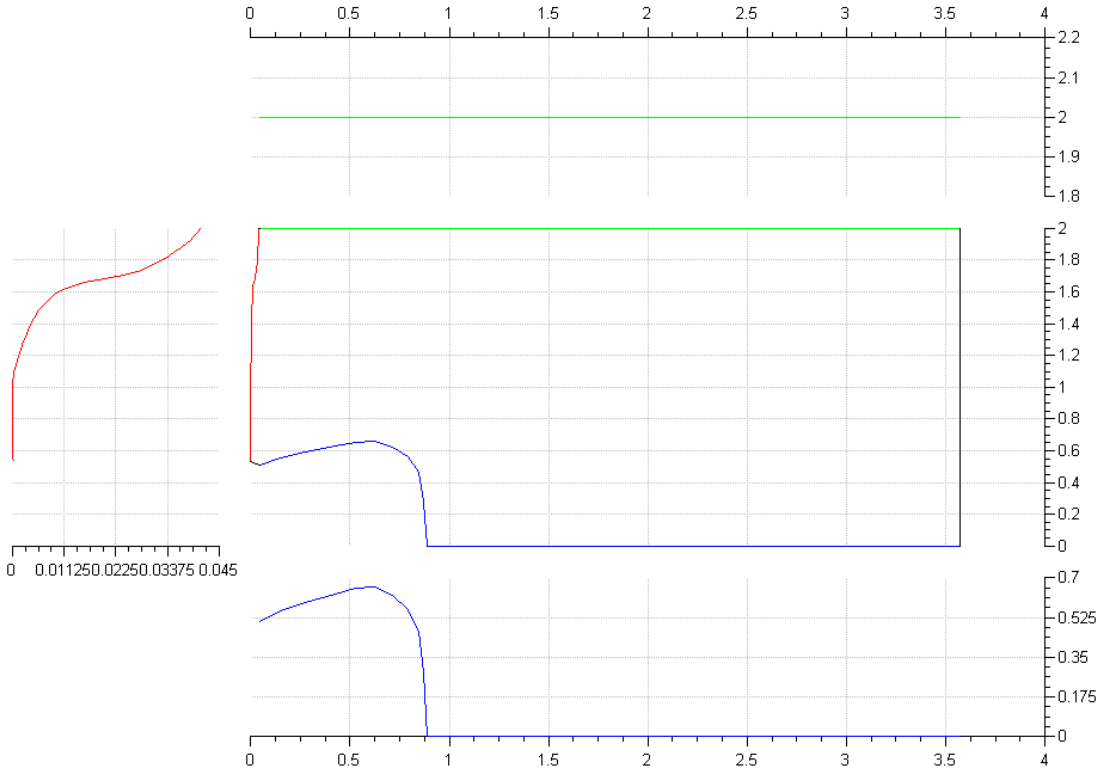

Figure A.5 : Second Compression Ring Profile

<u>Oil Ring:</u>

Ring Mass:	6.8 g
Center of Gravity:	0.04569 mm
Pre – Twist Angle:	0º
Tangential Force:	21 N
Ring End:	0.03 mm (variable)
Peripheral Edge:	0.02 mm
Summit Roughness:	0.55 µm
Radial Deviation:	-0.608 mm (above groove)
Radial Deviation:	-0.28 mm (below groove)
Groove Root Depth:	-3.55 mm
Distance from Piston Top:	24.345 mm
Groove Top Angle:	0º
Profile of Ring Face:	(Figure A.6)

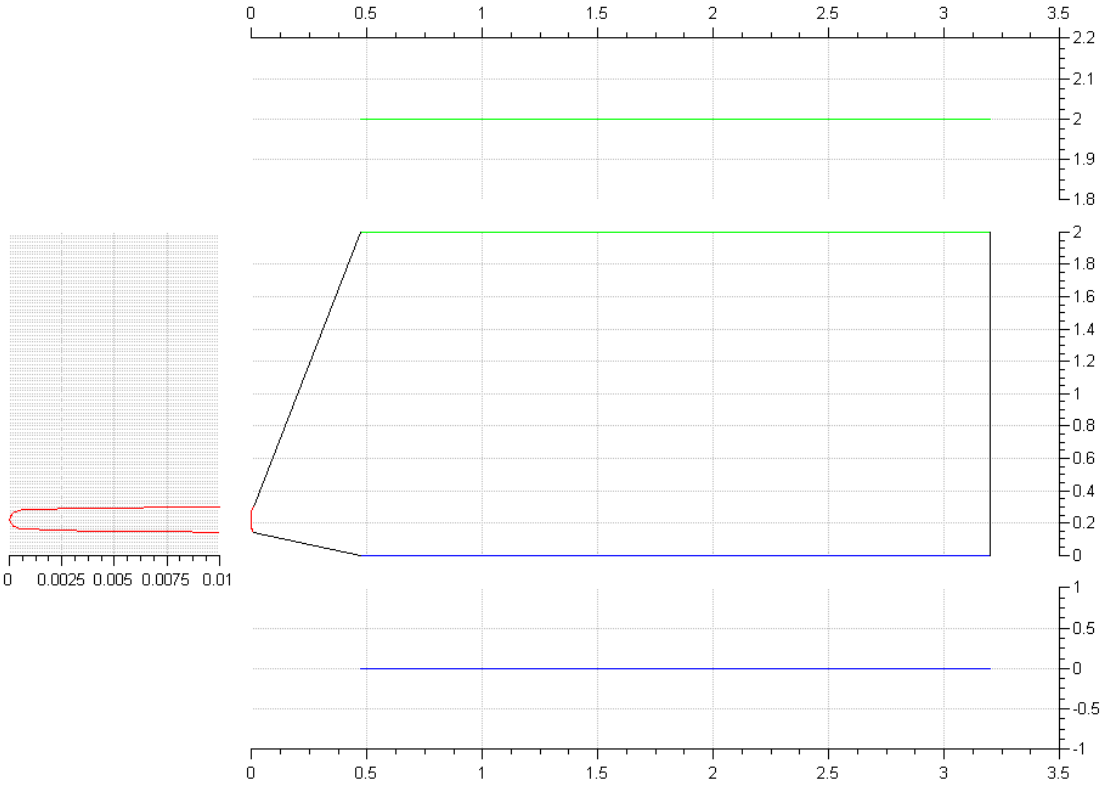

Figure A.6 : Oil Ring Profile

APPENDIX A.4

```
#
#  CONTROL OUTPUT OF
#  FORCE-DEFORMATION DATA
#
NODEPOS
 sym 1
 nmer     2
   phi     0
   numZ     7
          -24.816   !     1-Node
          -13.049   !     2-Node
           -3.228   !     3-Node
            6.594   !     4-Node
           16.635   !     5-Node
           34.558   !     6-Node
           44.163   !     7-Node

   phi     25
   numZ     3
          -9.121   !     8-Node
           10.522  !     9-Node
           34.558  !    10-Node
#
#
NODESTIFF
#
#---------------------------------------------------------------
#
#         Stiffness       Coupling         Interpolation mode
#       Characteristic    of piston         of bending lines
#                          nodes
#
# keyword   nonlin       coupled             intMod_lin
#          linear       uncoupled           intMod_quad
#                            uncoupAXIAL
#                     uncoupRADIAL
#
#---------------------------------------------------------------
#
       fact  1.0e-3       ! Change deformation data
#
          chara   linear   coupled                    intMod_lin
#
#---------------------------------------------------------------
#
#         LOAD ON NODE:     1
 newPos
```

```
        4500    -100,5          500     -11,165
        0       -51,012                 0       -5,668
        0       -20,858                 0       -2,3175
        0       -7,0623                 0       -0,7847
        0       -0,72284        0       -0,080316
        0       -4,6197                 0       -0,5133
        0       -6,7807                 0       -0,75341
#
        0       -8,8649                 0       -0,98499
        0       -0,24938        0       -0,027709
        0       -4,108          0       -0,45644

#
#       LOAD ON NODE:    2
 newPos
        0       -51,2           0       -5,6889
        4500    -48,852                 500     -5,428
        0       -22,153                 0       -2,4615
        0       -7,1713                 0       -0,79681
        0       -1,2095                 0       -0,13439
        0       -2,7867                 0       -0,30963
        0       -4,2544                 0       -0,47271
#
        0       -7,5841                 0       -0,84268
        0       -0,54582        0       -0,060646
        0       -2,3948                 0       -0,26609

#
#       LOAD ON NODE:    3
 newPos
        0       -20,948                 0       -2,3276
        0       -22,24          0       -2,4712
        4500    -25,682                 500     -2,8535
        0       -8,781          0       -0,97567
        0       -2,1889                 0       -0,24321
        0       -0,67515        0       -0,075017
        0       -1,4004                 0       -0,1556
#
        0       -4,7388                 0       -0,52653
        0       -1,0184                 0       -0,11315
        0       -0,43772        0       -0,048635

#
#       LOAD ON NODE:    4
 newPos
        0       -7,1114                 0       -0,79016
        0       -7,2412                 0       -0,80458
        0       -8,8879                 0       -0,98755
        4500    -12,504                 500     -1,3894
        0       -3,6585                 0       -0,4065
```

```
        0       -1,412          0       -0,15689
        0       -1,3033                 0       -0,14481
#
        0       -1,8138                 0       -0,20154
        0       -1,4778                 0       -0,1642
        0       -1,4738                 0       -0,16376

#
#       LOAD ON NODE:    5
 newPos
        0       -0,73629        0       -0,08181
        0       -1,2281                 0       -0,13645
        0       -2,219          0       -0,24656
        0       -3,7088                 0       -0,41209
        4500    -7,8923                 500     -0,87692
        0       -3,7338                 0       -0,41487
        0       -4,1953                 0       -0,46614
#
        0       -0,014392       0       -0,0015991
        0       -1,6944                 0       -0,18826
        0       -3,5668                 0       -0,39632

#
#       LOAD ON NODE:    6
 newPos
        0       -4,6282                 0       -0,51424
        0       -2,7927                 0       -0,3103
        0       -0,67972        0       -0,075525
        0       -1,4059                 0       -0,15621
        0       -3,7285                 0       -0,41427
        4500    -13,918                 500     -1,5465
        0       -11,494                 0       -1,2771
#
        0       -1,9093                 0       -0,21214
        0       -2,1943                 0       -0,24381
        0       -8,0614                 0       -0,89571

#
#       LOAD ON NODE:    7
 newPos
        0       -6,7837                 0       -0,75375
        0       -4,2561                 0       -0,4729
        0       -1,4009                 0       -0,15565
        0       -1,2999                 0       -0,14443
        0       -4,1902                 0       -0,46558
        0       -11,508                 0       -1,2787
        4500    -20,853                 500     -2,317
#
        0       -2,7421                 0       -0,30468
        0       -2,5845                 0       -0,28717
```

```
        0       -10,351             0       -1,1501

#
#       LOAD ON NODE:    8
 newPos
        0       -15,202732  0       -1,689163
        0       -12,983631  0       -1,442646
        0       -9,956344   0       -1,10624
        0       -7,272757   0       -0,808084
        0       -5,565882   0       -0,618435
        0       -4,792802   0       -0,532535
        0       -4,667358   0       -0,518596
#
        4500    -29,388324  500     -3,265386
        0       -7,389232   0       -0,821024
        0       -5,402492   0       -0,600275

#
#       LOAD ON NODE:    9
 newPos
        0       -4,828903   0       -0,536543
        0       -4,417962   0       -0,490885
        0       -4,090748   0       -0,454531
        0       -3,798011   0       -0,422003
        0       -3,370338   0       -0,374477
        0       -3,229307   0       -0,358812
        0       -3,306135   0       -0,367349
#
        0       -5,30522    0       -0,589474
        4500    -8,983826   500     -0,998206
        0       -2,854397   0       -0,317153

#
#       LOAD ON NODE:    10
 newPos
        0       -3,838738   0       -0,426526
        0       -2,295685   0       -0,255078
        0       -0,549542   0       -0,0610607
        0       -1,323873   0       -0,147096
        0       -3,254448   0       -0,361602
        0       -7,422403   0       -0,824706
        0       -9,535677   0       -1,059542
#
        0       -1,612428   0       -0,179165
        0       -2,243988   0       -0,249331
        4500    -13,241246  500     -1,471228
```

CURRICULUM VITA

Candidate's full name:	Fatih KAĞNICI
Place and date of birth:	Hekimhan, 13.10.1985
Permanent Address:	Kozyatağı Mah. Pınar Sok No:12/ B Blok/ Daire:1 Kadıköy/ İSTANBUL
Universities and Colleges attended:	Istanbul Technical University